Medical Applications of Thermoelectric Temperature Control

by

Connie Yu Jeong Lee

A dissertation submitted in partial fulfillment
of the requirements for the degree of
Doctor of Philosophy
(Mechanical Engineering)
in the University of Michigan
2022

Doctoral Committee:

Professor Kevin P. Pipe, Chair
Assistant Professor Cynthia A. Chestek
Professor Katsuo Kurabayashi
Professor Aditya S. Pandey

Connie Y. Lee

cyjlee@umich.edu

ORCID iD: 0000-0003-1940-3574

Dedication

This dissertation is dedicated to my family, my college and high school friends, my colleagues and professors in Ann Arbor, and my fiancé Gordon Peng.

Acknowledgement

This dissertation was only possible thanks to all the people and institutions who have supported my research projects.

My research group colleagues (past and present): Chen Li, Aman Jha, Shantonio Birch, Luyang Wang. Thank you all for your assistance in my projects, helping me move heavy equipment, and serving as mentors.

My adviser Kevin Pipe, who has encouraged me to be independent in my thinking.

The Mechanical Engineering department, for providing a warm community of scholars, academic support, and exceptional facilities.

Members of my dissertation committee: Aditya Pandey, Cynthia Chestek, Katsuo Kurabayashi.

My collaborators: Joan Greve, Richard Keep, and Arjun Adapa. Special thanks to Colleen Crouch, Autumn Bullard, Eric Kennedy and Samuel Nason, both who provided immeasurable research support and guidance.

Rob Pettigrew of ScholarSpace at the University of Michigan, whose amazing Word skills helped format this dissertation.

Funding for this work was provided by the University of Michigan Rackham Merit Fellowship (RMF), the Rackham Research Grants, and the Pipe lab discretionary fund.

Table of Contents

Dedication ii

Acknowledgement iii

List of Tables ix

List of Figures x

List of Equations xvi

List of Appendices xvii

Abstract xviii

Chapter 1 Introduction 1

1.1 Temperature's role in living systems 1

1.2 What is thermal medicine? 1

1.3 Temperature's role in sensation and perception 3

1.3.1 Temperature gated ion channels and sensory pathway 3

1.3.2 Gate control theory and cold 5

1.4 Basics of tissue cooling and bioheat transfer 6

1.5 Animal models and their limitations 8

1.5.1 Rodent models 8

1.5.2 Non-human primates 8

1.6 Thesis Structure 9

1.7 References 10

Chapter 2 Solid-state Temperature Control of In Vivo Blood Flow 12

2.1 Abstract 12

2.2 Introduction 13
2.3 Methods 15
2.3.1 System Description 15
2.3.2 Surgical Methods 20
2.3.3 Data processing and statistics 22
2.4 Results and Discussion 22
2.4.1 Device effect on RJV, LCA and rectal temperature 22
2.4.2 Limitations 25
2.4.3 Applications 27
2.5 Conclusion 30
2.6 Acknowledgements 31
2.7 References 31
Chapter 3 Selective Brain Cooling via Thermoelectric Extravascular Blood Cooling of a Carotid Artery 35
3.1 Abstract 35
3.2 Introduction 36
3.3 Methods 38
3.3.1 Device description 38
3.3.2 Animal preparation 39
3.3.3 Experimental procedure 40
3.3.4 Cooling blanket measurements 40
3.3.5 Cooling probe measurements 41
3.3.6 Blood and tissue sample collection 42
3.3.7 Data processing and statistical analysis 43
3.4 Results 44
3.4.1 Changes in temperature with cooling trials 44

3.4.2 Adverse effects of cooling 46
3.5 Discussion 50
3.5.1 Efficacy of brain cooling with cooling methods 50
3.5.2 Systemic hypothermia vs SBC 51
3.5.3 Safety of extravascular carotid cooling 52
3.5.4 Limitations 53
3.6 Conclusion 54
3.7 Acknowledgements 55
3.8 References 55
Chapter 4 Computational Modeling of Extravascular Blood Temperature Control for Selective Brain Cooling 58
4.1 Abstract 58
4.2 Introduction 59
4.3 Nomenclature 62
4.4 Methods 62
4.4.1 Governing physics 63
4.4.2 Model data extraction 65
4.4.3 Rat computational model 65
4.4.4 Methods for experimental rat blood flow and temperature measurements 66
4.4.5 Human model 68
4.4.6 Other metrics 72
4.4.7 FEM techniques 73
4.5 Results 74
4.5.1 Rat model: validation of model with prior rat experiments 74
4.5.2 Human model: cooling performed with open neck conditions 75

4.5.3 Human model: cooling performed with percutaneous conditions 77
4.6 Discussion 82
4.6.1 Rat model validation 82
4.6.2 Extravascular blood cooling in context of clinical therapy 83
4.6.3 Limitations of human scale models and possible sources of error 86
4.7 Conclusion 87
4.8 References 88
Chapter 5 Encoding of Thermosensation in the Layer V Sensory Cortex of Non-human Primates 92
5.1 Abstract 92
5.2 Nomenclature 93
5.3 Introduction 94
5.4 Assumptions 99
5.5 Experimental setup and protocol 99
5.5.1 Thermoelectric skin cooler and mechanical poker (clicker) 99
5.5.2 Animal preparation and selection 101
5.5.3 Experimental procedure 102
5.6 Data processing, machine learning, and statistics 107
5.6.1 Data preprocessing 108
5.6.2 Feature extraction 108
5.6.3 Visual encoding analysis: 110
5.6.4 Population analysis and classification 111
5.6.5 Other machine learning techniques 112
5.6.6 Broadband signal processing: FFT, Wavelet transformation 113
5.6.7 Statistical analysis 113

5.7 Results 113
5.7.1 Baseline neural response to the environment (20˚C) versus the probe 113
5.7.2 Response to constant T (-5, 0, 5, 35 ˚C) 114
5.7.3 Response to constant T (-5, 5, 35 ˚C) and innocuous MP (cold-induced numbing) . 116
5.7.4 Response to reheating after constant cooling 120
5.7.5 Response to a rapidly fluctuating temperature (|dT/dt| > 0) 121
5.7.6 Response to a periodic temperature 122
5.8 Discussion 124
5.8.1 Ice vs probe cooling 124
5.8.2 On the accuracy of classification and linear model generation 124
5.8.3 Limitations 125
5.9 Conclusion 127
5.10 Acknowledgements 128
5.11 References 128
Chapter 6 Summary and Future Work 131
6.1 Summary 131
6.2 Future work 132
Appendices 133

List of Tables

Table 2.1 Mean values of cooling rates calculated for the total lengths of each trial, ranging 15-30 mins. Values are calculated from the linear regression slopes of the time series data (per trial), which were initially smoothed in a 30 second window moving average. 24

Table 3.1 Animal Statistics 38

Table 3.2 Chart of experiments and methods. 40

Table 3.3 Summary of blood and tissue sample collection. G1 (pre- cooling blanket) was generally omitted in statistical comparison of test groups due to difficulty in sample collection. 42

Table 3.4 Compilation of all animals' averaged cooling rates per test group and location. 45

Table 3.5 Hematology results*,†,‡ 47

Table 4.1 Mean data from PCMRI (n = 10) scans. Body weight reported is weight measured on day of scan. 67

Table 4.2 Input values for rat open neck model 68

Table 4.3 Input values for human percutaneous model. *For open neck model, all values are the same except initial vessel temperature, which is assumed to be 32 ˚C 69

Table 5.1 Types of experiments performed. T: thermal stimuli, P: pressure/tactile stimuli 104

Table 5.2 Constant temperature trial sequence. Onset: placement of probe on the skin. Offset: removal of the probe from the skin/end of a trial. Each trial was repeated 5x minimum 105

Table 5.3 Constant T with MP trial sequence. MP: poking with the clicker. From 0-90 s, the probe T is held constant until at 91 s the probe is brought to 35 ˚C. The length of time to reach stable constant T varies with initial probe T, which results in longer wait times for restarting MP 106

Table 5.4 Mean accuracies for classification of population response in firing rates 117

Table 5.5 Statistical comparisons of latency values per trial and channels. Data from Aug 2019 dataset. 119

List of Figures

Figure 1.1 Taken from Vriens et al 2014[6]. A: Mechanosensitive channels, detects membrane properties change from dT B: Temperature dep. Production of ligands C: dT dep phosphorylation D: Ca activation E: dT leads to conformational changes in the channel complex. 4

Figure 1.2 Taken from Vriens et al[6]. Neural pathway of thermosensory signals from peripheral neurons into the sensory cortex, where it is processed as perception. 5

Figure 2.1 Rendering of a prototype cooling probe. The cooling bar has TECs layered inside to concentrate their cooling power onto the center bar. Tip dimensions that contact with blood vessel: 8.6 x 1.5 mm^2 (L x W). Not shown in image are thermal insulation around the cooling bar to reduce environmental heat leakage. 17

Figure 2.2 Theoretical heat flux of the probe tip with all 12 TECs engaged, the cooling power of which is concentrated into the 8.6 x 1.5 mm^2 flat tip area. 17

Figure 2.3 System prototype. From left to right: (1) probe with the cooling bar wrapped in thermal insulation, revealing only the tip, (2) electrical controller, (3) water chillers for TEC waste heat, (4) laptop for data collection and system control. 18

Figure 2.4 (Left) Blood temperature control concept. (Right) surgical schematic showing probe placement. Images created with BioRender.com. Adapted from icons “Rat (lateral)” and “Rat (supine, curved tail)”, by BioRender.com (2021). 19

Figure 2.5 (Left) Exposed RJV with thermocouple inserted into the vessel via a needle tip, shown inside dashed circles. (Middle) thermocouple placed on the LCA. White arrows point to the LCA. (Right) Probe applicator being placed atop the LCA for an experiment. Upon final placement, the probe tip (8.6 mm x 1.5 mm) is parallel and sitting flush on the LCA. 22

Figure 2.6 (Left) Sample temperature data taken for a 0 ˚C trial is shown for the first 15 minutes. LCA surface temperature drops rapidly, while intravenous blood and rectal temperatures fall gradually but at distinct rates. (Right) Average temperature changes after the first 15 minutes for all available data. Bars are in order of baseline, 0 ˚C, and -5 ˚C from left to right. 23

Figure 2.7 Comparing an animal’s RJV blood temperature levels at baseline versus with active cooling. Data shown is from a representative animal, for the first 15 minutes of the trial. Dashed lines indicate linear regression trendlines. Baseline (blue): $p < 0.001$ and $R^2 = 0.112$. 0 ˚C (red): $p < 0.001$ and $R^2 = 0.896$. 25

Figure 2.8 Possible embodiments of extravascular blood cooling devices. (A) Current prototype. (B) Percutaneous system. (C) Cooling loop. (D) Thermoelectric neck cooling cuff; similar cooling pads/blankets are currently in use in hospital settings. (E) Intranasal cooling. (F, G) Tip designs for the cooling bar. (H) Application of an array of probes on a single vessel to multiply cooling levels. Not included in the figure are ideas that combine the cooling device with existing tools, e.g., attaching cooling elements to surgical drills or other implements 29

Figure 3.1 Placement of cooling probe tip on the exposed LCCA of a rat. Other probe components, such as the power supply, thermoelectric modules, and thermocouples are not shown. 39

Figure 3.2 Images of the rat during experiments. Left: an ice-filled cooling blanket is used to induce whole-body cooling. Right: The animal is prepped for cooling probe trials. 41

Figure 3.3 Representative temperature traces for a sample rat in each test group. Baseline is when the probe in contact with the LCCA but deactivated. 45

Figure 3.4 Representative figure of brain temperature trace, comparing baseline trials with cooling trials in a sample rat. 46

Figure 3.5 Representative figures of rectal temperature change over time, comparing baseline trials with a cooling trial in a rat. Top: baseline vs. cooling blanket, Bottom: baseline vs. cooling probe at 0 ˚C and -5 ˚C..... 46

Figure 3.6 Representative blood smears from rats. No distinct hemolysis is detected at the time points spanning G2-G4. G1 is not shown due to a lack of samples, but it also displayed no obvious hemolysis..... 47

Figure 3.7 CBC results for G2 (n = 7), G3 (n = 6) and G4 (n = 7). All values were within normothermic ranges throughout the experimental manipulation, signifying no acute systemic damage from the probe. There were no statistically significant differences between groups for any parameter. There was a downward trend in total white blood cell count (WBC) and absolute lymphocyte count (Lym) across G2-4, but this is attributed to prolonged anesthesia. G1 was excluded due to low sample number and a sample was excluded from G3 due to clotting. *For the units and values of RBC parameters, refer to Table 3.5. 49

Figure 3.8 Representative images of hematoxylin and eosin-stained histology of experimental (LCCA: A, C, E, G) and contralateral control (RCCA: B, D, F, H). No arterial pathology was detected. Each pair of images are from one animal (A, B), (C, D), (E, F), (G, H). A total of 12 cross-sections (4 serial sections at each of 3 levels, separated by 100 μm each) were evaluated for each artery. Original magnification: 10x, bars = 200 μm. 50

Figure 3.9 Representative images of a sample LCCA. In some sections at level 2 (A) there was focal pericapillary degeneration in the adventitia with focal infiltration of acute inflammatory cells (B, arrow). This was consistent with mild tissue trauma on the adventitial surface but did not affect the artery itself. In two sections at level 3 (C, D) there was a focal tear in the vessel with hemorrhage but no tissue reaction in the artery wall or hemophagocytosis. In the absence of tissue reaction this was considered likely to be iatrogenic damage at the time of vessel collection.

Original magnifications: A, C, D = 10x, bar 100 μm; B = 40x, bar 20 μm. Box in A indicates area of focus in B. Staining for A, B, C: hematoxylin and eosin; D: trichrome-Verhoeff. 50

Figure 4.1 Locations for T, P, and V measurements. Primary results are collected along the midline, surface, and outlet locations. 65

Figure 4.2 PCMRI evaluation of CCA blood flow rates in vivo (n = 10). 67

Figure 4.3 Boundary conditions per delivery type. Constant temperature conditions apply in the center where the cooling is applied, with convection cooling on the fringes and bottom surface (top row) for open surgery and insulation for percutaneous (bottom row). The terminal ends of the carotid are insulated for both conditions..... 69

Figure 4.4 Pulsatile flow rate in carotid artery (top) and corresponding blood pressure waveform (bottom)..... 71

Figure 4.5 Comparison of pulsatile flow vs constant flow conditions result in minimal differences in outlet blood temperature in a sample trial..... 72

Figure 4.6 Comparison of experimental vs simulational results from rat probe cooling at T = 0 ˚ C. Experimental values are averaged from n = 10 rats. Filled area (blue) indicates 95% confidence interval of the experimental data. R^2 =0.75, p-value < 0.001..... 75

Figure 4.7 Midline blood temperature at open surgery boundary conditions, as measured at 10 min intervals. There is some fluctuation in the blood temperature with time as convection dominates and warm blood continues to enter at the inlet, leading to instances of nonmonotonic activity with T_p. Nonetheless, at steady state simulations, blood temperature is monotonic with T_p. Gray indicates area with extravascular cooling at constant temperature. 75

Figure 4.8 Using open surgery conditions, blood temperature decrease at carotid outlet at the corresponding L_p and T_p using a steady state model (time invariant). No monotonic dependence on L_p..... 76

Figure 4.9 Midline blood temperature at open neck conditions run with a time-invariant model (steady state). Midline temperature depends little on the conductive cooling and corresponding cooling length, but does monotonically decrease with applied temperature. Gray area indicates active extravascular cooling zone. 77

Figure 4.10 Outlet blood temperature with percutaneous cooling. Saturation occurs within 60 s of onset. 78

Figure 4.11 Midline blood temperature at percutaneous edge conditions. There are minor fluctuations with time, but the differences are near trivial (<0.1 ˚C). Note that for percutaneous results, after the first minute there is saturation in the results. Gray area indicates active extravascular cooling zone..... 78

Figure 4.12 Using percutaneous conditions, outlet blood temperature achieved at corresponding L_p and T_p at t = 300 s (quasi- steady state). Monotonic with L_p and T_p. 79

Figure 4.13 Midline blood temperature results at percutaneous conditions clearly depend on temperature and on cooling length. Data taken at t = 300 s. Gray area indicates active extravascular cooling zone..... 80

Figure 4.14. Thermal spread as measured for the edge cases in percutaneous cooling model. Right column depicts zoomed in plots of the left column, respectively. Gray areas highlight the regions of thermal spread..... 81

Figure 5.1 Taken from Vriens et al[7]. Neural pathway of thermosensory signals from peripheral neurons into the sensory cortex, where it is processed as perception..... 96

Figure 5.2 A commercial cryoanesthesia package consisting of vibrating cold packs. The combination of vibration and cold are thought to minimize pain. Image sourced from Pain Care Labs[14] 97

Figure 5.3 Applicator for cryoanesthesia for use before intravitreal injections[15]..... 97

Figure 5.4 Rendering of probe inner design, with TECs, mechanical clicker, and heat spreaders (copper plates) on the center bar..... 100

Figure 5.5 Skin cooling system. From left to right: water pump and reservoir, water chiller, power supply, cooling probe..... 100

Figure 5.6 (Left): Monkey in restraint chair. (Right): Probing and shaving receptive zone (marked in black square)..... 103

Figure 5.7 Experimental rig and cerebral data acquisition system (Cerebus) inside a faraday cage, which is used as the primary experimental theater 104

Figure 5.8 Conceptual drawing of a monkey plugged into neural data acquisition system. Monkey's seat, restraints, or other apparatus not shown. Graphic created using Biorender.com (2022)..... 104

Figure 5.9 Nominal T input for a rapidly changing T (dT/dt) trial, with no MP. This temperature trace was followed by a stepwise ramp up to 35 ˚C. 107

Figure 5.10 (Left): Referenced, broadband signal bandpass filtered to 300-5000 Hz range, with a moving -4.5*RMS threshold (red-dashed). (Right): Zooming in on the spikes that cross the thresholds 109

Figure 5.11 Conditional decision tree for returning optimal peak time value 110

Figure 5.12 Sample plot of firing rates vs time for a given channel and trial; this channel is clearly sensitive to MPs (dashed-black vertical lines) but less so to onset of cold T (1st blue-dashed line, 2nd line indicates probe offset)..... 111

Figure 5.13 Rasterplot of viable channels in a sample trial to visually assess for response to specific stimuli. (Top): no visible response to constant cold temperature; (Bottom): when probe is offset and skin rewarms to normal temperature, there is a surge of firing in all channels..... 112

Figure 5.14 From a representative channel from a trial, baseline recording during probe on vs off. 114

Figure 5.15 Firing rates from a sample channel with constant T inputs only at four T points... 115

Figure 5.16 Firing rates for a sample channel with onset/offset of ice, or 0 ˚C (blue), and the subsequent rewarming period (yellow). Red-dashed lines indicate a moving average of the firing rates. 116

Figure 5.17 Wavelet plot of ice trial, capturing the first two onset/offset pairs. Onset/offset are visible as hot spots in the wavelet plot..... 116

Figure 5.18 Preliminary attempt at decoding of T and MP stimuli with 16 viable channels. The actual T applied were 35 ˚C and -5 ˚C. MP = 1 indicates no stimuli and MP = 2 indicates with MP. Mean squared error for T: 608.6, MP: 0.31; Correlation for T: 0.07, MP: 0.42. 118

Figure 5.19 Mean accuracies for classification of applied T using population response in firing rates. 118

Figure 5.20 Position dependence and clustering based on k-means clustering. Figures created by Agnes M. Resto..... 119

Figure 5.21 For a sample responsive multiunit, firing rate for constant T and irregularly spaced MP, with return to skin T at MP 8-9. Horizontal labels indicate the i-th MP that was applied, not time. Trendlines are placed as a visual guide and are not regression lines..... 120

Figure 5.22 Response from a sample channel to dynamic T inputs. (Top row): firing rates from a sample channel compared to changing input T. (Bottom row): Mean moving RMS calculated from a sample channel for values of dT/dt. Only two trials are reported due to unforeseen experimental challenges with monkey cooperation. 122

Figure 5.23 Average MRS for a moving window (1 s) at points of constant dT/dt. An animation for the full rms trace is available in Appendix D..... 122

Figure 5.24 Wavelet analysis for a sample trial and channel for the first 60 seconds. Red-dashed indicates input T, colors indicate power of signal 123

Figure 5.25 Power spectra at ~ 0.1 Hz, red indicates peaks and black-dashed indicates T input, blue-dashed-horizontal line indicates threshold to define a peak. 123

Figure 5.26 Mean peak time vs sinusoidal input shows mean value falls during cooling period. Phase: -0.95 s ± 3.95 s at 0.1 Hz signal. 124

Appendix Figure 1. Rat surgical space setup. 1) Kopf stereotaxic frame, 2) anesthesia induction box and shaving area, 3) Vetamac isoflurane vaporizer, 4) oxygen tank with regulator, 5) 10x microscope, 6) surgical benchtop with anesthesia nose cone and cooling probe tip, 7) Koolance cooling probe chiller and power supply, 8) biohazardous waste disposal, 9) charcoal canister for waste isoflurane recovery, with another under the surgical benchtop. 134

Appendix Figure 2. Close up images of equipment used in surgical lab. 1) Zoomed heating pad for induction of anesthesia, 2) Kopf stereotaxic frame, 3) Vetamac vaporizer for isoflurane, 4) oxygen regulators, 5) Harvard Apparatus feedback controlled heating pad with rectal probe... 135

Appendix Figure 3. Close up of the surgical bench. 1) Surgical tools and anesthesia line from vaporizer (thin white tube to the left), 2) Harvard Apparatus feedback controlled heating pad, with the pad under the white surgical benchtop area, 3) 10x microscope, 4) 1”-1.25” diameter nose cone made with a syringe and latex gloves, 5) cooling probe tip, 6) Koolance water chiller, 7) Meerstetter TEC high voltage controller and Siteview data logger, 8) thermocopules, 9) hidden charcoal canister for waste isoflurane collection. 136

Appendix Figure 4. TEC specifications for rat (and monkey) probes. Manufactured by Custom Thermoelectrics..... 137

List of Equations

Equation 1 6
Equation 2 6
Equation 3 7
Equation 4 63
Equation 5 64
Equation 6 64
Equation 7 64
Equation 8 70
Equation 9 71
Equation 10 72
Equation 11 73
Equation 12 85
Equation 13 109
Equation 14 110
Equation 15 110

List of Appendices

Appendix A: Description of Rat Experimental Setup..... 134

Appendix B: Description of Parts in Cooling Probes (Rat and Monkey)..... 137

Appendix C: Custom Scripts and Functions for Study of Cold Sensation. 138

Appendix D: Cold Sensation Study-- Stepwise Dynamic Trials..... 142

Abstract

The human body is a complex machine that operates within a narrow thermal range. Alongside internal thermogenicity, local heat fluxes regulate various functions in the body that are critical for healthy living. For example, digestion, immune response, fitness, and hair/skin quality are all affected by bodily temperature. As significant as heat management is for good health, the body constantly monitors internal and environmental temperatures for homeostasis.

Humans have historically understood the importance of temperature, and leveraged heat to enhance or restore health. In 370 BC, Hippocrates was the first to identify cold (i.e., ice) as a therapeutic for swelling on soldiers. In the modern day, hypothermia is widely used to alleviate the detrimental effects of inflammation, cardiac arrest and fever. However, questions remain on how to best deliver cooling to deep tissues and quantify its responses to the external temperature. Current medical cooling technologies are uncontrollable in cooling rate, cooling region, and/or target temperature. Ethical and surgical barriers also discourage direct experimentation on humans. Overall, the lack of a sophisticated cooling and measuring method for deep tissue heat transfer inhibits the engineering and implementation of optimal cooling in clinics. Through a combination of animal models and computational simulations, this thesis aims to propose improved techniques for cooling therapy with concentrated thermoelectric cooling elements (TEC) and understand the mechanisms of cold therapy on the body. TECs are an advantageous tool for this purpose as they are feedback-controllable, precise, rapid, and can also quantify the heat that is removed.

Using TECs and rodent models, we developed a novel tool and surgical protocol for extravascular carotid blood cooling in vivo, for which we achieved a temperature change of -4.74 ± 2.9 ˚C/hr when a single artery is cooled at 0 ˚C. Following success with blood cooling, we demonstrated that cold blood in the carotid artery convectively cools rodent brain tissue independently of the core (carotid: -4.19 ± 3.15 ˚C/hr at core: -0.84 ± 2.59 ˚C/hr). This selective brain cooling technique is unique in the field as an extravascular (not intravascularly accessed), conduction-convection heat transfer medical device that can cool an organ by targeting its major artery. Computational models of human carotid arteries were used to identify the scope of cooling that is possible with the extravascular cooling technique (approximately 1 ˚C decrease in outlet blood temperature of the human carotid), subject to further technical improvements.

Concurrently, we quantitatively studied how cold information is delivered to and perceived in the brain. For this purpose, a skin cooling device that can accurately apply temperatures and simultaneously deliver nonpainful pokes to the same area was devised. Data from the sensory cortex of non-human primate models were used to train decoding algorithms linking neural firing rates to applied skin temperature. Preliminarily the algorithms reached a maximum of 76% accuracy when discriminating between cold and warm temperatures. Future improvements in the algorithm will allow for the prediction of cold sensation and cold-induced anesthesia.

This research will inform researchers and clinicians in quantifying and predicting the body's response to cold, how to manipulate the temperature of select regions in the body, and move towards an advanced cooling medical device and optimized clinical workflow. Ultimately, we seek to ensure medical application of cold as a precise and controlled therapy through which we heal and enhance the body.

Chapter 1 Introduction

1.1 Temperature's role in living systems

Healthy normothermic temperature is essential for proper physiological function and lifestyle. Temperature directly regulates internal biological processes (i.e. sweating, immune response, digestion), and influences a person's daily activities and behaviors. Maintaining normothermia ("normal temperature", around 36.5 ˚C) is most optimal, by balancing internal and external factors that can affect the temperature of living systems. Internal factors include metabolic heat generation, fever from infection/inflammation, thermoregulation, heat stress from exercise, and more. External factors are heat sources/sinks from the environment, such as exposure to inclement weather, getting wet, or being irradiated with intense sunlight. The consequences of a disbalanced internal body temperature, or prolonged exposure to extreme outdoor conditions are severe. Not only is there a risk of thermal damage (i.e. burns on the skin), but internal heat stresses can disable organs (i.e. cardiosuppression[1]) and permanently damage the brain[2]. In those with limited thermoregulatory abilities such as babies and the elderly[3], a summer heat wave can be fatal[4].

1.2 What is thermal medicine?

While maintaining normothermia is typically preferred, heating or cooling of tissue can be harnessed for therapeutic purposes. Thermal medicine is the use of heat and cold on the body to treat diseases or alleviate pain, and was used throughout human history (i.e. ice packs, warm baths). Hippocrates is known as one of the first users of thermal medicine, having applied ice to

treat swelling in patients[5]. He once said, “Those diseases that medicines do not cure are cured by the knife. Those that the knife does not cure are cured by fire. Those that fire does not cure, must be considered incurable.” In the modern day, thermal medicine has expanded to include cryotherapy, cryoablation, laser surgery, therapeutic hypothermia, cooling helmets for chemotherapy patients, and many more. Outside of the clinic, thermal therapies can also be used to improve athletic performance, comfort, and the quality of life.

Thermal therapies act by an intentional tissue temperature change, which can be a challenging task. Temperature change of living systems is highly difficult because of the following reasons: 1) deep tissues and organs are well protected from the environment by several layers of thermally resistive skin and fat, 2) a robust cardiovascular system continuously supplies warm blood flow, 3) metabolic heat generation resists external heat sinks and adult humans possess large thermal mass, 4) perfusion levels vary autonomically (vasodilation and vasoconstriction) in response to changing temperature, 5) the range of heat that can be applied must be moderated to avoid thermal damage 6) heat applied may cause discomfort in patients, and 7) variability in thermoregulatory ability with age and sex challenge standardizing some thermal interventions for clinical use. Even if temperature change is successfully induced, it is often difficult to quantify the amount of heat transferred as living systems are incredibly complex.

Of the many types of thermal medicine, this work focused on nondestructive, innocuous (nonpainful) tissue cooling via an external source. Meaning, the direct, intentional application of a cooling device or low temperature object to warm healthy tissue. Temperature changes due to internal or pharmacological factors (i.e. taking ibuprofen to reduce fever) was not investigated. Tissue heating was also not the focus of this work because: 1) the medical uses of heating is

already well explored in literature, 2) the technical challenges to building heating medical devices are low, and 3) the therapeutic benefits of cooling can be further optimized from its current state.

1.3 Temperature's role in sensation and perception

Temperature also plays a key role the processing of information about the environment. Without the ability to feel warmth, a person is deprived of sensory knowledge that alerts them to comfort and pain. Typical human behaviors like eating, exercising, and socializing are also affected by thermal perception. If a person who could not feel temperature tried to take a hot bath, they may accidentally burn themselves due to a lack of sensory feedback. Temperature as a stream of information informs an individual's perception and ultimately his/her behavior and health.

1.3.1 Temperature gated ion channels and sensory pathway

Temperature information is processed through nerve endings in the skin, which evoke action potentials in response to the stimulus. The nerve endings are comprised of ion channels, which are akin to biomechanical temperature sensors. Temperature changes regulate the opening and closing of ion channels, which evoke action potentials. Figure 1.1 depicts the possible ways for an ion channel to open due to temperature. These include the mechanical/conformational changes in membrane due to temperature, or production of temperature dependent channel activators that induce ion channel opening[6].

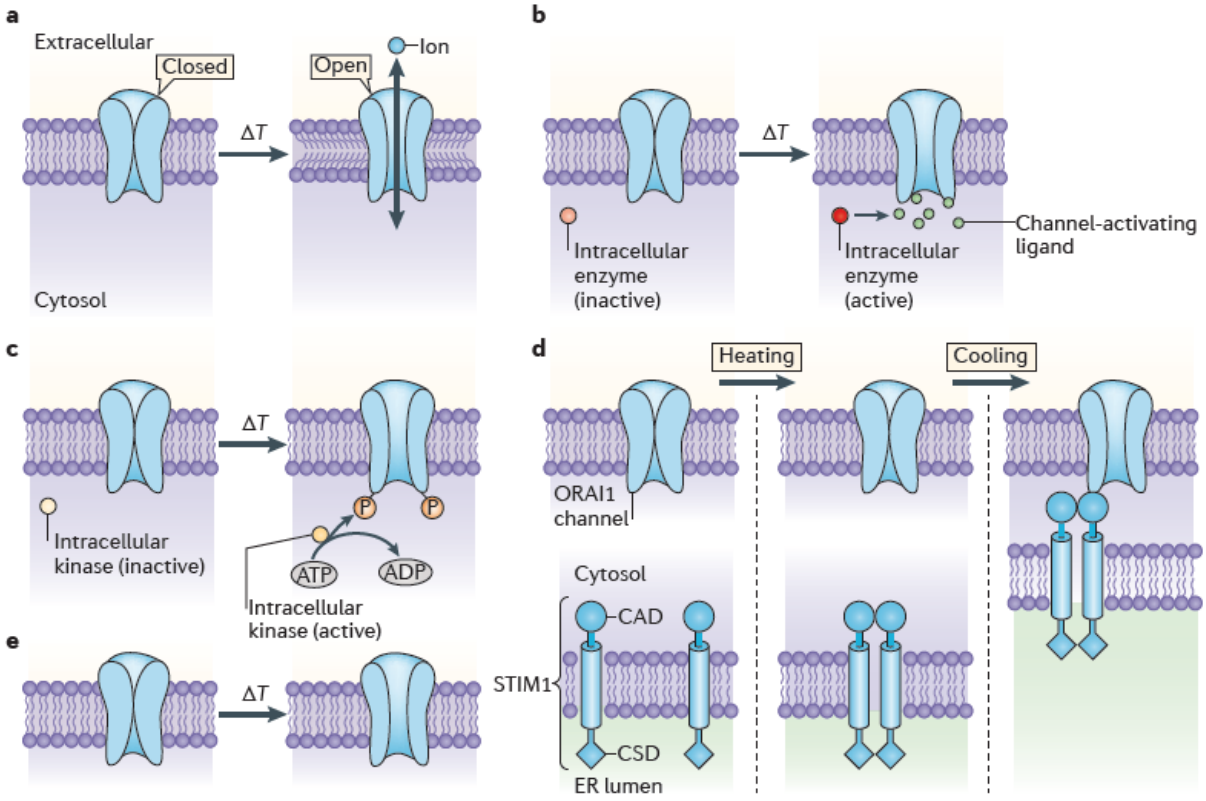

Figure 1.1 Taken from Vriens et al 2014[6]. A: Mechanosensitive channels, detects membrane properties change from dT B: Temperature dep. Production of ligands C: dT dep phosphorylation D: Ca activation E: dT leads to conformational changes in the channel complex.

Once an action potential is evoked, the signal travels down the nerves to the dorsal horn of the spine and delivered into the brain. The signals are then translated into perception (Figure 1.2). Not only thermal information transits by nervous pathways; pain, itch, and tactile sensations are initiated at corresponding receptors and delivered to the brain[7,8]. Some combination of these various sensations are perceived by the individual, but not all stimuli are felt equally. In fact it is both anecdotally and scientifically understood that certain stimuli (like cold) dull the perception of other sensations. A healthy person with regular sensory abilities could feel a loss of sensation with prolonged cold at the same site[9].

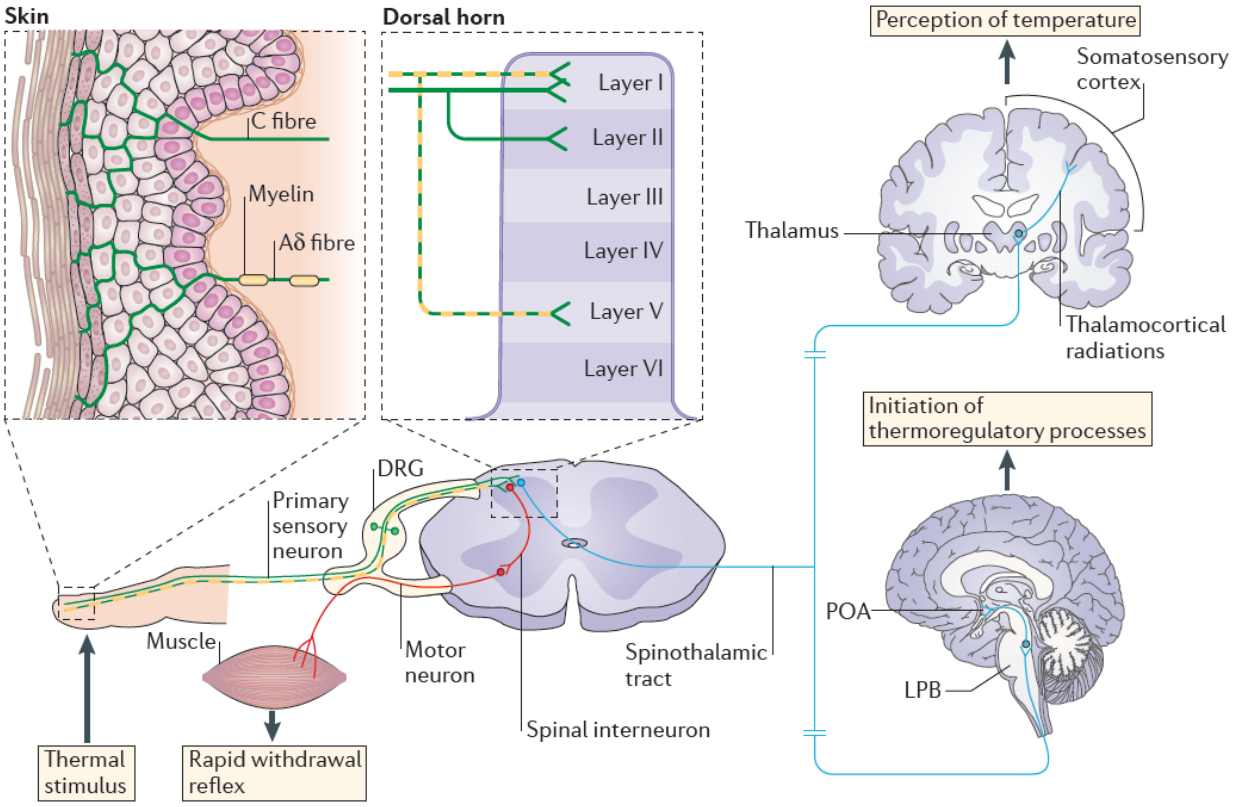

Figure 1.2 Taken from Vriens et al[6]. Neural pathway of thermosensory signals from peripheral neurons into the sensory cortex, where it is processed as perception.

1.3.2 Gate control theory and cold

The phenomenon for which prolonged innocuous cold reduces other sensation at the same location is termed the *gate control theory of pain*[10]. As previously discussed, this cold-induced numbing effect is not a novel finding (Hippocrates). However, the specific workings of how cold (and not hot) blocks painful stimuli in the spine/brain is yet unknown. It is also unclear if the driving factor is a cold temperature, or a rapid cooling rate[9]. There also exist thermomechanical confounders where pain may naturally be decreasing because lower temperatures induce a reduction in pressure (i.e. decreasing swelling with cold). The answers to these questions could help minimize pain in patients, particularly those suffering from chronic pain. Furthermore, engineering of sensation could assist patients with thermosensory disabilities and/or amputees with prosthetics.

1.4 Basics of tissue cooling and bioheat transfer

Heat transfer is the transit of thermal energy from one location to another due to a temperature difference. In the body, temperature varies with depth and location. Therefore, heat is continually moving all throughout the body, as well as to/from the environment. There are three modes of heat transfer relevant to living tissue: conduction, convection, and radiation.

In conduction, heat is transferred within the tissue medium or to another contacting solid. Conduction for tissue cooling is commonly seen with ice packs being placed on the skin, where the cold from the ice results in a heat transfer from the initially warm skin. The Pennes bioheat equation[11] (Equation 1) describes general conduction in terms of biological tissues:

Equation 1

$$\rho C_p \frac{\partial T}{\partial t} = k\nabla^2 T + C_{p,b}\omega_b(T - T_b) + q_m + q$$

where ρ, C_p, and k are the tissue density, heat capacity, and thermal conductivity, respectively. ω_b is the effective blood perfusion parameter, $C_{p,b}$ is the blood heat capacity, T is the local tissue temperature, T_b is the blood temperature, $\mathrm{q_m}$ is the metabolic heat generation rate of the tissue, q is the external heat being applied, and t is time. This equation applies throughout this work where the tissue cooling is applied via physical contact with a cooling device.

Convection occurs at a fluid to solid heat transfer boundary that is at different temperatures. In the context of cooling for thermal medicine, external convection is often utilized with ice baths and fans to reduce fevers in patients. Internally, convection is constantly occurring via the cardiovascular system, through which flowing blood delivers (or saps) heat to surrounding tissue. Newton's law of cooling (Equation 2) describes the one-dimensional convection that occurs at a fluid-solid boundary:

Equation 2

$$q'' = h(T_s - T_\infty)$$

where q'' is the heat flux (W/m^2), h is the heat transfer coefficient (W/m^2/K), and T_s and T_∞ are the surface temperature and fluid temperature respectively (K). This mode of convection exploiting the cardiovascular system is employed in this work to deliver cooling to select regions of the body. Note how convection is dependent on fluid flow (innately described within *h*), which is quadratic with the radius of the vessel. However, the heat transfer is linear with a temperature difference. Thus for thermal medicine, a limit likely exists where surface cooling/heating is constrained to temperature levels that avoids thermal damage, but the tissue/blood temperature is not cooled to desired levels because of blood vessel thickness.

Thermal radiation is the emission or absorption of energy from the environment via electromagnetic waves. The waves are present in all surfaces that have a finite temperature. Equation 3 describes the heat flux from radiation as a difference between the energies gained from emission versus absorption.

Equation 3

$$q'' = \varepsilon\sigma(T_s^4 - T_{sur}^4)$$

Here ε, σ are the emissivity, and the Boltzmann constant ($\sigma = 5.67\times10^{-8}$ W/m^2/K^4) respectively, and T_s and T_{sur} are the temperature of the surface and surroundings respectively. In thermal medicine, radiation is commonly utilized in the form of laser ablation. Radiative therapies tend to work via heating tissue, so excessive thermal damage is a particular concern for such treatments. As this work focuses on cold thermal therapies, and all experiments were performed indoors, radiation was not considered to be a factor in our studies.

1.5 Animal models and their limitations

Animal models are invaluable for testing preclinical treatments and devices for efficacy and safety without risk to human patients. Two animal species were used in this work, rodents (Sprague Dawley rats) and non-human primates (Rhesus Macaque monkeys).

1.5.1 Rodent models

Rodents were used in this work for studying hypothermia. As furred mammals, rats possess similar biology to humans, but are smaller and thus more sensitive to external heat sources. Therefore rats are suitable for heat transfer studies with experimental thermal devices. In addition, rats allow researchers to conduct experiments in a highly controlled manner, are relatively inexpensive (in both cost and space), and are readily manipulated with surgical interventions, anesthesia, and behavioral tests. Finally, rats also give researchers the ability to create transgenics, although this particular feature was not utilized in this work.

Rat models still pose limits to their ability to mimic human responses. Despite biological similarities, key differences remain in heat transfer conditions (i.e. cardiovascular system, surface boundary conditions, shape and size of organs). Their sensitivity to external heat can also be a complicating factor when attempting to only cool portions of the body or estimate the effectiveness of the thermal device.

1.5.2 Non-human primates

In this work, non-human primate models were used to test cold sensation on the skin. Monkeys are genetically and physically similar to humans, and are currently used as a standard model for brain-to-machine interface experiments. Monkeys are also allometrically similar to humans, meaning heat transfer on the skin will follow a similar temperature profile. They can

also be trained to perform tasks specific to the experiment. Much like rats, monkeys allow the researcher greater control in designing experiments and can be surgically implemented with electrodes for data collection.

On the other hand, monkeys are limited as models for several reasons. Monkeys are pricier than smaller animals like rodents, and can be expensive to maintain. Their size also makes them difficult to handle and perform surgery. The monkey's genetic similarity to humans is both an advantage and disadvantage-- while they are genetically good models, there is a higher risk of disease transmission to the researcher (i.e. tuberculosis, hepatitis, measles). Monkeys are also quite intelligent and (for studies without tranquilizers) can anticipate experimental steps, such as periodic delivery of cold on skin. This removes the element of surprise from the experiment and can affect neural responses.

1.6 Thesis Structure

This thesis describes the medical applications of thermoelectric cooling. Thermoelectric coolers are not only precisely controllable but rapid and can be maintained for long periods of time. Being electrically controlled makes TECs highly responsive and stackable (connect several elements in parallel) for concentrated cooling power. TECs can also be biased to heat and cool flexibly as the experiment demands, and can quantify the amount of cooling/heating power that is being applied. These factors make TECs highly desirable for tissue cooling studies that were previously hampered by low cooling power and imprecise methods. We hypothesized that precisely delivered cold could be used to optimize tissue cooling and inform existing knowledge on hypothermia and cold sensation. Here, we describe a new approach to delivering cooling on select portions of the body for multiple therapeutic purposes, keeping in mind weight, sex, and safety. The chapters henceforth are organized as follows. Ch. 2 introduces a novel device for

thermoelectric extravascular blood cooling in living systems. Ch. 3 demonstrates selective brain cooling in live rats by circulation of chilled blood flow. Ch. 4 describes a computational model of the human carotid artery for understanding cooling of human vessels. Ch. 5 investigates the cooling of a local area on the skin for numbing and pain relief. Ch. 6 is the summary and future work.

1.7 References

1. Nagao K, Nitobe E, Okamoto K, Miki T, Hayashi N. Advanced Challenge in Resuscitative Hypothermia in Patients with Cardiac Arrest on Arrival at the Emergency Room. In: *Hypothermia for Acute Brain Damage*. Springer, Tokyo; 2004:308-314. doi:10.1007/978-4-431-53961-2_50

2. Castillo J, Dávalos A, Marrugat J, Noya M. Timing for Fever-Related Brain Damage in Acute Ischemic Stroke. *Stroke*. 1998;29(12):2455-2460. doi:10.1161/01.STR.29.12.2455

3. Shibasaki M, Okazaki K, Inoue Y. Aging and thermoregulation. *J Phys Fit Sport Med*. 2013;2(1):37-47. doi:10.7600/jpfsm.2.37

4. Oudin Åström D, Bertil F, Joacim R. Heat wave impact on morbidity and mortality in the elderly population: A review of recent studies. *Maturitas*. 2011;69(2):99-105. doi:10.1016/J.MATURITAS.2011.03.008

5. Hippocrates. De vetere medicina. 460-375 BC.

6. Vriens J, Nilius B, Voets T. Peripheral thermosensation in mammals. *Nat Rev Neurosci*. 2014;15(9):573-589. doi:10.1038/nrn3784

7. Campero M, Serra J, Bostock H, Ochoa JL. Slowly conducting afferents activated by innocuous low temperature in human skin. 2001;535. http://doi.wiley.com/10.1111/j.1469-7793.2001.t01-1-00855.x. Accessed January 26, 2018.

8. Bini G, Cruccu G, Hagbarth KE, Schady W, Torebjörk E. Analgesic effect of vibration and cooling on pain induced by intraneural electrical stimulation. *Pain*. 1984;18(3):239-248. doi:10.1016/0304-3959(84)90819-4

9. Yarnitsky D, Ochoa JL. Studies of heat pain sensation in man: perception thresholds, rate of stimulus rise and reaction time. *Pain*. 1990;40(1):85-91. doi:10.1016/0304-3959(90)91055-N

10. Melzack R. Gate control theory: On the evolution of pain concepts. *Pain Forum*.

1996;5(2):128-138. doi:10.1016/S1082-3174(96)80050-X

11. Pennes HH. *Analysis of Tissue and Arterial Blood Temperatures in the Resting Human Forearm*. *J Appl Physiol*. 1948;1(2):93-122. doi:10.1152/jappl.1948.1.2.93

Chapter 2 Solid-state Temperature Control of In Vivo Blood Flow

2.1 Abstract

Background: Thermal therapies have strong potential for improving outcomes for patients suffering from cardiac arrest, neonatal hypoxic-ischemic encephalopathy, or medically refractory intracranial hypertension. We propose a novel tool to manipulate blood temperature through extravascular thermoelectric heat exchange of blood vessel walls and flowing blood.

Methods: This tool is a concentrated cooling probe with several thermoelectric elements combined to focus cooling at the application site. Using this tool, we aim to achieve desired levels of temperature control and potentially reduce complications associated with traditional intravascular or systemic thermal therapies. Leveraging the feedback control, speed, and reversible operation of thermoelectric cooling modules, the device can adapt to cool or heat as desired.

Results: Pre-clinical testing on rodent models confirmed rapid, significant reduction of intravenous jugular blood temperature when a prototype device was brought in contact with the left carotid artery (change in blood temperature of -4.74 ± 2.9 ˚C/hr and -4.29 ± 1.64 ˚C/hr for 0 ˚C and -5 ˚C cooling trials respectively). Declines in rectal temperature were also noted, but at lesser magnitudes than for jugular blood (0 ˚C: -3.09 ± 1.29 ˚C/hr; -5 ˚C: -2.04 ± 1.08), indicating proof-of-concept of thermoelectric extravascular blood cooling within a relatively localized region of the body.

Conclusion: With further improvements in the technique, there is potential for selective organ cooling via reduction in flowing blood temperature.

2.2 Introduction

Body homeostasis represents a physical and chemical equilibrium that allows optimal cellular, tissue, organ and system functioning. Thus maintaining a healthy body temperature (normothermia) is key to normal function and activity. Neonates[1], the obese[2], the elderly[3], and anesthetized patients[4] are especially susceptible to disbalance and subsequent injury from extreme thermal states due to their reduced ability to thermoregulate. Clinically, various tactics are used to reach and maintain normothermia, including the use of anti-inflammatory medications (e.g. NSAIDs) and external means such as cooling blankets[5], ice baths, ice vests, and cooling helmets[6]. Conversely, intentional heating or cooling away from normothermia can be harnessed for therapeutic applications such as: icing for local pain relief, thermal ablation of tumors [7], therapeutic hypothermia for mitigating hypoxic-ischemic encephalopathy[8], and neuroprotection in traumatic brain injury[9].

For inducing therapeutic hypothermia or helping patients maintain normothermia, methods that perform heat exchange with blood can be quite effective, as the cardiovascular system is pervasive and pumps blood in all regions of the body. This is advantageous over commonly used ice baths or cooling helmets, as the heat exchange is not through multiple layers of skin or bone which have very low thermal conductivities[10]. Existing techniques for thermal therapy via blood temperature control are primarily endovascular (intravascular). Endovascular techniques use needles to puncture and thread into a major blood vessel (e.g., femoral artery) to deliver cold therapy by routes such as: 1) cold saline infusion[11], 2) catheter-based heat exchange[12], 3) extracorporeal cooling[13–15], or 4) intra-arterial cold fluid balloons[16]. Such methods can achieve rapid cooling of the treatment site (e.g., reported brain temperature drop from 38.0 ˚C to 33.0 ˚C in 41 ± 17 minutes for extracorporeal cooling and 126 ± 37 minutes for

endovascular cooling[14]), but can also cause whole-body (systemic) hypothermia, which is associated with complications such as cardiac suppression[13,17] , coagulopathy[18], catheter-based thrombosis[19], and pneumonia [20]. Furthermore, endovascular techniques are often constrained in the duration they can be applied (for instance, cold-saline infusions pose a risk of blood thinning with prolonged treatment) and may lead to infection and vessel trauma. Lastly, systemic interventions by nature affect the whole body and therefore are unable to selectively cool deep tissues, vessels, or organs for targeted therapy.

While less explored than endovascular cooling systems, extravascular modes (affecting the surface of a vasculature without penetrating; extraluminal) obviate the risks that follow intravascular access and subsequent introduction of substances into the body. In extravascular techniques, sections of vessel walls are chilled in order to cool the blood flowing within. For example, a major artery supplying blood to an organ could be cooled while the venous return is warmed, thereby cooling the organ while maintaining core temperature. As a result, extravascular techniques potentially allow longer application than endovascular tactics and may be more suited for delivering selective cooling therapy while avoiding the deleterious effects of systemic hypothermia. Benefits of organ-specific or region-specific cold therapy include alleviating inflammation, reducing metabolic loads[21], and combating heat stresses from laser ablation or fevers [22].

Current extravascular blood cooling methods tend to utilize cold water loops as the primary mode of cooling. An experimental approach that circulates cold water through handmade loops wrapped around the common carotid artery (CCA) of a rat reported moderate selective cooling of the brain (brain temperature lowered by 2–5°C from baseline when cooling for 20 mins)[23]. Such approaches that circulate cold water, while effective, are not finely

controllable in terms of response time, temperature range, or ease of application. In general, water loops are difficult to heat/cool for rapid adjustment (within seconds) of temperature owing to the system's high thermal inertia; furthermore, such techniques are limited to a minimum applied temperature of 0˚C.

We propose to enhance extravascular cooling methods by using thermoelectric coolers (TEC) as the cooling element. TECs are ideal for rapid, precise temperature control and are readily suited for feedback-controlled heat exchange, enabling a responsive system that requires just seconds to reach a target temperature. Miniaturized TEC modules (mm- or cm-scale) possess significant cooling power despite their small size, and have previously been utilized for a handheld cooling device for local anesthesia of the eye[24]. Further adding to the suitability of TECs for blood cooling, recent advancements in TECs include organic, flexible[25], biocompatible, conformable[26], and thin-film devices[27]. These state-of-the-art modules may serve a role in advanced blood temperature control techniques.

In this work, we present a feedback-controlled, concentrated thermoelectric probe suitable for extravascular thermoelectric control of blood temperature and characterize its performance in cooling the CCA in rodents. This work is the first known to utilize a thermoelectric approach for extravascular blood temperature control, and is the first to utilize a concentrated thermoelectric tool for thermal management within the body.

2.3 Methods

2.3.1 System Description

A thermoelectric cooling probe was custom fabricated and composed of twelve TEC elements (6.6 x 6.6 mm^2 surface area, Custom Thermoelectrics LLC, Bishopville, MD) thermally mated to a central cooling bar (Figure 2.1). This configuration allows the TECs to achieve a good

(flat) thermal contact with the bar, concentrating the cooling power of several units at the applicator tip. The tip is placed on the target tissue for contact-based cooling, and its shape can be designed to best conform to the surface geometry of the target tissue. In addition to enabling cooling concentration, mating the TECs to a central bar rather than contacting one or more of them to the tissue itself lowers the risks of electrical shorts and tissue exposure to the toxic components of commonly-used TECs. The TECs are stacked in parallel, both electrically and thermally, to provide equal voltage and current to each module and ensure approximately equal cooling power per unit. This improves the usability and reliability of the system as the controller can simply vary the total current to control cooling levels, and a single failing TEC will not impact the electrical power supplied to the remaining elements. The TECs can be precisely controlled (± 0.01 ˚C) using a PID feedback loop (Meerstetter Engineering, Rubigen, Switzerland), and can provide total cooling power directly proportional to the number of elements employed (Figure 2.2). With this concentrated approach, significantly greater cooling power is reached compared to prior biomedical thermoelectric cooling methods (e.g., for pain research) that employed a single TEC element[28]. While this technology provides intense localized cooling, it is not intended to freeze tissue or blood, as freezing may have harmful consequences on the vasculature and blood cells along with undesirable changes in hemodynamics.

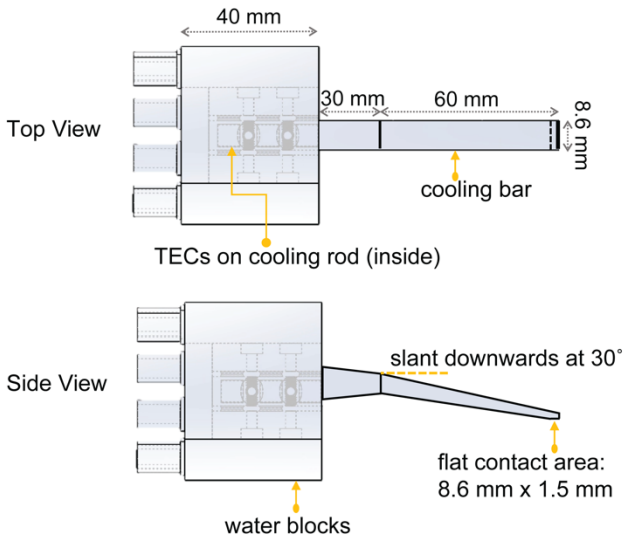

Figure 2.1 Rendering of a prototype cooling probe. The cooling bar has TECs layered inside to concentrate their cooling power onto the center bar. Tip dimensions that contact with blood vessel: 8.6 x 1.5 mm^2 (L x W). Not shown in image are thermal insulation around the cooling bar to reduce environmental heat leakage.

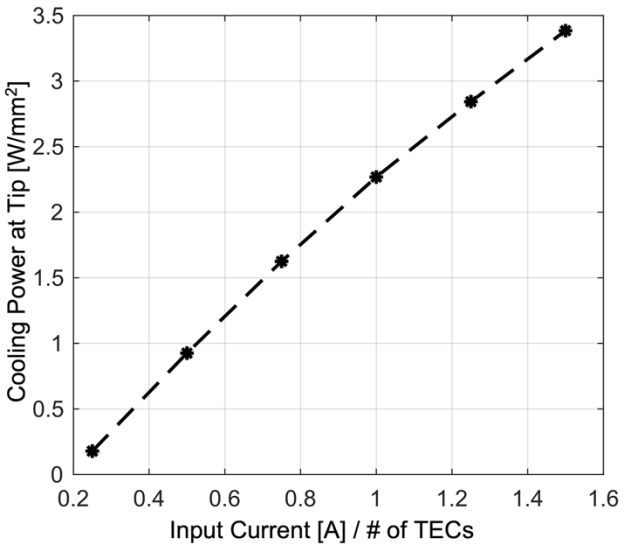

Figure 2.2 Theoretical heat flux of the probe tip with all 12 TECs engaged, the cooling power of which is concentrated into the 8.6 x 1.5 mm^2 flat tip area.

The current prototype has a temperature range of -10 to 50 ˚C, which may be expanded in future iterations of the device to suit specific applications. The number of TECs was chosen to be consistent with the number used in a probe developed previously to cool the surface of the eye, which had similar temperature characteristics [24]. The present design is an elongated, angled

cooling bar with a flat tip that can reach inside an incision and be placed along the exposed length of a CCA (tip contact area: 8.6 x 1.5 mm^2). Rodent CCAs were experimentally observed to be about 1 mm in diameter and could be surgically exposed up to a centimeter in length, guiding our choice of tip dimensions. Although a flat tip was used here for proof-of-concept of thermoelectric extravascular blood cooling, the tip can be customized to meet the heat transfer needs of a particular application, such as a clamp style end for maximum contact surface area and minimum thermal contact resistance. Except for the tip, the rest of the cooling bar is insulated and does not cool surrounding tissue. The current system utilizes a single probe for cooling only, but can be expanded to integrate multiple probes, each capable of independently cooling or heating different blood vessels in the body (Figure 2.3).

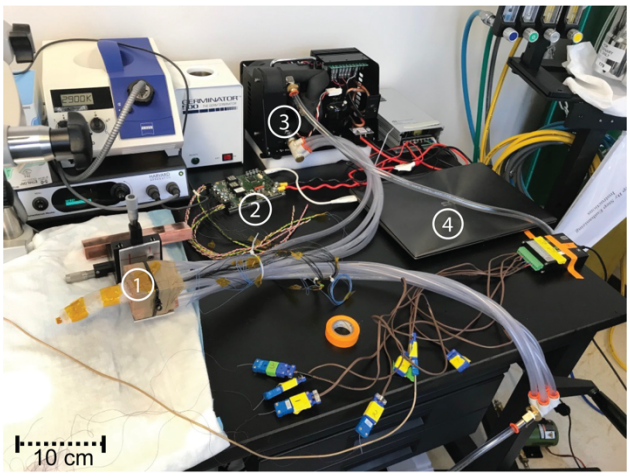

Figure 2.3 System prototype. From left to right: (1) probe with the cooling bar wrapped in thermal insulation, revealing only the tip, (2) electrical controller, (3) water chillers for TEC waste heat, (4) laptop for data collection and system control.

The performance of the current setup is as follows. At a tip temperature of 0 ˚C the maximum voltage and current supplied to each TEC are approximately 1.7 V and 1.17 A, corresponding to a probe input power of 23.9 W. At this bias point, each TEC removes approximately 2.7 W of heat, summing to a total of 32.4 W of heat removed. The coefficient of

performance (COP) at this bias point is then: 2.7 W/(1.7 x 1.17 W) = 1.28. Since the TECs are stacked in parallel, this is also the COP for the probe itself. This heat removal includes some parasitic losses from regions of the cooling bar other than the tip, although insulation was used to minimize these losses (Figure 2.3). When not in contact with tissue, the cooling probe is capable of ramping to a target temperature of 0 ˚C from an initial temperature of 20 ˚C in approximately 30 seconds. When the probe is at 20 ˚C, brought into contact with tissue, and then activated, it can reach 0 ˚C in less than 3 minutes. Once at target levels, the probe can maintain that temperature indefinitely. These ramping times were limited by the particular control system used and the maximum total current we allowed to be supplied to the probe (16 A); shorter times are achievable with different control systems or larger currents. However, we did not explore this regime of operation because the times given above are already less than the timescales of clinical relevance (e.g., the standard of care for hypothermia therapy in cardiac arrest patients is to begin treatment within the first few hours and continue the treatment for ~24 hours[29]). In this work, once anesthetized animals had their carotid and jugular vessels surgically exposed, the probe was first set to a target temperature before the tip was directed onto the CCA (Figure 2.4).

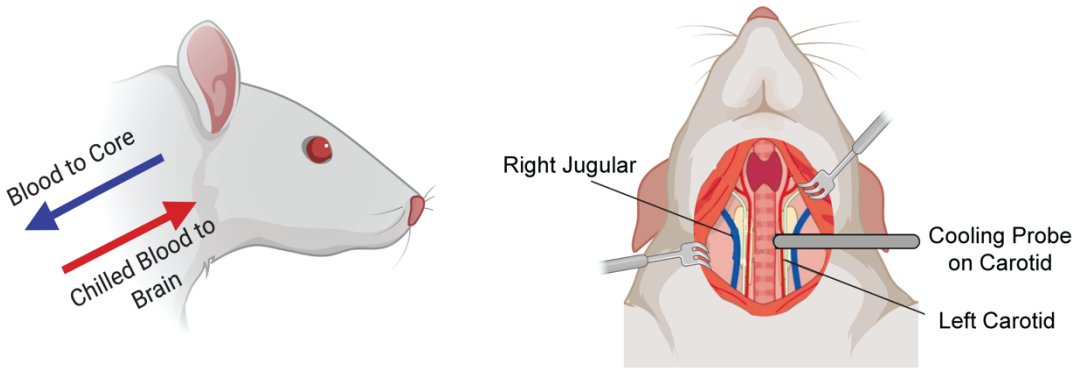

Figure 2.4 (Left) Blood temperature control concept. (Right) surgical schematic showing probe placement. Images created with BioRender.com. Adapted from icons "Rat (lateral)" and "Rat (supine, curved tail)", by BioRender.com (2021).

2.3.2 Surgical Methods

The University of Michigan is an Association for Accreditation of Laboratory Animal Care (AAALAC) accredited facility, and this research protocol was approved by the University of Michigan's Institutional Animal Care and Use Committee (IACUC). Healthy adult Sprague Dawley rats (Charles River Labs, Wilmington, MA) of both sexes were used to develop surgical techniques and to verify system efficacy (n = 10). The number of animals was selected based on prior experimentation with rodent models for which ≥ 5 animals were sufficient to collect temperature data at various locations in the body [30]. Animals were housed in controlled temperature (22 °C ± 2 °C) and humidity (~27%) vivaria.

Rats were anesthetized using 5% isoflurane at induction and maintained at 1-2.5% isoflurane in 1 L/min O_2 carrier gas[31]. The animal was placed supine atop a constant temperature heating pad set at 35-37˚C (Zoo Med Laboratories, San Luis Obispo, CA) in an attempt to maintain normothermic core temperature levels. Fur was removed in the upper chest for preparation of surgery. Several temperature probes were placed at multiple locations in the animal. Core temperature was monitored using a rectal temperature probe (time constant: 0.3 s; accuracy: +/- 0.1 ˚C; Harvard Apparatus, Cambridge, MA). Flexible thin thermocouples (time constant: 0.005 s; accuracy: +/- 0.1 ˚C; Physitemp Instruments LLC, Clifton, NJ) were implanted in the right external jugular vein (RJV) and placed on the surface of the contralateral left common carotid artery (LCA) through surgical exposure (Figure 2.4). Temperature data collection and monitoring were performed using a separate data logging system and software (Accsense, Chesterland, OH). The thermocouple time constants and data sampling interval (5 seconds) were small compared to both our experimental durations of 15-30 mins as well as the standard of care for potential applications (e.g., hypothermia treatment in cardiac arrest patients

lasts ~24 hours or more[29]). Therefore the thermocouples and data sampling interval were deemed suitable for the purposes of our study.

Following anesthesia and rectal probe placement, an incision was made midline/lateral over the cervical spine curvature, and blunt dissection was used to isolate the LCA and RJV from surrounding tissue. The severed tip of a 23-gauge needle was used to puncture the jugular, and was fixed in place with tissue glue (the placement of the needle did not occlude the vessel lumen from allowing continuous blood flow). Through the needle, a flexible thermocouple was guided into the RJV to record intravenous blood temperature[32]. This is in contrast to attaching thermocouples onto the vessel with tissue glue, which would give point measurements of the vessel wall and surrounding tissue, but not of the blood itself [33]. For reproducibility, the carotid thermocouple was placed on the LCA surface underneath the vessel opposite the probe rather than intravascularly due to the carotid being much more difficult to puncture without causing excessive bleeding.

Following the surgical interventions described above, the probe cooling tip was placed directly atop and in line with the exposed LCA (Figure 2.5). The following experiments were performed: a baseline (measurements with a deactivated probe atop the LCA), and two test temperatures of 0 and -5 ˚C. All trials were maintained for a minimum of 15 minutes, up to 30 minutes. Animals were used to test multiple trials (ex: baseline, followed by a cooling trial) for conservation of animals as well as experimental convenience. Total time under anesthesia from induction to conclusion of data collection was < 2.5 hours per animal.

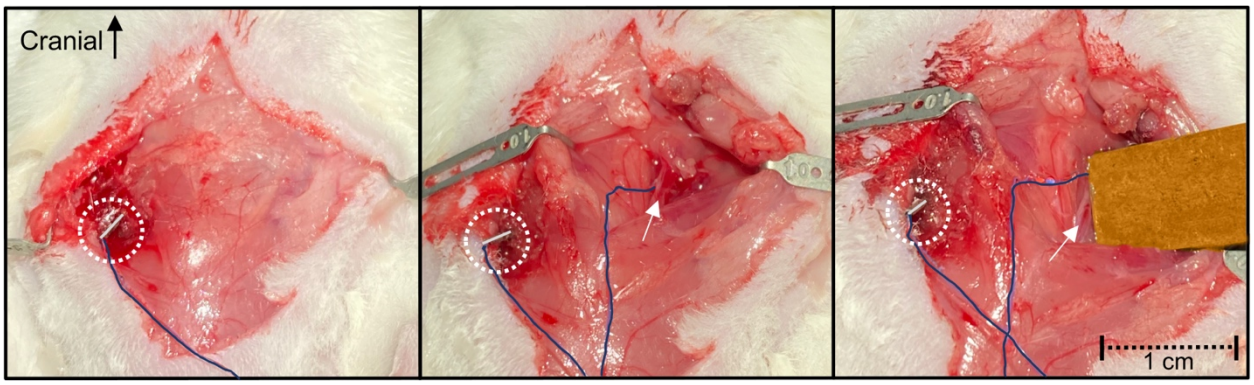

Figure 2.5 (Left) Exposed RJV with thermocouple inserted into the vessel via a needle tip, shown inside dashed circles. (Middle) thermocouple placed on the LCA. White arrows point to the LCA. (Right) Probe applicator being placed atop the LCA for an experiment. Upon final placement, the probe tip (8.6 mm x 1.5 mm) is parallel and sitting flush on the LCA.

2.3.3 Data processing and statistics

Data was collected using SiteVIEW (Accsense, Chesterland, OH) for rodent bodily measurements (1 sample/5 sec) and the TEC Service Software (Meerstetter Engineering, Rubigen, Switzerland) for probe measurements (1 sample/sec). Data analysis was performed using MATLAB (MathWorks, Portola Valley, CA) and in-house Python scripts. All data were smoothed using a moving average window of 30 seconds. Results are presented as mean ± standard deviation. A p-value of ≤ 0.05 was considered significant.

2.4 Results and Discussion

2.4.1 Device effect on RJV, LCA and rectal temperature

Use of the probe clearly achieved a lower RJV blood temperature than baseline and effectively chilled the LCA surface (Figure 2.6). While the probe tip is primed to -5 or 0 ˚C, the LCA surface remains between 10 to 20 ˚C. No obvious contact injury or physiological deformation was observed from our experiments. As every animal presented at unique temperature points at the start of each trial, we compared each animal's response to active cooling compared to its own baseline, and calculated the rate of blood cooling.

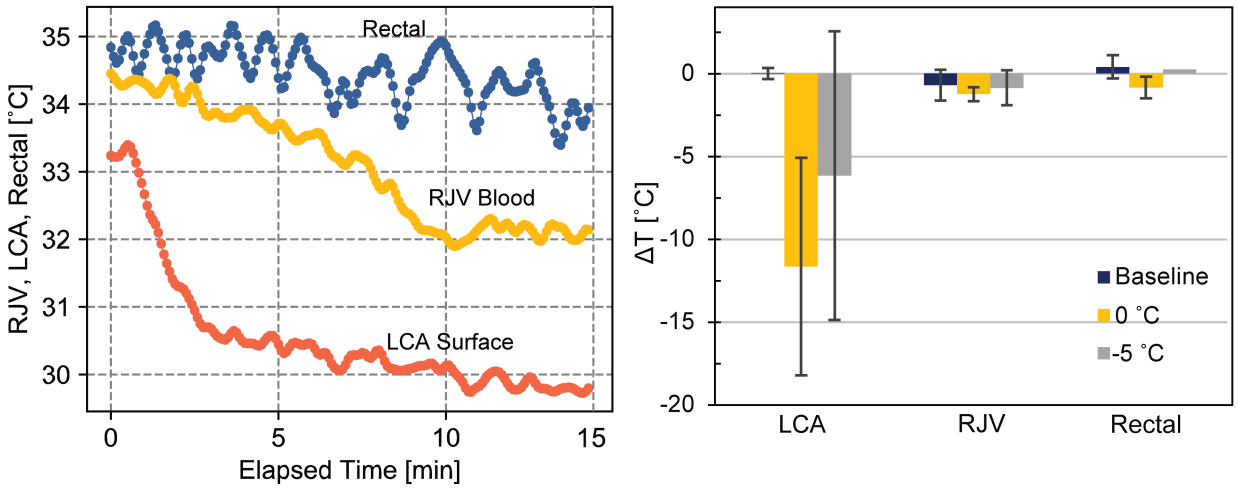

Figure 2.6 (Left) Sample temperature data taken for a 0 ˚C trial is shown for the first 15 minutes. LCA surface temperature drops rapidly, while intravenous blood and rectal temperatures fall gradually but at distinct rates. (Right) Average temperature changes after the first 15 minutes for all available data. Bars are in order of baseline, 0 ˚C, and -5 ˚C from left to right.

To determine the effects of the cooling probe on blood and core temperature, mean cooling rates were compared using a one-way ANOVA. RJV blood temperature in all test rats dropped with active cooling with the probe as compared to baseline levels (baseline vs 0 ˚C: $p = 0.035$; baseline vs -5 ˚C: $p = 0.021$). Baseline trials always preceded cooling trials, and on average caused little change to either blood or rectal temperature (Table 2.1). By comparison, blood cooled rapidly when the probe was powered on (for 0 ˚C trials, a mean 4.7 ˚C/hr decrease in RJV blood temperature; similar rates were found for -5 ˚C). Considering we have only cooled one of the CCAs, approximating 50% of blood volume in the brain, this level of cooling is a satisfactory outcome for validating and characterizing our methods. RJV blood cooling rates at the two temperature points (0 ˚C vs -5 ˚C) were not found to be significantly different ($p = 0.333$). On average, cooling trials did result in a decrease in rectal temperature, but at a lower magnitude than the rate of cooling for RJV blood. This indicates that the cooling of the blood flowing through the rat's brain is not driven by general heat loss in its whole body. Despite the

fluctuations in rectal temperatures during probe cooling, the rectal cooling rates at baseline and at active cooling were not found to be significantly different ($p = 0.22$ and 0.24 for 0 and -5 ˚C respectively). Rectal temperature also tended to stay above RJV blood temperature during experiments (Figure 2.6). Minor shifts in core temperature can likely be mitigated with the use of additional heating pads or a contralateral heating probe. Counterintuitively, the mean drop in RJV blood and rectal temperature was slightly less in the -5 ˚C trials than the 0 ˚C trials, likely due to the fact that the -5 ˚C trials were performed following the 0 ˚C trials for reasons of animal conservation. As such, for -5 ˚C trials, the animal's body was already chilled, and spent a longer period under anesthesia. All values in each set of compared groups were selected from the same set of animals.

Table 2.1 Mean values of cooling rates calculated for the total lengths of each trial, ranging 15-30 mins. Values are calculated from the linear regression slopes of the time series data (per trial), which were initially smoothed in a 30 second window moving average.

Trial	**RJV Blood ΔT/Δt [˚C/hr]**	**Rectal ΔT/Δt [˚C/hr]**
Baseline	0.22 ± 1.21	-0.50 ± 1.68
0 ˚C	-4.74 ± 2.90	-3.09 ± 1.29
-5 ˚C	-4.29 ± 1.64	-2.04 ± 1.08

Comparing individual rats' baselines against their cooling trials showed that cooling of the intravenous blood could be observed within the first 15 mins, while at baseline the blood temperature tended to remain relatively unchanged (Figure 2.7). From 15-30 mins, blood continued to cool and no lower limit was observed within that time.

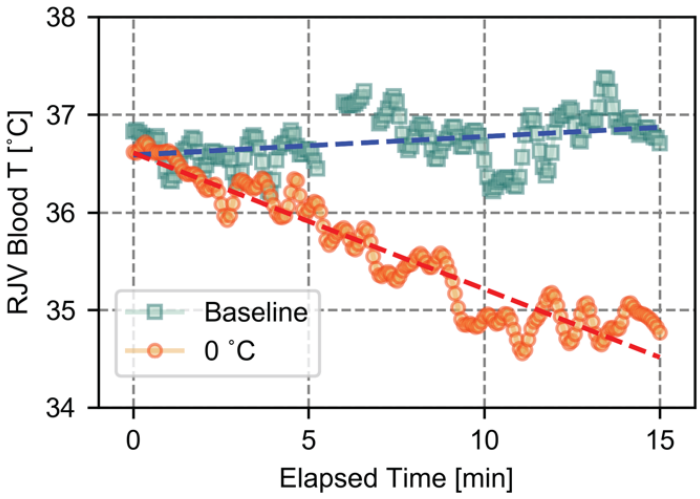

Figure 2.7 Comparing an animal's RJV blood temperature levels at baseline versus with active cooling. Data shown is from a representative animal, for the first 15 minutes of the trial. Dashed lines indicate linear regression trendlines. Baseline (blue): $p < 0.001$ and $R^2 = 0.112$. 0 ˚C (red): $p < 0.001$ and $R^2 = 0.896$.

2.4.2 Limitations

Generally, the baseline trials resulted in a slight dip in core temperature (-0.50 ± 1.68) despite the use of a heating pad. This is an unsurprising result as isoflurane has been reported to suppress shivering in anesthetized rats [34]; the decrease in temperature is most likely a combined effect from the isoflurane as well as reduced movement. Due to heat capacities associated with the blood and blood vessel walls, there is a thermal lag following initial application of the cooling probe (at time $t = 0$ in Figure 2.6) before the temperature of the carotid surface (measured on the underside of the vessel opposite the probe location) begins to decline. The precise delay from $t = 0$ to the initial reduction in temperature varied from experiment to experiment because the probe was occasionally adjusted slightly in the first several seconds to gain better contact with the vessel; regardless, we can generally say that the measured carotid surface temperature begins to decline less than a minute after probe contact. We note that this lag is significantly shorter than the timescales of clinical relevance discussed above, as is the

expected lag associated with applying the cooling probe to human blood vessels. We found the thermal lag associated with cooling of the jugular blood to be less well defined, as the temperature declines more gradually and is more oscillatory (such oscillations being natural and expected with bodily temperature measurements). However, we estimate it to be less than two minutes on average.

The contralateral jugular blood temperature recorded in this study does not necessarily capture temperature for the blood that flows in all regions of the head and neck. In our work, we assume that substantial mixing of blood occurs within the head (via the Circle of Willis [35]) before it exits through the contralateral vein. In actuality, there may be blood in remote regions of the head that require much greater than 15-30 mins to chill. A point measurement of the jugular blood is made assuming that there is radial uniformity in blood temperature within the jugular based on its small size and pulsatility. Experimentally, during insertion of the jugular thermocouple we observed relative uniformity in temperature. As this study only cooled a single CCA, it is possible to scale the total cooling power by cooling both arteries alongside improving on the technical capabilities of the probe. Animals used in the study were diverse in sex and weight, all elements of variance in the cardiovascular system. In future work, narrowly controlling weight ranges for animals will provide more precise thermal requirements for desired cooling outcomes.

Blood temperature control using an extravascular thermoelectric probe is a novel technique in the field of *in vivo* thermal therapies. While the effectiveness of direct contact cooling has been shown in this study, it also draws attention to the importance of probe tip design. In our trials, the flat blunt tip of the probe (Figure 2.1Figure 2.5) was designed to be laid in line with the rat's LCA, and it did not cause visible damage to the vasculature or surrounding

tissues. However, there may still be microscopic alterations to the LCA or the blood from the prolonged thermal stimuli and/or pressure from the probe. As this technique is still in its infancy, the limitations of the approach (e.g. maximum duration, tip material, pressure, etc.) for survival studies are yet to be fully determined. Understanding and improving on these limits are required to ensure the safety of our methods.

Despite our success in blood cooling with rodents, further analysis and device advancements are required to assess clinical relevancy in humans. Rats and humans differ in their brain-to-body proportions and hemodynamics (e.g. heartrate, blood volume, flow rate) which drives heat transfer in the body. In addition, rats are covered with fur, which affects heat transfer from the core to the environment. Allometric scaling and modeling, along with transition of the study to a larger scale model, are required for more accurate estimation of the efficacy of our methods in clinical settings.

2.4.3 Applications

The present thermoelectric cooling probe has several potential biomedical applications. The probe can be utilized for surface thermal therapies such as cooling for swelling and pain relief[24]. Provided that the blood temperature control demonstrated in this study can also be utilized for subsequent tissue temperature control (via convective heat exchange from cold blood circulation), brain cooling via chilling of the carotid may be feasible. There are numerous clinical benefits to brain cooling, such as mitigating neuronal damage from cardiac arrest[29], neonatal hypoxic-ischemic encephalopathy[36], or medically refractory intracranial hypertension[37].

Beyond the brain, this technology may be applied to cool other organs by cooling (and if required, downstream heating) their major vasculatures. Perhaps equally valuable is the probe's potential utility for the experimental validation of thermal coefficients in deep tissue (muscles,

vessels, lipids, nerves, organs) *in vivo* or in resected tissue. Tissue thermal coefficients (e.g., thermal conductivity) are often presented as constants, when they may be more accurately represented as temperature-dependent relations. This is especially likely as temperature affects core vasculature and blood perfusion in living systems[30]. Perfusion/reperfusion studies utilizing *in vivo* versus *ex vivo* systems could also provide valuable knowledge for transplant medicine and stroke. Lastly, current knowledge of the effects on temperature on metabolic rates are based on biochemical models from *ex vivo* systems (organ perfusion culture systems)[38]. The optimal cold temperature for cell viability while minimizing oxidative stress may be explored for *in vivo* systems and inform biochemical models. The cooling probe prototype presented in this paper is but one possible method of accomplishing selective hypothermia with blood temperature control; various embodiments, at varying levels of invasiveness and for different clinical indications are envisioned (Figure 2.8). Depending on the form and limitations of such embodiments, additional clinical and academic applications may be suggested.

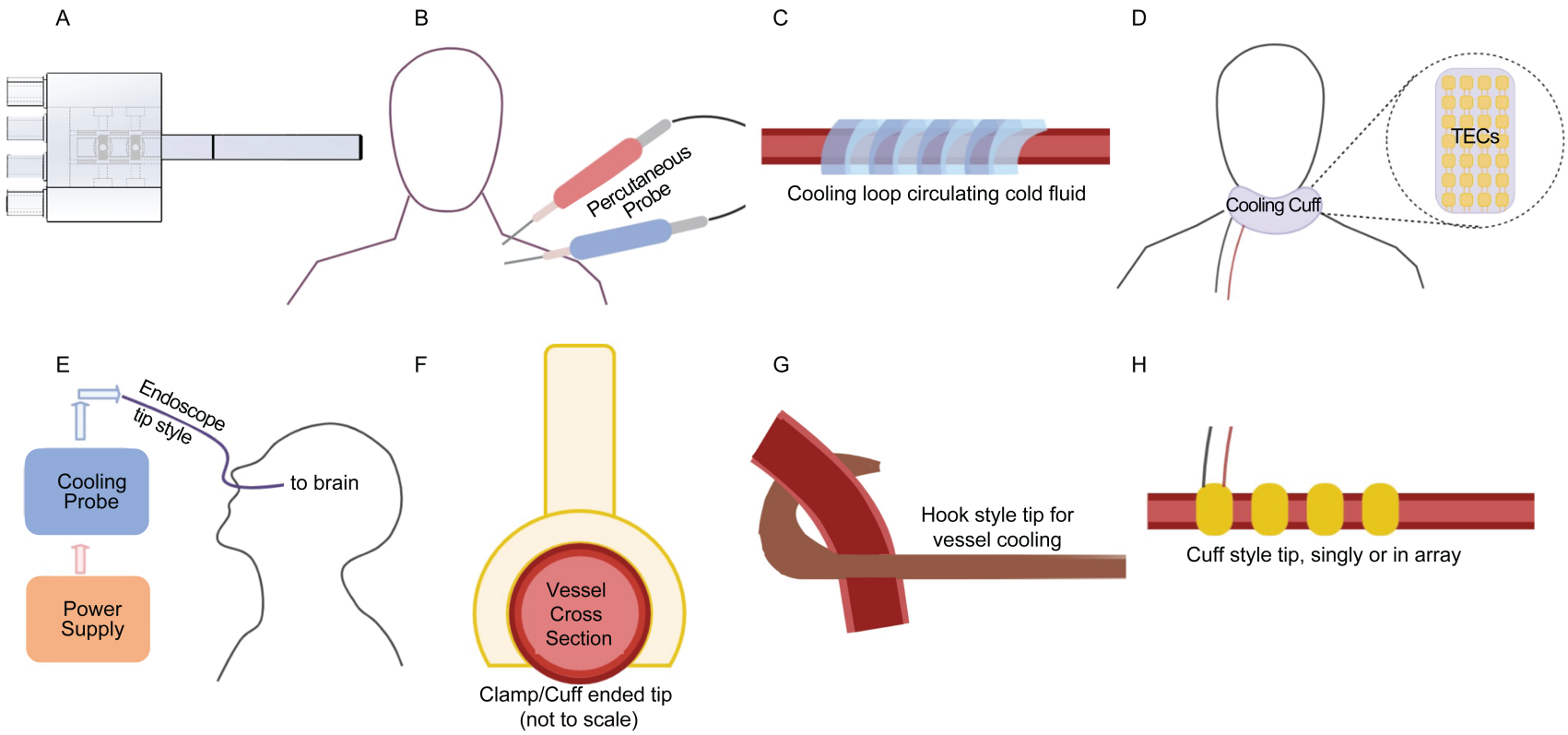

Figure 2.8 Possible embodiments of extravascular blood cooling devices. (A) Current prototype. (B) Percutaneous system. (C) Cooling loop. (D) Thermoelectric neck cooling cuff; similar cooling pads/blankets are currently in use in hospital settings. (E) Intranasal cooling. (F, G) Tip designs for the cooling bar. (H) Application of an array of probes on a single vessel to multiply cooling levels. Not included in the figure are ideas that combine the cooling device with existing tools, e.g., attaching cooling elements to surgical drills or other implements

2.5 Conclusion

We have demonstrated the successful extravascular control of blood temperature using a custom-built, concentrated thermoelectric probe. In future work, results gathered for varying allometric groups and sexes should be presented, along with histological analyses to confirm local and systemic safety of our technique. Tissue temperature should be monitored to ascertain levels of tissue cooling derived from our chilled blood circulation. We may also investigate the extent of the thermal spread in the region surrounding where the cooling probe is applied. While cooling is the primary focus, a study of tissue heating with the probe is also possible.

Of the many embodiments discussed above, percutaneous cooling/heating probes (Figure 2.8) are envisioned to be our end goal in developing this novel tool for clinical applications. Such probes (in which the probe system will approach and clamp onto key vessels through a small incision in the skin) will hypothetically maximize the therapeutic window for patients. Smaller incisions will reduce risk of complications such as infection and scarring, and result in a less invasive procedure. Moreover, percutaneous systems have implications for future users and use settings. Unlike cut-down procedures that would require a surgeon (as employed in this study with the rodent models), it is possible that emergency medicine or intensive care clinicians may be able to use the percutaneous probe to deliver prompt care. In light of these uses, the next generation probe system will be percutaneous and trialed with the goal of informing clinical workflows.

This thermoelectric probe system is a powerful tool for scientific and clinical research. Scientifically, it can be used to induce and quantify cooling in different locations in the body, as well as investigate disease, pain, thermoregulation and tissue thermal properties. Clinically, many of the potential benefits of tissue cooling have been confounded by numerous

complications brought on by systemic hypothermia. With the proposed probe system, the benefits of selective organ cooling may be made clear, informing clinical recommendations for several diseases. The system's ability to flexibly cool or heat may streamline thermal therapeutics in clinics and inform established clinical workflows. Though hypothermia itself remains a hotly debated intervention in the clinical arena, through the use of our probe system we anticipate new developments in medicine and science.

2.6 Acknowledgements

I thank Aman Jha, Colleen Crouch, Joan Greve, Jose Diaz, Aditya Pandey and Badih Junior Daoh for their contributions to this work.

2.7 References

1. Smales ORC, Kime R. Thermoregulation in babies immediately after birth. *Arch Dis Child*. 1978;53(1):58-61. doi:10.1136/adc.53.1.58

2. Speakman JR. Obesity and thermoregulation. In: *Handbook of Clinical Neurology*. Vol 156. Elsevier B.V.; 2018:431-443. doi:10.1016/B978-0-444-63912-7.00026-6

3. Shibasaki M, Okazaki K, Inoue Y. Aging and thermoregulation. *J Phys Fit Sport Med*. 2013;2(1):37-47. doi:10.7600/jpfsm.2.37

4. Lenhardt R. *Body Temperature Regulation and Anesthesia*. Vol 157. Elsevier B.V.; 2018. doi:10.1016/B978-0-444-64074-1.00037-9

5. Milhaud D, Thouvenot E, Heroum C, Escuret E. Prolonged moderate hypothermia in massive hemispheric infarction: Clinical experience. *J Neurosurg Anesthesiol*. 2005;17(1):49-53.

6. Qiu W, Shen H, Zhang Y, et al. Noninvasive selective brain cooling by head and neck cooling is protective in severe traumatic brain injury. *J Clin Neurosci*. 2006;13(10):995-1000. doi:10.1016/j.jocn.2006.02.027

7. Chu KF, Dupuy DE. Thermal ablation of tumours: Biological mechanisms and advances in therapy. *Nat Rev Cancer*. 2014;14(3):199-208. doi:10.1038/nrc3672

8. Shankaran S, Laptook AR, Ehrenkranz RA, et al. Whole-Body Hypothermia for Neonates

with Hypoxic–Ischemic Encephalopathy. *N Engl J Med*. 2005;353(15):1574-1584. doi:10.1056/nejmcps050929

9. Dietrich WD, Bramlett HM. The Evidence for Hypothermia as a Neuroprotectant in Traumatic Brain Injury. *Neurotherapeutics*. 2010;7(1):43-50. doi:10.1016/j.nurt.2009.10.015

10. itis.swiss. Thermal Conductivity » IT'IS Foundation. https://itis.swiss/virtual-population/tissue-properties/database/thermal-conductivity/. Accessed March 3, 2021.

11. Choi JH, Marshall RS, Neimark MA, et al. Selective brain cooling with endovascular intracarotid infusion of cold saline: A pilot feasibility study. *Am J Neuroradiol*. 2010;31(5):928-934. doi:10.3174/ajnr.A1961

12. Keller E, Imhof H-G, Gasser S, Terzic A, Yonekawa Y. Endovascular cooling with heat exchange catheters: a new method to induce and maintain hypothermia. *Intensive Care Med*. 2003;29(6):939-943. doi:10.1007/s00134-003-1685-3

13. Nagao K, Nitobe E, Okamoto K, Miki T, Hayashi N. Advanced Challenge in Resuscitative Hypothermia in Patients with Cardiac Arrest on Arrival at the Emergency Room. In: *Hypothermia for Acute Brain Damage*. Springer, Tokyo; 2004:308-314. doi:10.1007/978-4-431-53961-2_50

14. Holzer M, Bernard SA, Hachimi-Idrissi S, Roine RO, Sterz F, Müllner M. Hypothermia for neuroprotection after cardiac arrest: Systematic review and individual patient data meta-analysis. *Crit Care Med*. 2005;33(2):414-418. doi:10.1097/01.CCM.0000153410.87750.53

15. Ohta T, Kobayashi T. US6336910B1 - Extracorporeal circulation apparatus for selective cooling method - Google Patents. https://patents.google.com/patent/US6336910B1/en. Accessed February 9, 2021.

16. Dobak JDI. US6149677A - Circulating fluid hypothermia method - Google Patents. https://patents.google.com/patent/US6149677A/en. Accessed June 10, 2021.

17. Bernard SA, Gray TW, Buist MD, et al. Treatment of Comatose Survivors of Out-of-Hospital Cardiac Arrest with Induced Hypothermia. *N Engl J Med*. 2002;346(8):557-563. doi:10.1056/nejmoa003289

18. Polderman KH. Hypothermia and coagulation. *Crit Care*. 2012;16(S2):1-42. doi:10.1186/cc11278

19. Maze R, Le May MR, Froeschl M, et al. Endovascular cooling catheter related thrombosis in patients undergoing therapeutic hypothermia for out of hospital cardiac arrest. *Resuscitation*. 2014;85(10):1354-1358. doi:10.1016/j.resuscitation.2014.05.029

20. Woo JH, Lim YS, Yang HJ, et al. Factors associated with pneumonia in post-cardiac arrest patients receiving therapeutic hypothermia. *Am J Emerg Med*. 2014;32(2):150-155. doi:10.1016/j.ajem.2013.10.035

21. ROSOMOFF HL, HOLADAY DA. Cerebral blood flow and cerebral oxygen consumption during hypothermia. *Am J Physiol*. 1954;179(1):85-88. doi:10.1152/ajplegacy.1954.179.1.85

22. Schwartz MJ, Faiena I, Cinman N, et al. Laparoscopic bowel injury in retroperitoneal surgery: Current incidence and outcomes. *J Urol*. 2010;184(2):589-594. doi:10.1016/j.juro.2010.03.133

23. Wei G, Hartings JA, Yang X, Tortella FC, Lu X-CM. Extraluminal Cooling of Bilateral Common Carotid Arteries as a Method to Achieve Selective Brain Cooling for Neuroprotection. *J Neurotrauma*. 2008;25(5):549-559. doi:10.1089/neu.2007.0498

24. Pipe, Kevin; Besirli, Cagri G.; Kim, Gun-Ho; Smith S. (2) Patent Application Publication (10) Pub . No .: US 2015 / 0164398 A1. 2015;1(19).

25. Chen G, Xu W, Zhu D. Recent advances in organic polymer thermoelectric composites. *J Mater Chem C*. 2017;5(18):4350-4360. doi:10.1039/c6tc05488a

26. Hossain MS, Li T, Yu Y, Yong J, Bahk JH, Skafidas E. Recent advances in printable thermoelectric devices: Materials, printing techniques, and applications. *RSC Adv*. 2020;10(14):8421-8434. doi:10.1039/c9ra09801a

27. Yu Y, Zhu W, Kong X, Wang Y, Zhu P, Deng Y. Recent development and application of thin-film thermoelectric cooler. *Front Chem Sci Eng*. 2020;14(4):492-503. doi:10.1007/s11705-019-1829-9

28. Jankowski MP, Soneji DJ, Ekmann KM, Anderson CE, Koerber HR. Dynamic changes in heat transducing channel TRPV1 expression regulate mechanically insensitive, heat sensitive c-fiber recruitment after axotomy and regeneration. *J Neurosci*. 2012;32(49):17869-17873. doi:10.1523/JNEUROSCI.3148-12.2012

29. Arrich J, Holzer M, Havel C, Müllner M, Herkner H. Hypothermia for neuroprotection in adults after cardiopulmonary resuscitation. *Cochrane Database Syst Rev*. 2016;2016(2). doi:10.1002/14651858.CD004128.pub4

30. Crouch AC, Castle PE, FitzGerald LN, Scheven UM, Greve JM. Assessing structural and functional response of murine vasculature to acute β-adrenergic stimulation in vivo during hypothermic and hyperthermic conditions. *Int J Hyperth*. 2019;36(1):1137-1146. doi:10.1080/02656736.2019.1684577

31. Yang CF, Yu-Chih Chen M, Chen TI, Cheng CF. Dose-dependent effects of isoflurane on cardiovascular function in rats. *Tzu Chi Med J*. 2014;26(3):119-122.

doi:10.1016/j.tcmj.2014.07.005

32. Diaz JA, Hawley AE, Alvarado CM, et al. Thrombogenesis with continuous blood flow in the inferior vena cava: A novel mouse model. *Thromb Haemost*. 2010;104(2):366-375. doi:10.1160/TH09-09-0672

33. He Q, Zhu L, Weinbaum S. Effect of Blood Flow on Thermal Equilibration and Venous Rewarming. *Ann Biomed Eng 2003 316*. 2003;31(6):659-666. doi:10.1114/1.1569265

34. Shimaoka H, Shiina T, Suzuki H, Horii Y, Horii K, Shimizu Y. Successful induction of deep hypothermia by isoflurane anesthesia and cooling in a non-hibernator, the rat. *J Physiol Sci*. 2021;71(1):10. doi:10.1186/s12576-021-00794-1

35. Neimark MA, Konstas A-A, Laine AF, Pile-Spellman J. Integration of jugular venous return and circle of Willis in a theoretical human model of selective brain cooling. *J Appl Physiol*. 2007;103(5):1837-1847. doi:10.1152/japplphysiol.00542.2007

36. Tagin MA, Woolcott CG, Vincer MJ, Whyte RK, Stinson DA. Hypothermia for Neonatal Hypoxic Ischemic Encephalopathy: An Updated Systematic Review and Meta-analysis. *Arch Pediatr Adolesc Med*. 2012;166(6):558-566. doi:10.1001/ARCHPEDIATRICS.2011.1772

37. Harris OA, John M. Colford J, Good MC, Matz PG. The Role of Hypothermia in the Management of Severe Brain Injury: A Meta-analysis. *Arch Neurol*. 2002;59(7):1077-1083. doi:10.1001/ARCHNEUR.59.7.1077

38. Bellini, Yiu, Nozdrin, Papalois. The Effect of Preservation Temperature on Liver, Kidney, and Pancreas Tissue ATP in Animal and Preclinical Human Models. *J Clin Med*. 2019;8(9):1421. doi:10.3390/jcm8091421

Chapter 3 Selective Brain Cooling via Thermoelectric Extravascular Blood Cooling of a Carotid Artery

3.1 Abstract

Background: We demonstrate selective brain cooling (SBC) via extravascular cooling of the carotid artery in rat models using a contact-based, thermoelectric concentrated cooling probe.

Methods: The efficacy of this technique is verified with direct monitoring of brain tissue, rectal, and intrajugular blood temperatures. SBC was achieved by bringing the cooling probe in contact with the surgically exposed left common carotid artery. We compare our technique's ability to induce brain cooling to that of classical methods (systemic hypothermia). Placement of a large ice pad across the rat's abdomen from neck to the tips of the feet simulated a clinical hypothermia intervention.

Results: Brain temperature decreased independently of the core at a rate of -4.19 ± 3.15 ˚C/hr (rectal: -0.84 ± 2.59 ˚C/hr) when a cooling probe temperature of 0 ˚C was applied. Histology of the vasculatures and blood composition revealed that extravascular cooling with our probe did not cause adverse pathological changes on the animal. In contrast to our technique, whole body cooling resulted in rapid brain cooling rates (-8.22 ± 3.35 ˚C/hr) but at the expense of severe hypothermia at the core (-15.31 ± 6.60 ˚C/hr).

Conclusion: Isolated cooling of the brain as achieved by our technique suggests greater controllability in future thermal therapies provided it is validated in larger animal models. Rapid SBC may allow further studies into reducing and decoupling the deleterious side effects of systemic hypothermia from its benefits at the treatment site.

3.2 Introduction

The application of cold has historically been a useful therapy for patients suffering from trauma, fever, and cardiac arrest. Systemic hypothermia ("whole-body hypothermia", "hypothermia") is currently indicated for adult cardiac arrest patients with return of spontaneous circulation[1], medically refractory intracranial hypertension from severe traumatic brain injury (TBI)[2], and for patients with neonatal hypoxic-ischemic encephalopathy[3]. Though not yet standard of care, mild hypothermia has also shown promise in mitigating neurologic damage from TBI[4], ischemic stroke[5,6], and intracranial hemorrhage[7]. In these cases, the primary objective of the hypothermia was in cooling of the brain so to preserve neurological function and improve patient outcomes. The benefits of brain cooling are attributed to decreases in brain inflammation[8], oxygen and metabolic demand[9], and neuronal injury from free radical damage[10]. However, such benefits are weighed against the toxicities (e.g., cardiac suppression[11], coagulopathy[12], immune suppression[13]) that arise from systemic hypothermia as a side effect of current brain cooling technologies. Selective brain cooling (SBC) however, has the potential to enhance patient outcomes in diseases where it is already standard of care (e.g., cardiac arrest) as well as to improve clinical outcomes for other cerebral insults (e.g., ischemic stroke). In clinical trials, the injurious effects of systemic hypothermia often discouraged its use in TBI or stroke, where brain cooling may be beneficial. Therefore, it is essential to identify and develop a method of brain cooling that is independent of systemic hypothermia.

Clinically established brain cooling interventions include the intravascular cold saline infusion[14], ice baths/blankets[15], and extracorporeal cooling loops[16]. Each approach causes steep reductions in core temperature alongside to reductions in brain temperature. In addition to the toxicities arising from systemic hypothermia, intravascular techniques also raise the risk of

catheter-based thrombosis[17] and vessel trauma from needle punctures. Ice baths tend to overwhelm patients and are often not controllable in temperature or cooling rate. Current methods are therefore limited to short use times and cannot target specific organs, vessels, or select regions of deep tissue.

Compared to systemic hypothermia, SBC acts on a smaller thermal load and contains the cascading effects of tissue cooling (e.g. vasodilation) within a smaller region to minimize disruptions in core physiological systems. Emerging SBC methods include: ice helmets and neck cuffs[18], intranasal chillers[19], carotid cold saline injections[20], epidural coolers[21], and extravascular cooling water loops[22]. At various stages of development and use, these techniques report low efficacy (e.g. decrease of 0.32 ˚C/hr in brain temperature[18]), narrow temperature ranges, and slow system responsiveness (e.g. a water loop is limited to a minimum of ~ 0 ˚C and possesses high thermal inertia[22]). Despite the potential for SBC in the clinical arena, no sophisticated local cooling device existed with the capacity for feedback control and flexibility in cooling rate and temperature. In response, we have improved our solid-state extravascular blood cooling probe[23] and applied it for SBC. This technology was previously demonstrated to chill the blood flowing in the rat carotid artery. The probe can precisely cool or heat for extended periods, which is advantageous for maintaining desired intensity of thermal stimulus. While a single probe is used here for arterial cooling, there is potential to utilize a complementary heating probe for jugular heating to further enable SBC.

In this study, we demonstrate SBC with rodent models, in which thermoelectric extravascular cooling of arterial blood promotes convective heat loss of brain tissue. The key aims of this study are to: (1) demonstrate the feasibility of SBC in rats using the custom probe, (2) prove non-toxicity of our methods, and (3) compare the results against a cooling blanket as

an analog for clinical hypothermia in terms of effectiveness and selectivity. To prove non-toxicity, we report blood and local tissue analyses both prior to and immediately following experiments to assess acute adverse systemic effects and localized damage caused by the cooling probe. To accomplish these goals, temperature data were acquired under various cooling conditions and locations in the animal.

3.3 Methods

This research protocol was approved by the University of Michigan's Institutional Animal Care and Use Committee. Healthy adult Sprague Dawley rats (Charles River Labs, Wilmington, MA) of both sexes were used to characterize SBC in terms of their cooling rates at various locations in the body (n = 10). The number of animals was selected based on prior experimentation with rodent models, for which ≥ 5 animals were sufficient for data analysis[24]. Animals were housed in a controlled temperature (22 ± 2 °C) and humidity (~27%) vivarium. All animals were initially selected within weight ranges of 200-275 g. Animals weighed ~250-450 g by their date of experiment, which was randomly assigned within a two week period (Table 3.1). A subset of animals for each sex was randomly selected for blood/tissue collection.

Table 3.1 Animal Statistics

Sex	Male	Female
# of animals	4	6
Mean weight (g)	395 ± 44	275 ± 13

3.3.1 Device description

A concentrated thermoelectric cooler (TEC) probe system ("cooling probe") with a range of -10 to 50 ˚C was custom-built for extravascular cooling of the left common carotid artery (LCCA)[23]. The probe extends in a thermally conductive tip that contacts the outer surface of the LCCA (contact area: 8.6 x 1.5 mm^2), rapidly cooling the arterial wall and the blood flowing into the brain (Figure 3.1). Only the tip edge is exposed for contact cooling with tissue, and other surfaces are completely insulated. The cooling applied is not intended to freeze tissues or blood. For this study, a single probe was used to cool the LCCA, approximating 50% of the blood flow into the brain.

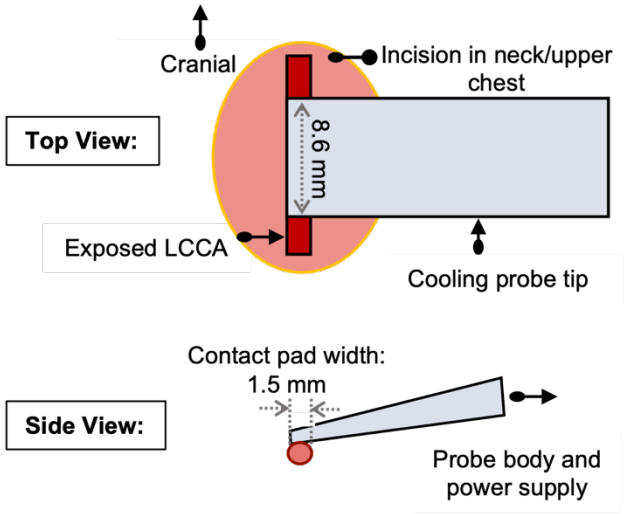

Figure 3.1 Placement of cooling probe tip on the exposed LCCA of a rat. Other probe components, such as the power supply, thermoelectric modules, and thermocouples are not shown.

3.3.2 Animal preparation

Rats were anesthetized using 5% isoflurane at induction and maintained at 1-2.5% isoflurane in 1 L/min O_2 carrier gas[25]. Following induction, fur was removed in the upper chest and head area. Thermocouples were placed at multiple locations in the animal: rectal (core), brain, right external jugular vein (RJV), and LCCA exterior (carotid temperature data not shown). To monitor brain temperature, a flexible, 23-gauge thermocouple (time constant: 0.005 sec; accuracy: +/- 0.1 ˚C; Physitemp Instruments, Clifton, NJ) was surgically implanted in the

left hemisphere of the brain. For this, the anesthetized rat was secured prone in a stereotaxic frame (Kopf Instruments, Tujunga, CA), and an incision made between the ears approximately following the sagittal midline (1-1.5 cm long). A 1 mm diameter burr hole was placed 3 mm lateral and 2 mm posterior to the bregma with a dental drill[26]. The thermocouple was implanted 3-4 mm below the skull surface (approximately reaching into the outer cortex), and fixed in place using tissue glue. The rat was then released from the frame and placed supine atop a feedback-controlled heating pad (Harvard Apparatus, Holliston, MA) set at 36 ˚C. Core temperature was monitored using a rectal thermocouple (time constant: 0.3 sec; accuracy: +/- 0.1 ˚C; Harvard Apparatus, Cambridge, MA). The remaining thermocouples at intrajugular and LCCA wall locations were placed immediately prior to the baseline/cooling probe trials, which require surgical exposure of the relevant vasculature. Since the time scales for clinical hypothermia treatment are on the order of hours, the time constants of the equipment described above were sufficient to characterize the cooling that occurred.

3.3.3 Experimental procedure

3.3.4 Cooling blanket measurements

A flat ice gel pack was placed on the rat's abdomen to mimic the effects of a cooling blanket or ice bath used in clinics. All ice packs were kept temperature controlled (0 ˚C) prior to use, and was wrapped in a vinyl sleeve to reduce the risk of freeze injury to the animal. Temperature was recorded at brain and rectal locations. Cooling blanket trials, when administered, always followed brain thermocouple placement and preceded all other surgical interventions and trials with the probe (Table 3.2, Figure 3.2).

Table 3.2 Chart of experiments and methods.

Cooling Blanket*	**Baseline**	**Cooling probe: 0 ˚C/-5 ˚C†**

	(n = 7)	(n = 10)	(n = 10)
Animal Prep	○ Animal anesthetized ○ Thermocouples inserted at brain and rectal locations ○ Shaved and placed ons heating pad	○ Animal anesthetized ○ Thermocouples inserted at brain and rectal locations ○ Shaved and placed on heating pad ○ LCCA, RJV surgically exposed and thermocouples placed at intrajugular and carotid wall	○ Animal anesthetized ○ Thermocouples inserted at brain and rectal locations ○ Shaved and placed on heating pad ○ LCCA, RJV surgically exposed and thermocouples placed at intrajugular and carotid wall
Procedure	○ Ice pad wrapped in vinyl protective sleeve ○ Interfacial thermocouple placed atop rat stomach under the pad ○ Temperature measured for ≥ 15 mins, or until rectal temperature < 30 ˚C.	○ Deactivated probe placed atop LCCA ○ Temperature measured for ≥ 15 mins	○ Probe primed at target temperature (0 or -5 ˚C) and placed atop LCCA ○ Temperature measured for ≥ 15 mins

* Experiments performed in order of cooling blanket (if applicable), baseline, then cooling probe. Cooling blanket experiments were performed on 7 animals only.

†Probe trials of 0 or -5 ˚C performed alternately. In about half of the animals, 0 ˚C was performed first, followed by -5 ˚C, and vice versa for the remaining.

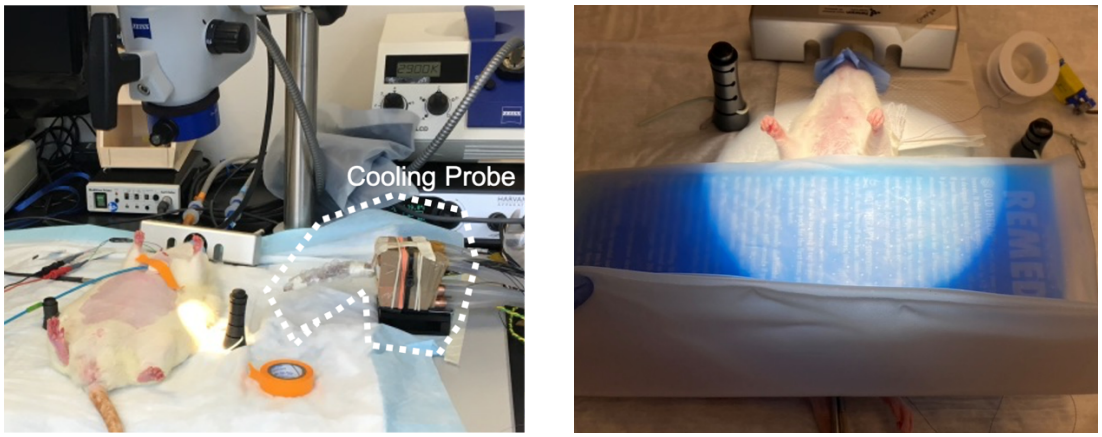

Figure 3.2 Images of the rat during experiments. Left: an ice-filled cooling blanket is used to induce whole-body cooling. Right: The animal is prepped for cooling probe trials.

3.3.5 Cooling probe measurements

An incision was made on the supine rat's neck, midline/lateral over the cervical spine curvature and blunt dissection used to isolate the LCCA and RJV from surrounding tissue. Another thermocouple was inserted into the RJV[27], fixed in position using tissue glue (3M, Saint Paul, MN), and used to record intravenous blood temperature. A thermocouple was also placed

on the LCCA wall. The central cooling bar in the probe was then primed at a target temperature and gently brought into contact with the LCCA (Figure 3.1). Three types of cooling probe trials were performed: a baseline (cooling probe atop the carotid but not activated), followed by trials with probe target temperatures of 0 ˚C and -5 ˚C.

All trials lasted 15-20 minutes, with early discontinuation should rectal temperature drop below 30 ˚C. The maximum duration of anesthesia from induction to end of data collection was 3 hours, with an average of 158 ± 15 mins.

3.3.6 Blood and tissue sample collection

Blood and tissue samples were collected for a subset of rats. Blood (vol: 0.5-1 mL, n = 7) was drawn intravenously (at jugular) at the following times: Post-brain thermocouple insertion / pre-cooling blanket (Group 1, G1), pre-baseline (G2), pre-cooling probe (G3), post-cooling probe (G4). To assess hemolysis and other systemic changes with the experimental manipulations, complete blood count (CBC) and blood smears were conducted and compared against each group. To study the effects of probe cooling on arterial tissue, samples of the carotid arteries (LCCA: test, RCCA: control) were collected in pairs in a subset of rats (n = 4) for histology. Hematological and histological evaluations were performed by an independent pathologist at the University of Michigan (Table 3.3).

Table 3.3 Summary of blood and tissue sample collection. G1 (pre- cooling blanket) was generally omitted in statistical comparison of test groups due to difficulty in sample collection.

Sample Description	Male (n=4)	Female (n=6)	Procedure
Hematology: Post-brain thermocouple / Pre-cooling blanket (G1)*	2	0	Sample collected immediately following brain thermocouple insertion, within 20 mins of anesthesia induction.

Hematology: Post-cooling blanket / Pre-jugular thermocouple and Pre-baseline (G2)	4	3	Immediately following jugular/carotid exposure, prior to thermocouple insertion in jugular
Hematology: Post- baseline (G3)	3†	3	Immediately following baseline trial with the inserted thermocouple
Hematology: Post- cooling probe (G4)	4	3	Immediately following a cooling trial of 0 ˚C and -5 ˚C with the cooling probe
Histology: pair of RCCA, LCCA	2	2	Carotid arteries harvested immediately following euthanasia (overdose with anesthesia), within 10 mins of exsanguination. Tissues fixed in a 20:1 ratio of 10% buffered formalin to single artery sample

*Lack of blood samples in G1 due to difficulty in obtaining samples at this stage in experiments; †A blood sample was omitted due to undesirable clotting in the collected sample prior to analysis.

3.3.7 Data processing and statistical analysis

All temperature data were collected using SiteVIEW (Accsense, Chesterland, OH) for *in vivo* measurements (1 sample/5 sec) and the TEC Service Software (Meerstetter Engineering, Rubigen, Switzerland) for the probe (1 sample/sec). All data analyses were completed using MATLAB (MathWorks, Portola Valley, CA) and custom Python scripts. All data were smoothed using a moving average window of 30 seconds. Results are presented as mean ± standard deviation. A p-value of ≤ 0.05 was considered significant.

Due to variability in the initial temperature of animals, the rate of cooling is our primary metric for comparison. Graphically, only data from the same animal is plotted together for visual analysis. To test if the brain and rectal temperature cooling rates differed significantly for baseline (deactivated probe on LCCA) versus a cooling trial, a one-way ANOVA was used. Due to the oscillatory nature of blood and tissue temperatures, the cooling rate was determined using simple linear regression. To test significance across hematology results, a two-way ANOVA was

used. Histological findings were used for visual and qualitative analysis and were not evaluated statistically.

3.4 Results

3.4.1 Changes in temperature with cooling trials

To determine the effects of the cooling probe on brain and core temperature, the following comparisons were made: brain cooling rates at baseline vs 0 ˚C ($p = 0.002$), and baseline vs -5 ˚C ($p < 0.0001$). Rectal cooling rates at baseline vs 0 ˚C ($p = 0.67$) or vs -5 ˚C ($p = 0.49$) were not significantly different. Brain cooling rates at 0 ˚C vs -5 ˚C were also not significantly different ($p = 0.54$). To test for SBC, brain and rectal cooling rates were compared: rectal vs brain at 0 ˚C ($p = 0.02$), and at -5 ˚C ($p = 0.0004$). Brain cooling rates did not depend significantly on sex or weight. Figure 3.3 shows the effects of each cooling trial on rat body temperature. Figure 3.4 and Figure 3.5 compare the effects of cooling trials on the brain and core with baseline. Mean values of all results are summarized in Table 3.4.

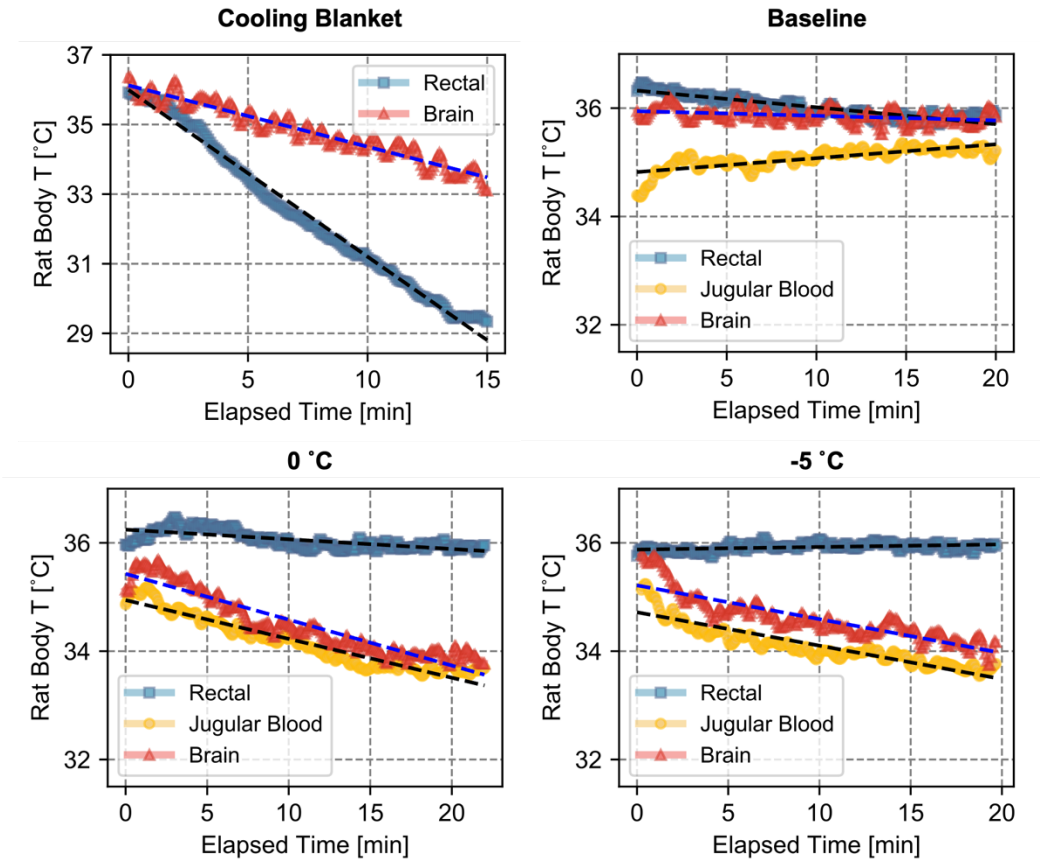

Figure 3.3 Representative temperature traces for a sample rat in each test group. Baseline is when the probe in contact with the LCCA but deactivated.

Table 3.4 Compilation of all animals' averaged cooling rates per test group and location.

Trial	Intrajugular ΔT/Δt (˚C/hr)	Brain ΔT/Δt (˚C/hr)	Rectal ΔT/Δt (˚C/hr)
Cooling blanket	*N/A*	-8.22 ± 3.35	-15.31 ± 6.60
Baseline	0.24 ± 1.74	-0.14 ± 1.41	-0.32 ± 2.71
0 ˚C	-3.24 ± 2.08	-4.19 ± 3.15	-0.84 ± 2.59
-5 ˚C	-2.90 ± 2.07	-3.52 ± 1.34	-0.97 ± 1.30

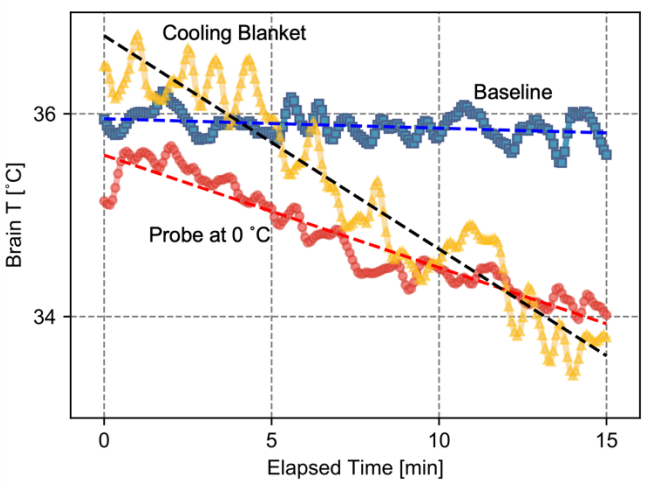

Figure 3.4 Representative figure of brain temperature trace, comparing baseline trials with cooling trials in a sample rat.

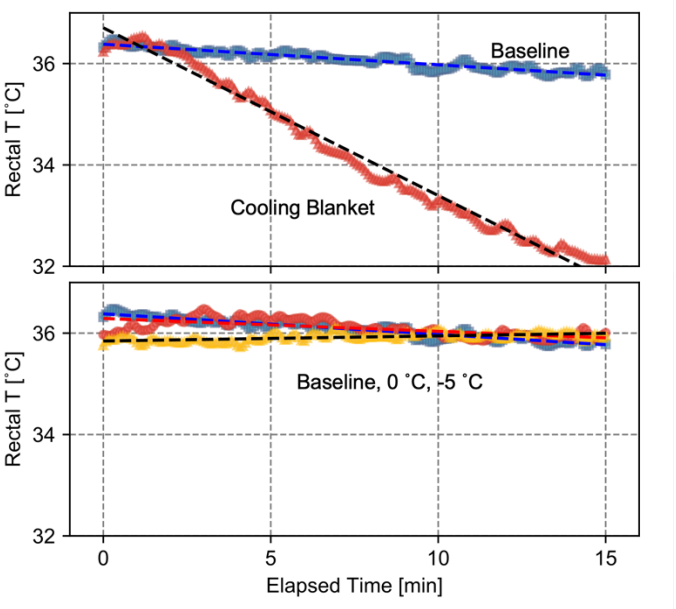

Figure 3.5 Representative figures of rectal temperature change over time, comparing baseline trials with a cooling trial in a rat. Top: baseline vs. cooling blanket, Bottom: baseline vs. cooling probe at 0 ˚C and -5 ˚C.

3.4.2 Adverse effects of cooling

To assess the relative toxicity of the experiments on the animal, hematological and histological evaluations were reviewed. Blood samples did not show evidence of hemolysis as a

result of cooling with the probe (Figure 3.6), and CBC values also did not change significantly across the sample groups (Table 3.5, Figure 3.7). Histology confirmed benign use of the probe for our experimental durations, with no clinically relevant damage to the LCCA compared to the RCCA (Figure 3.8, Figure 3.9).

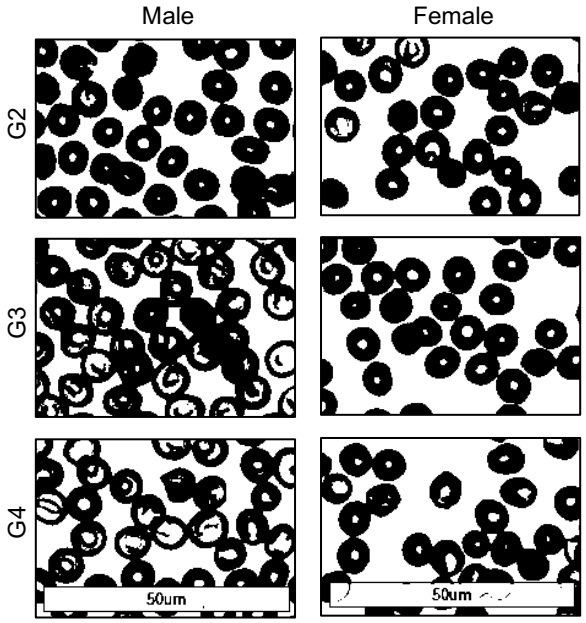

Figure 3.6 Representative blood smears from rats. No distinct hemolysis is detected at the time points spanning G2-G4. G1 is not shown due to a lack of samples, but it also displayed no obvious hemolysis.

Table 3.5 Hematology results,†,‡*

Sample IDs	**G2 (n=7)**	**G3 (n=6)†**	**G4 (n=7)**
White Blood Cell Count, WBC (10e3/ul)	9.924 ± 3.513	7.917 ± 3.099	6.337 ± 2.932
Neutrophils, Neut (10e3/ul)	1.179 ± 0.503	0.985 ± 0.408	0.979 ± 0.347
Lymphocytes, Lym (10e3/ul)	8.154 ± 3.066	6.472 ± 2.677	4.961 ± 2.476
Monocytes, Mono (10e3/ul)	0.446 ± 0.230	0.333 ± 0.194	0.283 ± 0.194
Eosinophils, Eos (10e3/ul)	0.110 ± 0.047	0.097 ± 0.035	0.091 ± 0.055
Basophils, Baso (10e3/ul)	0.036 ± 0.010	0.030 ± 0.011	0.023 ± 0.011
Neutrophils (%)	12.329 ± 5.328	12.833 ± 5.216	16.457 ± 5.359
Lymphocytes (%)	81.871 ± 5.414	81.400 ± 4.967	77.457 ± 4.812
Monocytes (%)	4.271 ± 1.107	4.067 ± 1.019	4.171 ± 0.996
Eosinophils (%)	1.129 ± 0.189	1.283 ± 0.483	1.514 ± 0.426
Basophils (%)	0.400 ± 0.163	0.417 ± 0.117	0.400 ± 0.115
Red Blood Cell Count, RBC (10e6/ul)	6.779 ± 0.375	6.817 ± 0.230	6.346 ± 0.366
Hemoglobin (g/dL)	14.886 ± 0.367	14.717 ± 0.117	13.957 ± 1.107
Hematocrit (%)	40.529 ± 1.045	40.467 ± 0.821	38.171 ± 2.961
Mean Corpuscular Volume, MCV (fL)	59.929 ± 2.906	59.467 ± 2.791	60.086 ± 2.377

Mean Corpuscular Hemoglobin, MCH (pg)	21.943 ± 1.089	21.600 ± 0.841	22.014 ± 0.869
MCH Concentration, MCHC (g/dL)	36.657 ± 0.637	36.383 ± 0.631	36.629 ± 0.550
Red Cell Distribution Width, RDW (%)	12.357 ± 1.122	12.100 ± 1.022	12.229 ± 1.137
Platelets (10e3/uL)	811.286 ± 321.794	975.500 ± 175.896	930.286 ± 214.082

*G1 not evaluated statistically due to lack of samples (n=2) and the presence of visible clots in one of the samples. The clots formed due to improper storage and is unrelated to our probe usage.

†A G3 sample was omitted due to the presence of visible clots (error in storage).

‡No statistical differences (two-way ANOVA).

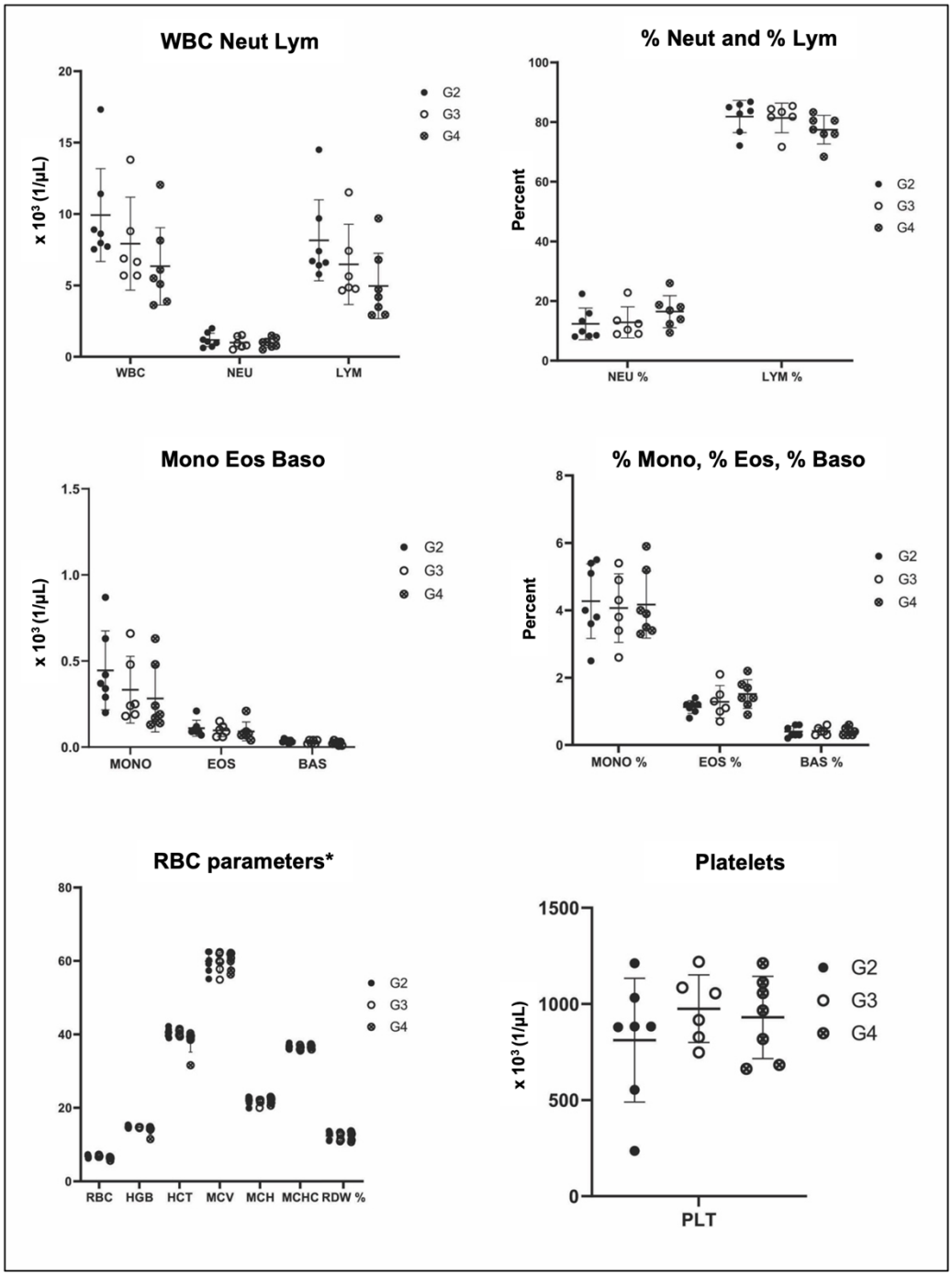

*Figure 3.7 CBC results for G2 (n = 7), G3 (n = 6) and G4 (n = 7). All values were within normothermic ranges throughout the experimental manipulation, signifying no acute systemic damage from the probe. There were no statistically significant differences between groups for any parameter. There was a downward trend in total white blood cell count (WBC) and absolute lymphocyte count (Lym) across G2-4, but this is attributed to prolonged anesthesia. G1 was excluded due to low sample number and a sample was excluded from G3 due to clotting. *For the units and values of RBC parameters, refer to Table 3.5.*

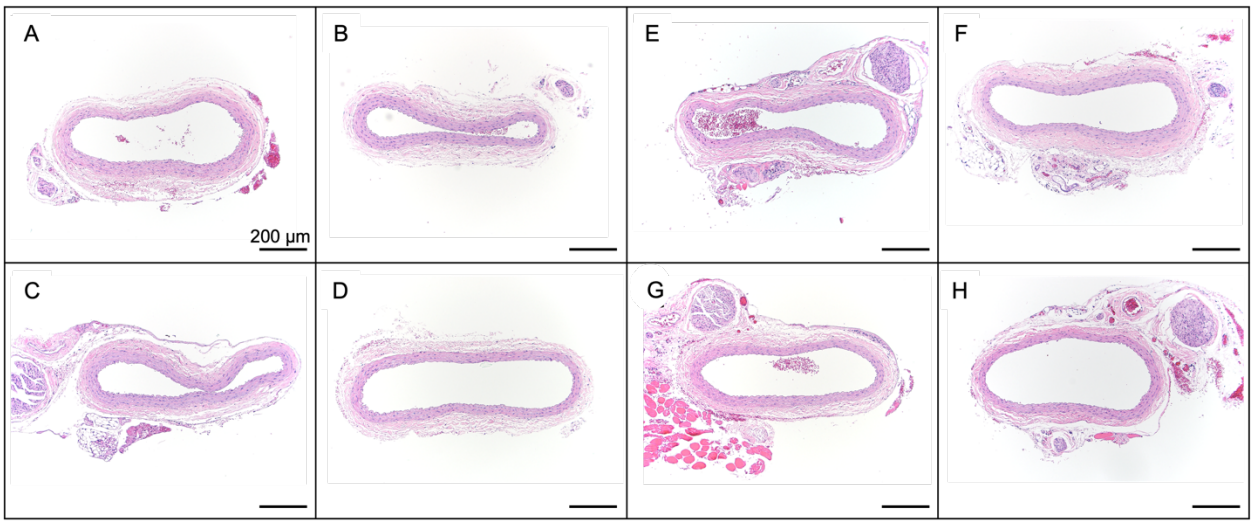

Figure 3.8 Representative images of hematoxylin and eosin-stained histology of experimental (LCCA: A, C, E, G) and contralateral control (RCCA: B, D, F, H). No arterial pathology was detected. Each pair of images are from one animal (A, B), (C, D), (E, F), (G, H). A total of 12 cross-sections (4 serial sections at each of 3 levels, separated by 100 µm each) were evaluated for each artery. Original magnification: 10x, bars = 200 µm.

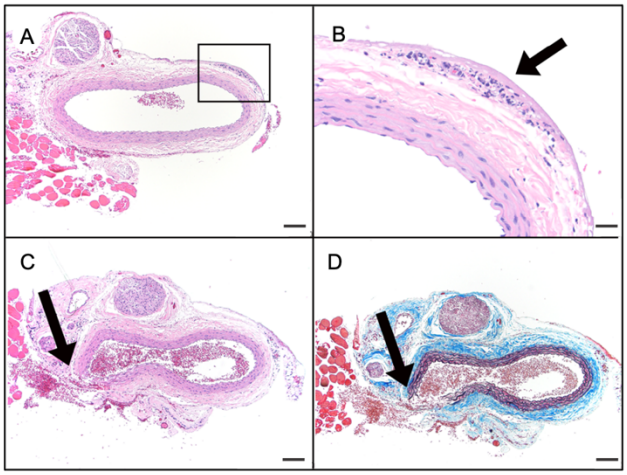

Figure 3.9 Representative images of a sample LCCA. In some sections at level 2 (A) there was focal pericapillary degeneration in the adventitia with focal infiltration of acute inflammatory cells (B, arrow). This was consistent with mild tissue trauma on the adventitial surface but did not affect the artery itself. In two sections at level 3 (C, D) there was a focal tear in the vessel with hemorrhage but no tissue reaction in the artery wall or hemophagocytosis. In the absence of tissue reaction this was considered likely to be iatrogenic damage at the time of vessel collection. Original magnifications: A, C, D = 10x, bar 100 µm; B = 40x, bar 20 µm. Box in A indicates area of focus in B. Staining for A, B, C: hematoxylin and eosin; D: trichrome-Verhoeff.

3.5 Discussion

3.5.1 Efficacy of brain cooling with cooling methods

For all cooling conditions, brain cooling was rapidly achieved relative to baseline ($p < 0.05$) and was differentiated from the depressant effects of isoflurane[28]. At baseline, brain temperature remained at normothermia (Figure 3.3), while during the cooling blanket and probe trials the brain temperature was greatly reduced (Figure 3.4). In a subset of baseline trials, the jugular and brain temperature appeared to increase because the baseline trials followed cooling blanket trials, and were rewarming (Figure 3.3). The cooling blanket surpassed other cooling methods for fastest brain cooling (-8.22 ± 3.35 ˚C/hr). Probe trials at 0 ˚C (4.19 ± 3.15 ˚C/hr) and -5 ˚C (-3.52 ± 1.34 ˚C/hr) resulted in similar brain cooling rates, possibly because of the proximity of the two temperatures. Reduction in blood temperature may also contribute to reduced cerebral blood flow, which reduces convective heat transfer from brain tissue to the chilled blood[29].

Overall, sex and weight were not found to significantly affect brain cooling results. Males were consistently heavier than females, and while weight was not found to be a significant factor in cooling, we observed a general increase in cooling rate with decreasing weight. This is in line with our expectation that smaller masses are more affected by cooling. Note that our results, while promising, are gained with rodents and are not wholly representative of human physiological and thermal states. Allometric scaling and analysis is required to determine the ranges of cooling that are both optimal and clinically significant, and how to improve our technique to achieve that target level of cooling.

3.5.2 Systemic hypothermia vs SBC

The cooling blanket trials used to induce systemic hypothermia resulted in a sharp decrease in all temperatures compared to its baseline (Figure 3.3, Figure 3.4). During our experiments, cooling blanket trials were occasionally aborted midway due to the animals' core

temperature reaching 30 ˚C or lower. The cooling blanket not only affects the core (-15.31 ± 6.60 ˚C/hr) to a greater extent than the brain (-8.22 ± 3.35 ˚C/hr), but its resultant cooling rate is also harder to control beyond simple loss of contact. Furthermore, the substantial reduction in core temperature likely resulted in subsequent reductions in the brain due to the cooled blood circulating throughout all parts of the body (Figure 3.5). By contrast, cooling with the probe achieved SBC with minimal changes to core temperature. Brain temperature was generally slower to decrease than with the cooling blankets, but the brain and core rates were independent ($p = 0.018$, $p < 0.001$ for 0 ˚C and -5 ˚C trials respectively), suggesting targeted cooling of brain tissue. With the probe, the heating pad below the animal was sufficient to maintain normothermia in the core. The resulting probe brain cooling was also considerable for but a 15 min application on a single carotid at modest cooling temperatures and contact areas.

Though our study did not explore the effects of deep systemic hypothermia (core temperature <20 ˚C), its adverse effects are well established in literature. In rats, cardiac arrest was reported to occur at rectal temperatures below 30 ˚C during anesthesia with 1-2% isoflurane, along with increased risk of organ damage[28]. As rats are known to be revivable from these isoflurane levels at normothermia, the cardio-suppressive effect of deep systemic hypothermia is implicit. Regardless, the toxicity from prolonged isoflurane use itself cannot be ignored as it certainly aids in achieving a deep hypothermic state by suppressing shivering in animals[28]. In our work, we have shown minimal effects of isoflurane on animals with steady core temperature and CBC levels during baseline and SBC. Hence, it may be possible for the brain to be selectively under deep hypothermia while minimizing risks of organ damage as the rest of the body is still at normothermic levels.

3.5.3 Safety of extravascular carotid cooling

Hematology for G1-G4 showed CBC values to be within normal physiologic ranges for rats and were not statistically different across groups, indicating no apparent damage from the surgical interventions or the cooling probe. From G2-G4, total white cell counts and lymphocyte counts displayed a downward trend (Figure 3.7). However, as the groups were composed of samples collected at successive timepoints throughout the experiments, such a decline is most likely due to prolonged anesthesia and stress rather than experimental manipulation. Despite this downward trend, the values remained within normal ranges and were not considered clinically significant. Manual differential of blood smears also confirmed no considerable increase in hemolysis as compared to baseline (Figure 3.6).

Histology of harvested carotid arteries also showed no clinically adverse alterations (Figure 3.8, Figure 3.9). Locally and systemically, there were no degenerative effects on the rat from use of the cooling probe at the given experimental temperatures and durations. However, as we collected blood and tissue samples within minutes of completing an experiment, only acute injury (i.e. chemical or temperature related damage) would be detected. It is still possible that inflammation and downstream molecular and biophysical changes may occur several hours following the procedure. A longer survival period would be required to test for such findings.

3.5.4 Limitations

While we assessed the local and systemic safety of extravascular cooling of the carotid, this was with an application period of ~2 hours, for cooling periods of 15-20 mins interspersed throughout. Therefore safety may not be assumed past the first few hours. In addition, this study cooled a single artery and recorded brain temperature in the corresponding hemisphere. We assumed that the point temperature measurement of the brain tissue is representative of the whole brain. Literature on heat transfer models have indicated that the perfusion of cooled blood in the

brain eventually leads to a temperature distribution that is quite uniform, as opposed to the distributions achieved by alternative methods such as the ice helmet which cool from the outside of the brain inward (for a cooling period of up to 6 hrs)[30]. Here with rats, we have assumed that 15-20 mins of cooling was sufficient to circulate chilled blood into all regions of the rat's brain. However, such short timeframes have not revealed the full limitations of this approach, such as minimum application time for uniform temperature distribution in the brain, optimal target temperature, cooling rates, and more. Identifying and improving on these limits will allow future optimization studies for clinical therapy.

3.6 Conclusion

We demonstrate SBC with solid-state extravascular cooling of the carotid artery in rodents. Brain tissue was successfully cooled without acute systemic or local damage from the experimental manipulations performed. Beyond validation for SBC, this technique may be used to validate *in vitro* or computational models of tissue cooling, the cardiovascular system, and other bioheat transfer (e.g., hypothermia models of head and neck[31]) using preclinical animal models. Future work should identify and improve on the limitations of our technique. With regards to eventual clinical testing and application, scaling and modeling the technique to human-sized power requirements is required. Then, the benefits and risks of brain cooling in clinical settings may be identified without confoundment from systemic toxicities. Through further study, we aim to inform thermal therapies and clinical workflows, as well as extend the technique to additional organs.

3.7 Acknowledgements

Special thanks to: Aman Jha, Joan Greve, Colleen Crouch, Richard Keep, Aditya Pandey, and Arjun Adapa for their guidance, input, equipment, and research spaces.

3.8 References

1. Arrich J, Holzer M, Havel C, Müllner M, Herkner H. Hypothermia for neuroprotection in adults after cardiopulmonary resuscitation. *Cochrane Database Syst Rev*. 2016;2016(2). doi:10.1002/14651858.CD004128.pub4

2. Harris OA, John M. Colford J, Good MC, Matz PG. The Role of Hypothermia in the Management of Severe Brain Injury: A Meta-analysis. *Arch Neurol*. 2002;59(7):1077-1083. doi:10.1001/ARCHNEUR.59.7.1077

3. Tagin MA, Woolcott CG, Vincer MJ, Whyte RK, Stinson DA. Hypothermia for Neonatal Hypoxic Ischemic Encephalopathy: An Updated Systematic Review and Meta-analysis. *Arch Pediatr Adolesc Med*. 2012;166(6):558-566. doi:10.1001/ARCHPEDIATRICS.2011.1772

4. Dietrich WD, Bramlett HM. The Evidence for Hypothermia as a Neuroprotectant in Traumatic Brain Injury. *Neurotherapeutics*. 2010;7(1):43-50. doi:10.1016/j.nurt.2009.10.015

5. Busto R, Dietrich WD, Globus MY, Ginsberg MD. The importance of brain temperature in cerebral ischemic injury. *Stroke*. 1989;20(8):1113-1114. doi:10.1161/01.STR.20.8.1113

6. Yenari MA, Han HS. *Neuroprotective Mechanisms of Hypothermia in Brain Ischaemia*. Vol 13. Nature Publishing Group; 2012:267-278. doi:10.1038/nrn3174

7. Melmed KR, Lyden PD. Meta-Analysis of Pre-Clinical Trials of Therapeutic Hypothermia for Intracerebral Hemorrhage. *Ther Hypothermia Temp Manag*. 2017;7(3):141-146. doi:10.1089/ther.2016.0033

8. Deng H, Han HS, Cheng D, Sun GH, Yenari MA. Mild hypothermia inhibits inflammation after experimental stroke and brain inflammation. *Stroke*. 2003;34(10):2495-2501. doi:10.1161/01.STR.0000091269.67384.E7

9. Chihara H, Blood AB, Hunter CJ, Power GG. Effect of Mild Hypothermia and Hypoxia on Blood Flow and Oxygen Consumption of the Fetal Sheep Brain. *Pediatr Res 2003 545*. 2003;54(5):665-671. doi:10.1203/01.pdr.0000084115.31416.17

10. McManus T, Sadgrove M, Pringle AK, Chad JE, Sundstrom LE. Intraischaemic hypothermia reduces free radical production and protects against ischaemic insults in

cultured hippocampal slices. *J Neurochem*. 2004;91(2):327-336. doi:10.1111/j.1471-4159.2004.02711.x

11. Bernard SA, Gray TW, Buist MD, et al. Treatment of Comatose Survivors of Out-of-Hospital Cardiac Arrest with Induced Hypothermia. *N Engl J Med*. 2002;346(8):557-563. doi:10.1056/nejmoa003289

12. Polderman KH. Hypothermia and coagulation. *Crit Care*. 2012;16(S2):1-42. doi:10.1186/cc11278

13. Polderman KH. Hypothermia, immune suppression and SDD: Can we have our cake and eat it? *Crit Care*. 2011;15(2). doi:10.1186/cc10080

14. Kim F, Olsufka M, Carlbom D, et al. Pilot study of rapid infusion of 2 L of 4°C normal saline for induction of mild hypothermia in hospitalized, comatose survivors of out-of-hospital cardiac arrest. *Circulation*. 2005;112(5):715-719. doi:10.1161/CIRCULATIONAHA.105.544528

15. Larsson IM, Wallin E, Rubertsson S. Cold saline infusion and ice packs alone are effective in inducing and maintaining therapeutic hypothermia after cardiac arrest. *Resuscitation*. 2010;81(1):15-19. doi:10.1016/J.RESUSCITATION.2009.09.012

16. Holzer M, Behringer W, Janata A, et al. Extracorporeal venovenous cooling for induction of mild hypothermia in human-sized swine. *Crit Care Med*. 2005;33(6):1346-1350. doi:10.1097/01.CCM.0000166356.45902.A2

17. Maze R, Le May MR, Froeschl M, et al. Endovascular cooling catheter related thrombosis in patients undergoing therapeutic hypothermia for out of hospital cardiac arrest. *Resuscitation*. 2014;85(10):1354-1358. doi:10.1016/j.resuscitation.2014.05.029

18. Poli S, Purrucker J, Priglinger M, et al. Induction of cooling with a passive head and neck cooling device: Effects on brain temperature after stroke. *Stroke*. 2013;44(3):708-713. doi:10.1161/STROKEAHA.112.672923

19. Abou-Chebl A, Sung G, Barbut D, Torbey M. Local brain temperature reduction through intranasal cooling with the rhinochill device: Preliminary safety data in brain-injured patients. *Stroke*. 2011;42(8):2164-2169. doi:10.1161/STROKEAHA.110.613000

20. Duan Y, Wu D, Huber M, et al. New Endovascular Approach for Hypothermia with Intrajugular Cooling and Neuroprotective Effect in Ischemic Stroke. *Stroke*. 2020:628-636. doi:10.1161/STROKEAHA.119.026523

21. King C, Robinson T, Dixon CE, Rao GR, Larnard D, Nemoto CEM. Brain temperature profiles during epidural cooling with the ChillerPad in a monkey model of traumatic brain injury. *J Neurotrauma*. 2010;27(10):1895-1903. doi:10.1089/neu.2009.1178

22. Wei G, Hartings JA, Yang X, Tortella FC, Lu X-CM. Extraluminal Cooling of Bilateral Common Carotid Arteries as a Method to Achieve Selective Brain Cooling for Neuroprotection. *J Neurotrauma*. 2008;25(5):549-559. doi:10.1089/neu.2007.0498

23. Lee CY, Crouch AC, Jha AK, et al. Extravascular Cooling of Blood Using a Concentrated Thermoelectric Cooling Probe. *J Med Device*. 2022;16(3):31004-31005. doi:10.1115/1.4054003

24. Crouch AC, Manders AB, Cao AA, Scheven UM, Greve JM. Cross-sectional area of the murine aorta linearly increases with increasing core body temperature. *Int J Hyperth*. 2018;34(7):1121-1133. doi:10.1080/02656736.2017.1396364

25. Yang CF, Yu-Chih Chen M, Chen TI, Cheng CF. Dose-dependent effects of isoflurane on cardiovascular function in rats. *Tzu Chi Med J*. 2014;26(3):119-122. doi:10.1016/j.tcmj.2014.07.005

26. Diao C, Zhu L. *In Vivo Experimental Study of Brain Temperature Distribution in Rats during Head Surface Cooling*. Vol 374.; 2003. doi:10.1115/IMECE2003-41994

27. Diaz JA, Hawley AE, Alvarado CM, et al. Thrombogenesis with continuous blood flow in the inferior vena cava: A novel mouse model. *Thromb Haemost*. 2010;104(2):366-375. doi:10.1160/TH09-09-0672

28. Shimaoka H, Shiina T, Suzuki H, Horii Y, Horii K, Shimizu Y. Successful induction of deep hypothermia by isoflurane anesthesia and cooling in a non-hibernator, the rat. *J Physiol Sci*. 2021;71(1):10. doi:10.1186/s12576-021-00794-1

29. Walter B, Bauer R, Kuhnen G, Fritz H, Zwiener U. Coupling of cerebral blood flow and oxygen metabolism in infant pigs during selective brain hypothermia. *J Cereb Blood Flow Metab*. 2000;20(8):1215-1224. doi:10.1097/00004647-200008000-00007

30. Keller E, Mudra R, Gugl C, Seule M, Mink S, Fröhlich J. Theoretical evaluations of therapeutic systemic and local cerebral hypothermia. *J Neurosci Methods*. 2009;178(2):345-349. doi:10.1016/j.jneumeth.2008.12.030

31. Li H, Chen RK, Tang Y, Meurer W, Shih AJ. An experimental study and finite element modeling of head and neck cooling for brain hypothermia. *J Therm Biol*. 2018;71(May 2017):99-111. doi:10.1016/j.jtherbio.2017.10.022

Chapter 4 Computational Modeling of Extravascular Blood Temperature Control for Selective Brain Cooling

4.1 Abstract

Background: In vivo blood cooling is a promising technique for uniform cooling of deep brain tissue for therapeutic hypothermia. We assess the potential of extravascular techniques for blood cooling and downstream brain cooling.

Methods: Computational models of extravascularly cooled common carotid arteries were developed and solved with the finite element method. Three models were created: rat carotid model with open neck extravascular cooling validated with past rat experiments, human model scaled up from the validated rat model, and human model of percutaneous extravascular cooling. Temperature data was extracted from the vessel surface, midline and outlet locations for analysis. Parametric studies varying extravascular zone's length and temperature were performed.

Results: Simulations of outlet blood temperature of an open neck cooling approach in rats were in good agreement (R^2 =0.75, p-val < 0.001) with past experimental data. A human carotid blood temperature simulation from same boundary conditions resulted in > 9˚C drop. The human percutaneous simulations resulted in ~1˚C drop and is estimated to induce brain cooling by a similar level. Sensitivity analysis of percutaneous results showed extravascular cooling length to be a more significant parameter than the applied temperature. Thermal spread along the vessel increased effective cooling length and aided in reduction of blood temperature.

Conclusion: Extravascular cooling of human common carotid arteries successfully cool flowing blood entering the brain. Future work will analyze the magnitude of brain cooling from the chilled blood in the context of clinical use. We will also investigate methods to increase the cooling delivered via extravascular means.

4.2 Introduction

Brain cooling is significant in the clinical arena as a thermal therapy for mitigating neuronal damage from diseases. For instance, brain cooling (delivered via whole-body hypothermia) is the Class 1 recommendation for adult cardiac arrest patients with return of spontaneous circulation. Standard of care is to initiate cooling within the first few hours and continue cooling for at least 24 hours, with a target brain temperature of 32-36 ˚C[1,2]. Clinically, brain cooling is often administered through whole-body hypothermia using methods such as ice baths or cold saline infusions[3]. Maintenance of whole-body hypothermia for several hours is not only highly stressful to the patient (i.e. discomfort, shivering, cardiac suppression[4]), but is also thermally inefficient (i.e. greater thermal load/heat capacity). By contrast, selective brain cooling (SBC) is a mode of brain cooling that concentrates solely on reducing brain temperature while maintaining normothermia at the core. The benefits of SBC include reduction of damaging heat stress, inflammation[5], and metabolic load[6] on the brain, while minimizing hypothermic shock in core systems[7] by isolating the cold to the brain. In addition to cardiac arrest, SBC has been proposed as a potential treatment for brain trauma[8] and ischemic stroke[9].

Despite the possible benefits of SBC, approved techniques for SBC are currently limited to ice helmets (decrease of 0.32 ˚C/hr in brain temperature)[10]. Emerging SBC methods tested nasal cooling (1.4 ± 0.4°C reduction of brain temperature in 1 hr)[11] and intra-arterial cold saline injections[12] as potentially more efficient alternatives to ice helmets. While these methods were

experimentally found to be effective at lowering brain temperature, they still impact on core temperature levels (nasal cooling resulted in -1.1± 0.6 °C change alongside brain cooling[11]) and are challenging to maintain for prolonged periods of time. For example, saline injections risks blood thinning and hypotension with extended use. As such, research continues in the study of brain heat transfer and engineering of a selectively effective and safe cooling technique. In particular, extravascular ("outside of the vessel") cooling modes are being considered due to their potential for SBC as a minimally invasive technique. The advantage of extravascular blood cooling is that it chills the entire vessel/blood flow without needle punctures or intravascular fluids, lowering the risks of infection[13], hypotension, coagulopathy[14] and catheter-based thrombosis[15]. However, cooling through the vessel walls dissipates cooling power via thermal spread. It is unclear whether thermal spread is a beneficial or detrimental side-effect of vessel cooling. As an emerging technique, the effectiveness and limitations of extravascular cooling are yet to be fully characterized.

Computational simulations are a useful tool to understand brain cooling requirements and predict the performance of novel cooling methods without the complications of a clinical study. Computational heat transfer models on brain temperature compared blood-based brain cooling (chilled blood from whole-body hypothermia) versus brain/scalp cooling with ice helmets. Simulations revealed that not only does chilled blood circulation lower brain temperature to a greater extent than ice helmets, but also uniformly cools deep brain tissue[16]. This result clearly highlights the potential for blood-based brain cooling methods in terms of cooling penetration and magnitude. In studies of extravascular carotid cooling, investigators modeled cooling of the entire carotid artery and neck tissue to for possible brain hypothermia. In one work, carotid temperature was reduced by 0.13 ˚C after 60 mins of neck cooling (including the skin and 15 cm

of the common and internal carotid) at normal blood flow conditions[17]. By contrast, another computational work simulating interstitial carotid coolers showed a 2.8 ˚C reduction in carotid temperature and a subsequent 3.1 ˚C drop in brain temperature, though simulated with smaller diameter vessels than typical (instead of a diameter of ~6 mm for a typical adult CCA, used 2.5 mm)[18]. Key differences in these works are: the layer of neck tissue that dissipate cooling (a thermal resistance to/near the vessel) and the simulated carotid diameter. All of these factors are critical in assessing the potential of extravascular blood cooling, because heat capacity (i.e. total tissue being cooled), flow rate (which is quadratic with vessel radius), and effective cooling power directly impact final blood temperature.

In this work, we seek to understand the impact of direct cooling of the common carotid arterial wall (no interfacial neck tissue) on flowing blood temperature and downstream vasculature. For this purpose, a computational model of an adult common carotid artery (CCA) was developed. The model is distinct from existing works in literature as it simulates direct vascular cooling, and incorporates predicted thermal constraints posed by human physiological/clinical limits for an extravascular technique (e.g., length of CCA that can surgically be exposed, nontoxicity of application temperature, practical duration of use, etc). Two extravascular cooling conditions were explored: 1) carotid cooling via open surgery of the neck, and 2) percutaneous cooling with minimal incisions. At these cooling conditions, our primary aim was to understand the levels of blood cooling achieved from the extravascular cooling. A secondary aim was to characterize the thermal spread and transient cooling response in the artery, and determine whether it is beneficial for blood cooling. If possible, a tertiary aim was to identify design parameters necessary for developing the ideal, minimally invasive

percutaneous cooling probe, keeping in mind possible downstream applications such as brain cooling.

4.3 Nomenclature

Acronym/Symbol	Definition
T_p	(Model) Applied extravascular temperature / (Experimental) extravascular probe temperature
L_p	Length of vessel cooled extravascular technique
t_{sat}	Saturation time
T_{blood}	Blood temperature
$\dot{V}_{avg}$	Average volumetric blood flow rate
P_{blood}	Blood pressure
h	Heat transfer coefficient
k	Thermal conductivity of tissue
q_m	Metabolic heat generation of tissue
r_{cca}	Internal radius of carotid artery
t_{cca}	Total wall thickness of carotid
$\dot{Q}$	Heat flow
l_{cca}	Length of carotid, prescribed in model
Z	Axial direction along carotid artery
CCA	Common carotid artery
$\|\Delta T\|$	Absolute change in outlet blood temperature

4.4 Methods

Computational models were developed in-house for the common carotid arteries (CCA) of 1) an adult Sprague Dawley rat, and 2) an adult human, using Solidworks (Dassault Systemes, France), and COMSOL Multiphysics (COMSOL, Sweden). Past experimental work performed with rodents informed the rat computational model inputs, initial states, and boundary conditions. The model was supplemented with relevant physics pertaining to the cooling

conditions of interest. Model outputs were validated with the experimental data. Following validation, the rat model physics and boundary conditions informed the custom-built model of a human CCA. All inputs were scaled appropriately for human physiology.

4.4.1 Governing physics

A 3-dimensional, transient model of the CCA was used to simulate the effects of extravascular cooling on temperature profiles in the blood and vessel. The CCA is the key artery supplying blood to the brain, and understanding its response to extravascular cooling is key to pursuing further studies in brain cooling with the chilled arterial blood. The CCA was modeled as a straight, rigid, tubular cylinder (Figure 4.1). The extravascular cooling applied was modeled as a constant-temperature boundary condition on sections of the vessel wall, assuming perfect contact. The cooled surfaces were the top hemisphere of the artery, or a cuff style that cools the artery all around its circumference.

The following mathematical formulas were used to model the artery. The modified Pennes bioheat equation (linear transient bioheat transfer equation[19]) can be expressed as the conduction equation with an additional term for an external heat source. This was used to model the extravascular (conduction-based) cooling that was applied onto the vessel (Equation 4).

Equation 4

$$\rho C_p \frac{\partial T}{\partial t} = \boldsymbol{k\nabla^2 T} + C_{p,b}\omega_b(T - T_b) + q_m + \boldsymbol{q}$$

Here ρ, C_p, and k are the tissue density, heat capacity, and thermal conductivity, respectively. ω_b is the effective blood perfusion parameter, $C_{p,b}$ is the blood heat capacity, T is the local tissue temperature, T_b is the blood temperature, $\mathrm{q_m}$ is the metabolic heat generation rate of the tissue, q is the external heat being applied, and t is time. The boundary conditions were applied at

specified locations on the carotid model, with active cooling regions of the artery modeled as "constant temperature" (Equation 5), sections open to air and passive flow as "convection" (Equation 6), and the rest as "insulation" (Equation 7).

Equation 5

$$T = T_{probe}$$

Equation 6

$$-\boldsymbol{n} \cdot \boldsymbol{q} = h(T_{\text{ext}} - T)$$

Equation 7

$$-\boldsymbol{n} \cdot \boldsymbol{q} = 0$$

Arterial flow was modeled as uniform, laminar, and fully developed. This assumed that the pulsatile flow that is observed in live cardiovascular systems may be averaged to a mean flow rate for simplicity in the model (see Methods Section 4 below). The laminar flow was coupled to the extravascular heat transfer using non-isothermal multiphysics in COMSOL Multiphysics vr. 5.6 (COMSOL, Sweden). All model parameters such as flow rate, vessel geometry, and pressure were varied to simulate different size vasculatures and thermal conditions. The following is a list of all assumptions made in developing the models for both the rat and human scale vessels.

- The carotid is simplified as a straight, smooth, rigid tube.
- Vasoconstriction, vasodilation, or changes in perfusion of the vessel are not considered.
- Perfect contact with extravascular cooling mechanism, i.e. perfect constant temperature boundary condition.
- Convection cooling boundaries are referenced to experimentally measured temperatures in prior rat work
- Segments of the vessel that are not being cooled (either by conduction or convection) are perfectly insulated, i.e. no heat transfer to surrounding neck tissue.
- The extravascular cooling is perfectly insulated to neck tissue.
- Atmospheric pressure = 1 atm.
- Applied a steady, uniform, and fully developed blood flow, rather than pulsatile flow as is in real-life.
- Material properties (i.e. thermal conductivity) are assumed constant with temperature. This is because 1) projected changes in temperature are small (< 10 ˚C) and are not

expected to cause a great difference in material properties, and 2) because there are complex surface conditions that can't be modeled (i.e. moisture) that also affects effective material property.

- For rats, not all tissue material properties or flow dynamics are known. In such cases, human values were substituted.

4.4.2 Model data extraction

Models were solved using the finite element method (FEM), and temperature, pressure, and flow data (T, P, $\dot{V}$) were recorded from the inlet, outlet, midline, and surface locations of the carotid (Figure 4.1). As a time-dependent study, data was also recorded at various time intervals.

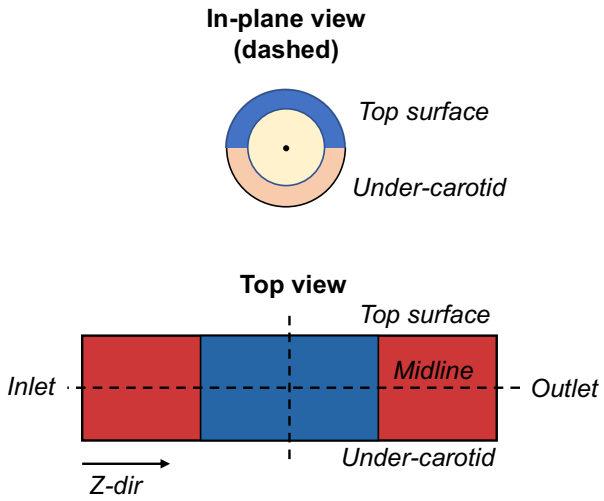

Figure 4.1 Locations for T, P, and $\dot{V}$ measurements. Primary results are collected along the midline, surface, and outlet locations.

4.4.3 Rat computational model

A rat scale model was created first to validate the modeling approach with past experimental work. In prior work, we introduced an extravascular blood cooling device ("cooling probe", "probe") and surgical technique that cooled the blood and brain tissue in rodents (-4.19 ± 3.15 ˚C/hr at a probe temperature of 0 ˚C)[20]. This technique was uniquely delivered through a long cooling tip which contacted the carotid through a long incision in the skin. No superficial neck cooling or implantation of an interstitial device in the neck muscles was required.

Physiological inputs (i.e., initial temperature, flow rate) and boundary conditions in the present rat scale model were derived from this past experimental work (methods for the experimental measurements is described in the following section).

The boundary conditions for the "open neck surgery" rat model are as follows. Based on experimental observations, a slight air gap of approximately 32 ˚C was imposed on the under-carotid surface in the model, and the top surface fringes adjacent to the extravascular cooling zone were modeled as exposed to ambient air (20 ˚C). Natural convective transfer to the environment was assumed at these exposed surfaces, except for the extravascular cooling zone (constant *T* condition). The total boundary conditions for the rat scale model are summarized in Figure 4.3. A natural convection heat transfer coefficient (*h*) of 25 W/m^2/K was applied based on literature[21]. Flow conditions were taken as the mean volumetric flow rate collected from PCMRI measurements (Table 4.1), applied as steady laminar flow in this model. The rat open surgery model was validated by comparing its under-carotid temperature values with experimental measurements (see next section) at the same location. Following successful validation, the initial/boundary conditions were applied to a human scale carotid model.

4.4.4 Methods for experimental rat blood flow and temperature measurements

The following research protocols (PRO8910, PRO9557) were approved by the University of Michigan's Institutional Animal Care and Use Committee. Healthy adult Sprague Dawley rats of both sexes (n = 20) were used to gather physiological input parameters on flow characteristics and temperature for the computational model. Phase contrast magnetic resonance imaging (PCMRI) was used to non-invasively measure volumetric blood flow in key vasculatures (PRO8910, n = 10, male, mean weight = 513.6 g ± 31.2), These measurements were used to create the rat model in this study. Rats were anesthetized with 1.25–2% isoflurane in 1 L/min of

oxygen Animals were imaged in the supine position at 7 T field strength using a Direct Drive console (Agilent Technologies, Santa Clara, CA) and a 60 mm inner diameter transmit-receive volume coil (Morris Instruments, Ontario, Canada). Field of view was $(60\ mm)^2$ and resolution $(117\ \mu m)^2$. See Figure 4.2 and Table 4.1 for flow rate measurements.

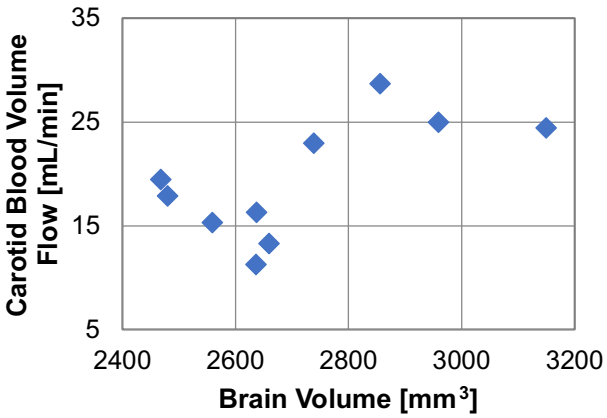

Figure 4.2 PCMRI evaluation of CCA blood flow rates in vivo (n = 10).

Table 4.1 Mean data from PCMRI (n = 10) scans. Body weight reported is weight measured on day of scan.

Vessel	**Vessel Area [mm²]**	**Velocity [cm/s]**	**Volumetric Flow Rate [mL/min]**
Jugular	3.35 ± 0.3	8.9 ± 1.2	20.9 ± 3.1
Carotid	1.1 ± 0.1	25.8 ± 2.5	19.5 ± 1.8
Sex	**Brain Volume [mm³]**	**Body Weight [g]**	**Arterial Flow/Brain Volume [1/min]**
Male	2714.5 ± 217	514 ± 31	7.12 ± 1.7

Temperature was measured in the remaining subset of rats (PRO9557, n = 10, male and female, mean weight = 323 g ± 67.8) at the rectal (core), under-carotid, and intra-jugular locations by surgically exposing and cooling the left CCA artery ("open neck") with the cooling probe. Under-carotid temperature was measured experimentally in lieu of intracarotid blood temperature because rodent carotids are narrow and flow blood at high pressures. These factors prohibited reliable thermocouple placement in rodent carotids without causing severe blood loss

in the animal. The complete set of experimentally measured parameters, initial conditions, and rat material properties (i.e. initial body temperature, probe length, applied probe temperature, etc) are summarized in Table 4.2. Specific methods for the open neck surgery on rodents, measurement tools/data collection techniques, and extravascular cooling probe design are described in Lee et al[20]. The core and jugular temperatures are not reported.

Table 4.2 Input values for rat open neck model.

Physical constants		**Initial conditions**		**Variable parameters**	
f^b	350 [1/min]	$T_{vessel}{}^a$	32 [°C]	T_p	0 [°C]
$r_{cca}{}^a$	0.594 [mm]	T_b	36.5 [°C]	L_p	8.6 [cm]
$\dot{V}_{avg}{}^a$	19.46 [mL/min]	T_{amb}	20 [°C]		
q_m	0 [W/m^3]	P_{amb}	1 [atm]		
$l_{cca}{}^a$	1.5 [cm]				
$t_{cca}{}^a$	80 [um]				
$k_{cca}{}^c$	0.46 [W/m/°C]				
$k_b{}^c$	0.52 [W/m/K]				
ρ^c	1102 [kg/m^3]				
$\rho_b{}^c$	1050 [kg/m^3]				
$C_{p,b}{}^c$	3617 [J/kg/K]				
$C_p{}^c$	3306 [J/kg/K]				
ω_b	0 [1/s]				
$T_{core}{}^a$	36.5 [°C]				
$P_{blood}{}^d$	130 [mmHg]				

Values were gathered both experimentally[a] and from literature[b, c, d]. For physiological parameters that could not be found for rodents, human values were substituted. All other values are prescribed as per model assumptions and control variables.

[b] Azar et al 2011

[c] IT'IS Foundation

[d] Olmstead et al 1957

4.4.5 Human model

For human scale models, two extravascular cooling conditions were investigated, 1) open neck surgery as experimentally demonstrated with rodents and re-created in the computational model above, and 2) minimally invasive percutaneous cooling conditions as would be ideal to perform on human patients. For both cases, transient simulations were performed, and a non-

pulsatile, steady blood flow and pressure was assumed for ease of computation. Figure 4.1 depicts the layout of the boundary conditions per cooling condition. Temperature, pressure, and flow data (T, P, $\dot{V}$) were collected as described in Figure 4.1. Table 4.3 contains the initial conditions and parameters for a human model for both cooling conditions. Human model parameters were limited to practically possible values, such as the cooling length (L_p), of which up to 6 cm was deemed surgically possible to implement in a clinical setting (out of $l_{cca,}$ which is the total length of the common carotid itself). Ranges of T_p were also constrained to temperatures that could be reasonably implemented in real-life extravascular cooling probes while inserted in warm tissue.

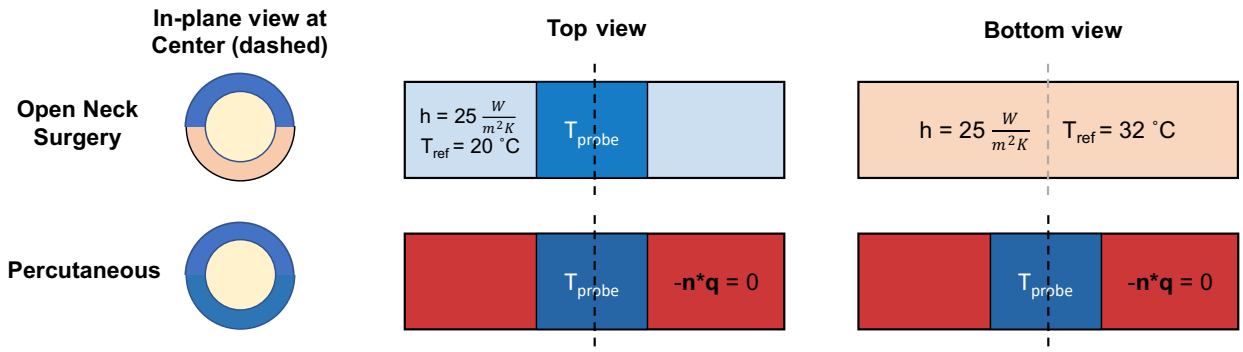

Figure 4.3 Boundary conditions per delivery type. Constant temperature conditions apply in the center where the cooling is applied, with convection cooling on the fringes and bottom surface (top row) for open surgery and insulation for percutaneous (bottom row). The terminal ends of the carotid are insulated for both conditions.

*Table 4.3 Input values for human percutaneous model. *For open neck model, all values are the same except initial vessel temperature, which is assumed to be 32 ˚C.*

Physical constants		**Initial conditions***		**Variable parameters**	
f [e]	80 [1/min]	T_{vessel}	36.5 [˚C]	T_p	-10 to 5 [˚C]
r_{cca} [a]	3.05 [mm]	T_b	36.5 [˚C]	L_p	1 to 6 [cm]
$\dot{V}_{avg}$ [f]	7.99 [mL/s]	T_{amb}	20 [˚C]		
q_m [b]	180.2 [W/m^3]	P_{amb}	1 [atm]		
l_{cca} [d]	12.4 [cm]				
t_{cca} [g]	1.6 [mm]				
k_{cca} [c]	0.46 [W/m/K]				
k_b [c]	0.52 [W/m/K]				

ρ[c]	1102 [kg/m^3]
ρ_b[c]	1050 [kg/m^3]
$C_{p,b}$[c]	3617 [J/kg/K]
C_p[c]	3306 [J/kg/K]
ω_b	0 [1/s]
T_{core}[a]	36.5 [°C]
P_{blood}[d]	120 [mmHg]

Values from the following sources (a-g). All other values are prescribed as per model assumptions and control variables.

[a] Ku et al 1985 [b] Wang et al 2007
[c] IT'IS Foundation [d] Choudhry et al 2016
[e] Perktold et al 1991 [f] Uematsu et al 1983
[g] Hodges et al 1994

Pulsatile flow rates and pressure waveforms:

Although most simulations in this work were run with mean steady flow, for verification of our assumptions a pulsatile flow was briefly simulated for human scale models (a rat's pulsatile flow is not well documented in literature, and was ultimately considered irrelevant to this study). The pulsatile flow was modeled as a fully developed flow at inlet with a corresponding pressure waveform. To simulate a typical pulse waveform for a healthy heart rhythm[25], the following piecewise function was devised.

Equation 8

$$\begin{cases} 0.66\dot{V}_{avg}[1 + 1.5\,sin\,4\pi fx] & 0 < x < 0.2 \\ 0.66\dot{V}_{avg}[1 + 0.2\,sin\,5.5\pi fx] + 0.33x10^{-8} & 0.2 \leq x < 0.3 \\ 0.66\dot{V}_{avg} - 2x10^{-7} & 0.3 \leq x < 1 \end{cases}$$

Here $\dot{V}_{avg}$ is the average volumetric flow rate for an adult (7.99 mL/s)[28], f is the heartbeat rate (set to 80 beats/min), and x is time in seconds. Equation 9 was created to simulate healthy blood pressure[30]. The pulse wave and corresponding pressure waveform are depicted in Figure 4.4.

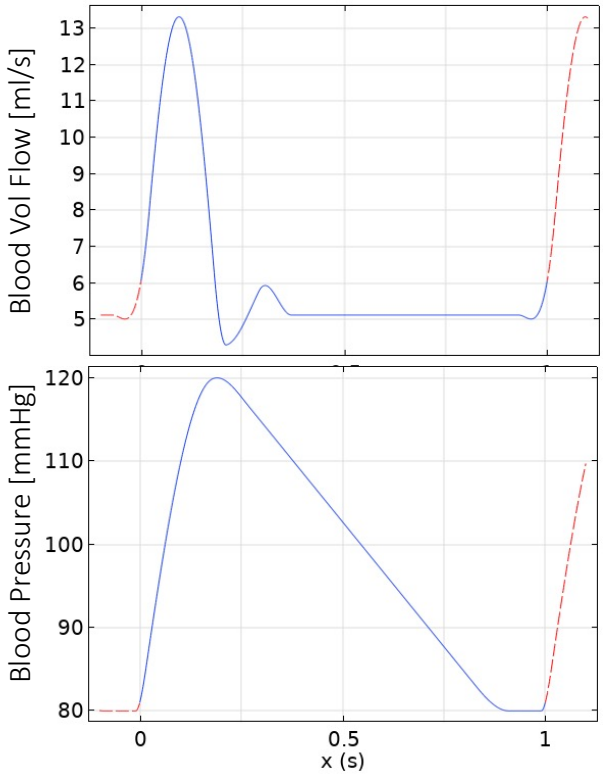

Figure 4.4 Pulsatile flow rate in carotid artery (top) and corresponding blood pressure waveform (bottom).

Equation 9

$$\begin{cases} P_{blood,dia}[1 + 0.5\,sin\,2\pi f x] & 0 < x < 0.2 \\ -8000x + P_{blood,sys} + P_{blood,dia}[0.16\,sin\,0.4\pi f] & 0.2 \leq x < 0.9 \\ P_{blood,dia} & 0.9 \leq x < 1 \end{cases}$$

Here $P_{blood,dia}$ (80 mmHg) and $P_{blood,sys}$ (120 mmHg) are the diastolic and systolic blood pressure levels for a healthy adult human, respectively. Units of time are in seconds. Pulsatile flow/pressure modeled with Equation 8 and Equation 9, when compared with averaged constant flow, resulted in near similar temperature profiles (Figure 4.5). Therefore the assumption of constant flow was applied for the remainder of the simulations.

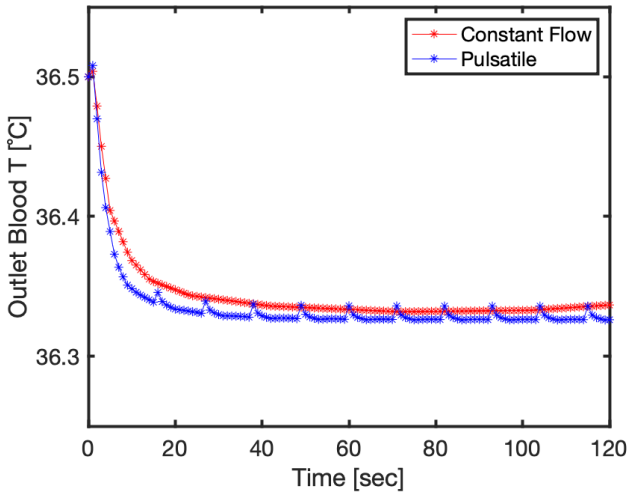

Figure 4.5 Comparison of pulsatile flow vs constant flow conditions result in minimal differences in outlet blood temperature in a sample trial.

4.4.6 Other metrics

From the model outputs (T, P, $\dot{V}$), the following were calculated to better understand the heat transfer response of the cooling conditions.

Induced change in outlet blood temperature ($|\Delta T|$*):*

Change in outlet blood temperature (midline outlet of the carotid artery, $Z = l_{cca}$) was defined as the difference in the blood temperature at a specified time point in the transient study relative to the initial (Equation 10).

Equation 10

$$|\Delta T| = T_{outlet}(t) - T_{outlet}(t = 0)$$

Thermal spread:

Thermal spread was defined as the length of carotid artery that experiences a temperature change of ≥0.5 ˚C from the initial vessel temperature. The spread was calculated for both sides of the cooling zone on the carotid. The CCA is modeled at a length greater than the L_p to assess levels of thermal spread.

Saturation:

Saturation time was defined as the time to reach quasi-steady state in outlet blood temperature. Specifically, it was defined as at least ten consecutive output temperature values of ≤ 0.05% change from the previous value. In cases where saturation time could not be easily determined from the transient model (due to computational memory/runtime constraints), a time-invariant model was used to find the steady state temperature.

Sensitivity analysis:

Sensitivity (s) to the variables of interest (L_p and T_p) was calculated with the desired goal of minimizing the outlet blood temperature. Equation 11 was used to calculate sensitivity of outlet blood temperature to changes in a parameter.

Equation 11

$$s = \left. \frac{\Delta J}{J} \right/ \frac{\Delta p}{p} [\%/\%]$$

Here J is the outlet blood temperature (or its difference from core temperature), and p is an input variable (the parameters L_p and T_p). Note that in this work, p was not perturbed with a small change. Instead it was incremented by a specified step size (i.e., 1 cm increase in L_p).

4.4.7 FEM techniques

The models were compiled and solved using the 3D FEM solver in COMSOL, which allows coupled bioheat transfer and laminar flow physics. The mesh size for each model type (rat, human) was determined by varying the mesh refinement feature into progressively denser meshes, with concentrated nodes around boundaries, until the solution at the outlet of the carotid did not vary by more than 2% at the target run time. The resulting mesh had 135451 total elements in the rat models, and 232736 elements in the human models. Once mesh independence was established, the same mesh was used for all computations. Finer meshes were not pursued

due to increasing computational load on the computer system and solver. The solvers were run on a computer with a Intel Xeon E-2236 CPU 3.40GHz processor with 32 GB RAM.

4.5 Results

4.5.1 Rat model: validation of model with prior rat experiments

To assess the accuracy and quality of the rat carotid model created with experimental input terms, the under-carotid temperature from the model was compared with the under-carotid temperature measurements performed on live rats (n = 10). Under-carotid vessel temperature was used in lieu of intracarotid blood temperature for the reasons described in Section 4.4.4. Figure 4.6 depicts the computationally generated under-carotid temperatures, alongside the mean under-carotid temperatures measured across animals. This simulation was performed with steady, averaged flow from experimental measurements, and closely adhered to the experimental results (R^2 =0.75, $p < 0.001$). On the accuracy of results for mean steady blood flow versus pulsatile flow, no clear data was available in literature to allow for a pulsatile simulation. However, we expect no significant difference in the results based on the quality of fit in experimental and computational results with the steady flow input.

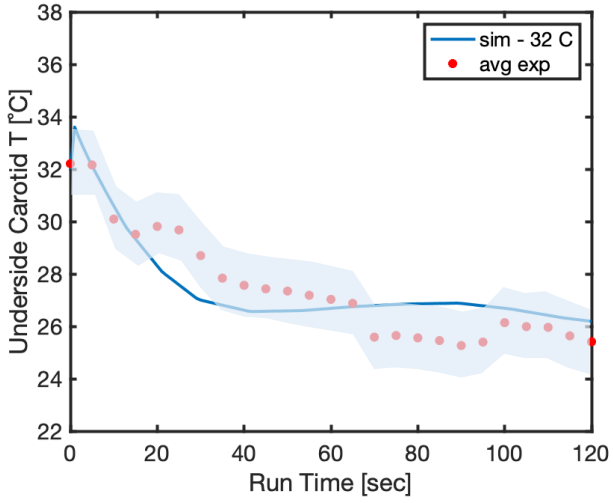

Figure 4.6 Comparison of experimental vs simulational results from rat probe cooling at T = 0 ˚C. Experimental values are averaged from n = 10 rats. Filled area (blue) indicates 95% confidence interval of the experimental data. R^2 =0.75, p-value < 0.001.

4.5.2 Human model: cooling performed with open neck conditions

Saturation time:

Saturation time (time to reach quasi-steady state) for all models were extracted to assess the magnitudes of |ΔT| achievable within a reasonable time frame (constrained by clinical and practical needs). In open neck models, saturation was often not reached, or required at least 600 s. Therefore results from the open neck condition continued to fluctuate slightly within a 2 ˚C window past the initial 600 s (Figure 4.7). In such cases, steady state values were found using stationary (time-invariant) simulations, which resulted in a monotonic decrease in blood temperature with T_p (Figure 4.8).

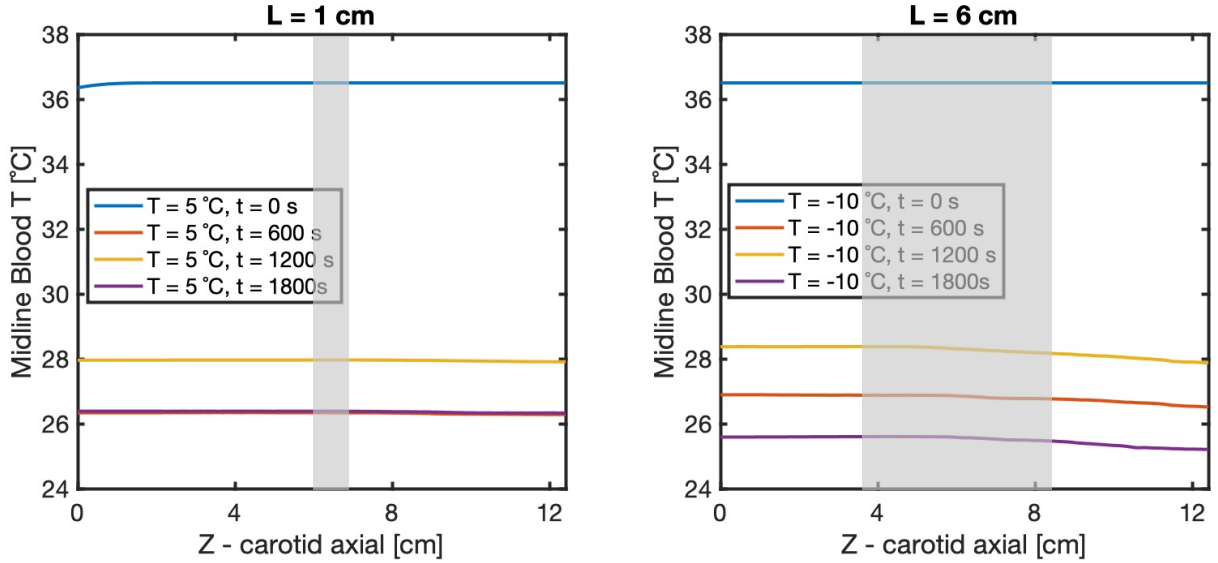

Figure 4.7 Midline blood temperature at open surgery boundary conditions, as measured at 10 min intervals. There is some fluctuation in the blood temperature with time as convection dominates and warm blood continues to enter at the inlet, leading to instances of nonmonotonic activity with T_p. Nonetheless, at steady state simulations, blood temperature is monotonic with T_p. Gray indicates area with extravascular cooling at constant temperature.

Changes in outlet blood temperature from CCA cooling:

Change in outlet blood temperature (|ΔT|) was assessed by calculating a relative difference between initial blood temperature (36.5 ˚C) and final outlet blood temperature ($t = t_{final}$, $Z = l_{cca}$). In open neck surgery conditions, the model resulted in |ΔT| ≥ 9 ˚C within 5 mins of run time for all variable combinations of L_p and T_p (Figure 4.8). At steady state (using time-invariant simulations), |ΔT| monotonically increased with T_p but was independent of L_p.

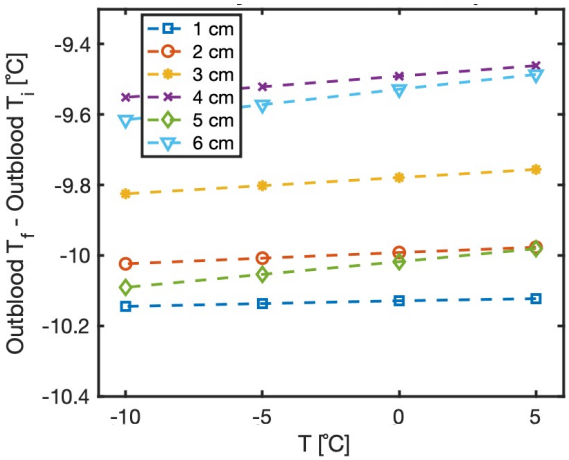

Figure 4.8 Using open surgery conditions, blood temperature decrease at carotid outlet at the corresponding L_p and T_p using a steady state model (time invariant). No monotonic dependence on L_p.

Midline T vs Z:

For open neck conditions, blood temperature was not highly dependent on L_p. However, at steady state, blood temperature monotonically decreased with lower T_p (Figure 4.9). The magnitude of blood temperature change along the midline ($Z = 0$ *to* l_{cca}) was < 0.5 ˚C, indicating greater dependence of final blood temperature on convection cooling and its thermal spread to all areas of the vessel (|ΔT| at $Z = 0$ was > 8 ˚C) rather than on conduction cooling (|ΔT| from $Z =$ *upstream cooling edge* to l_{cca} was < 0.5 ˚C).

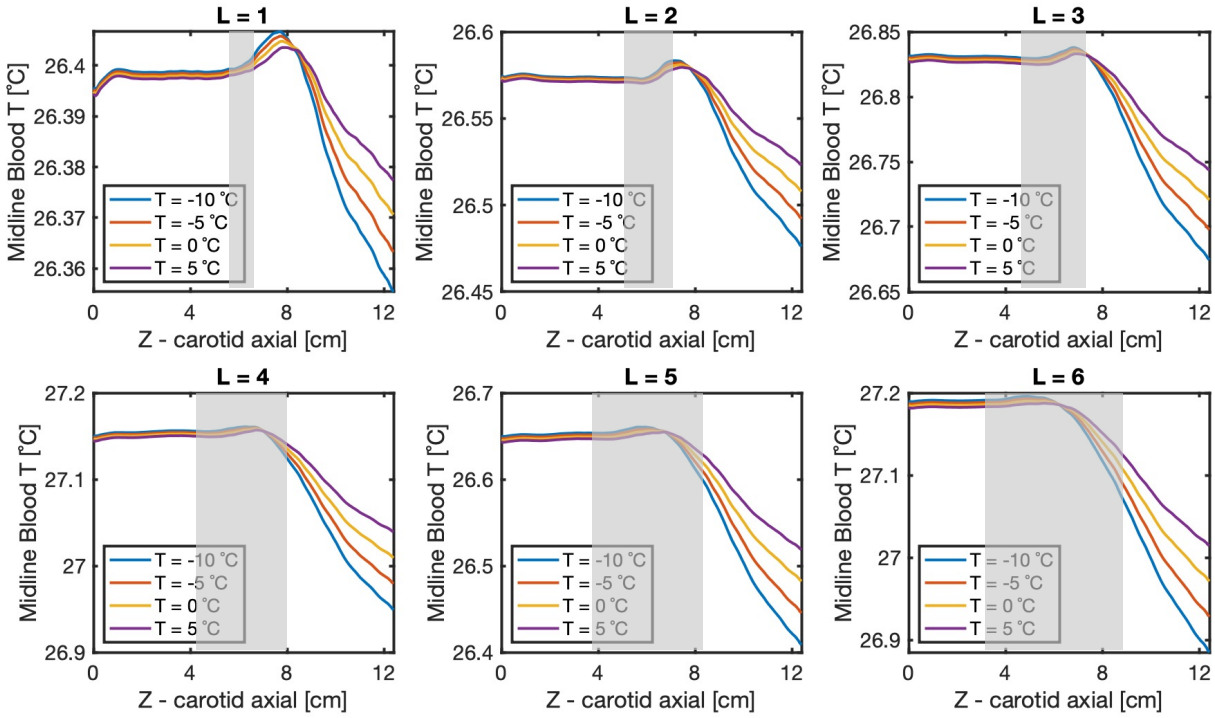

Figure 4.9 Midline blood temperature at open neck conditions run with a time-invariant model (steady state). Midline temperature depends little on the conductive cooling and corresponding cooling length, but does monotonically decrease with applied temperature. Gray area indicates active extravascular cooling zone.

Thermal spread on carotid artery:

For the open neck condition, thermal spread was detected in the whole length of the carotid artery ($Z = 0$ to l_{cca}). There was a significant drop in midline blood temperature (from normothermia) across the whole of the modeled artery that was much greater than the temperature change across just the extravascular cooling zone (Figure 4.9).

4.5.3 Human model: cooling performed with percutaneous conditions

Saturation time:

Saturation was detected in percutaneous models at t_{sat} ~15 sec for all L_p and T_p, with the greatest change in temperature occurring in the first several seconds (Figure 4.10). Past the saturation point, any fluctuations in the output temperature were near trivial (< 0.1 °C change).

Figure 4.11 shows that percutaneous cooling at the edge cases of L_p and T_p all resulted in near identical outlet blood temperature and midline blood temperature traces past the saturation point.

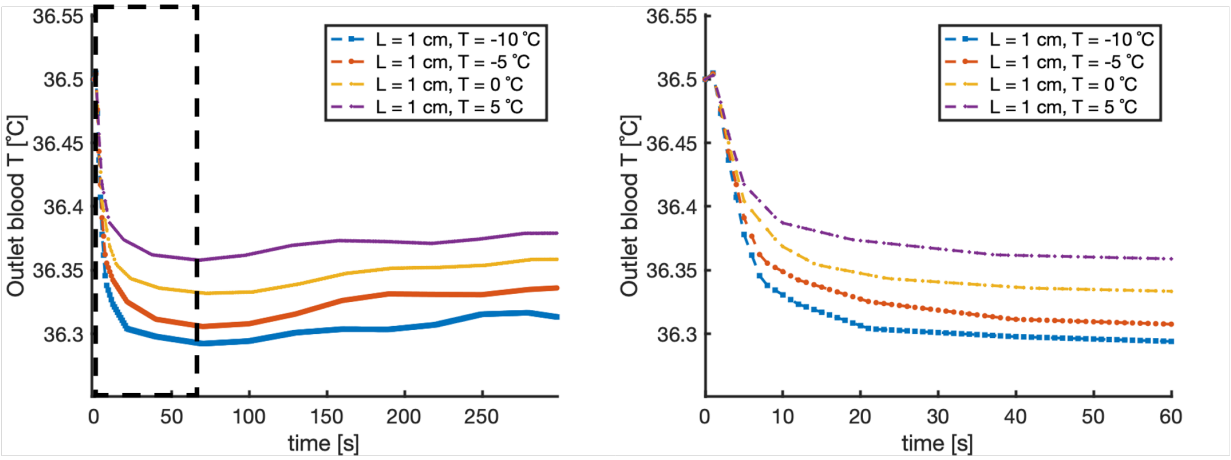

Figure 4.10 Outlet blood temperature with percutaneous cooling. Saturation occurs within 60 s of onset.

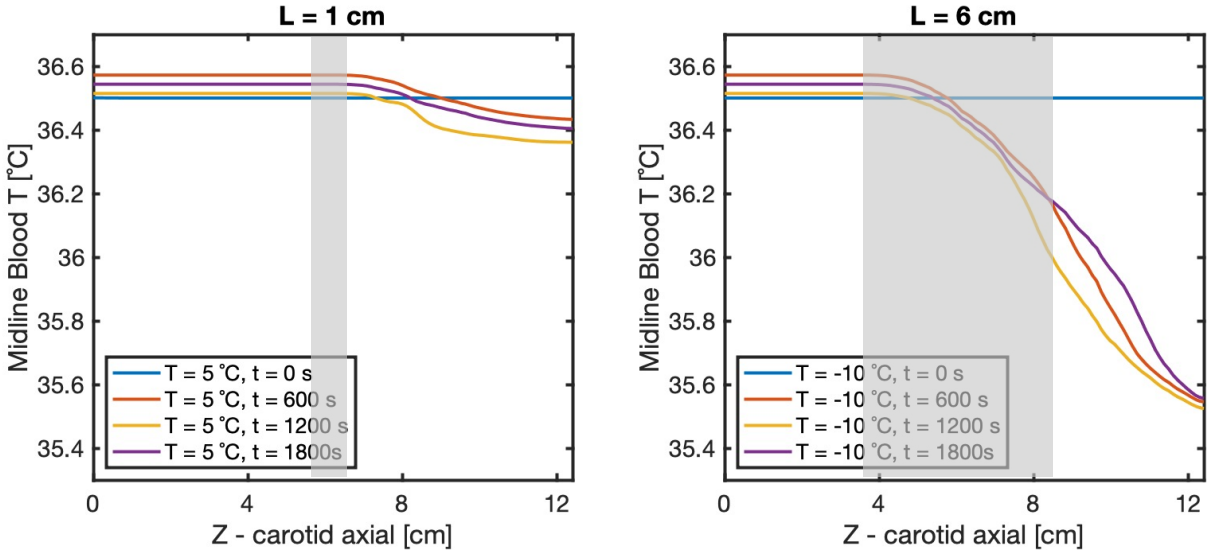

Figure 4.11 Midline blood temperature at percutaneous edge conditions. There are minor fluctuations with time, but the differences are near trivial (<0.1 °C). Note that for percutaneous results, after the first minute there is saturation in the results. Gray area indicates active extravascular cooling zone.

Changes in outlet blood temperature from CCA cooling:

For simulations with percutaneous conditions, the model reached a maximum |ΔT| of ~1 ˚C just at t = 300 s (effectively steady state) and at the maximum extravascular cooling zone length and minimum cooling temperature (Figure 4.12). Percutaneous results were monotonic for both L_p and T_p.

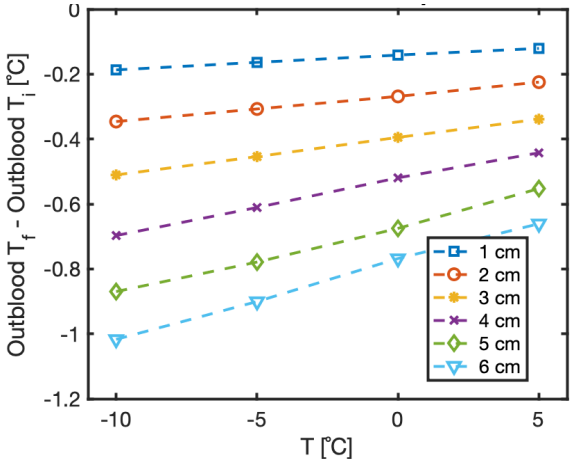

Figure 4.12 Using percutaneous conditions, outlet blood temperature achieved at corresponding L_p and T_p at t = 300 s (quasi- steady state). Monotonic with L_p and T_p.

Sensitivity analysis:

Sensitivity analysis of the human percutaneous model post saturation (the open neck model is less clinically impactful and thus omitted from sensitivity analysis) revealed greater dependence on L_p (maximum 6 % change with 1 cm step increase) than T_p (< 0.5 % change with 5 ˚C step increase) at their respective increments. No significant changes to perturbations in q_m were detected.

Midline T vs Z:

In the percutaneous model, L_p and T_p were stratified monotonically in a smooth decline. The extravascular cooling zone was the only heat sink in this condition and blood temperature immediately dropped following the cooling zone (Figure 4.13). The greater the L_p, there was greater decrease in temperature along Z.

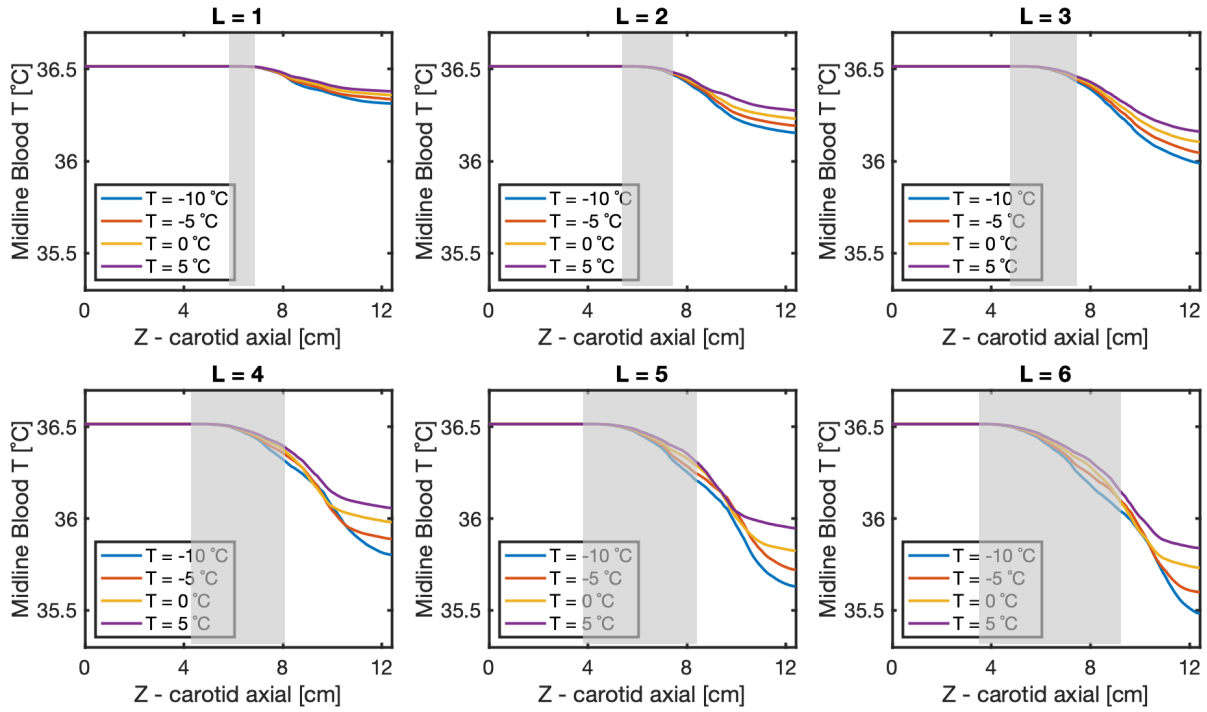

Figure 4.13 Midline blood temperature results at percutaneous conditions clearly depend on temperature and on cooling length. Data taken at t = 300 s. Gray area indicates active extravascular cooling zone.

Thermal spread on carotid artery:

In the percutaneous condition, thermal spread had clear differences between the upstream and downstream regions of the CCA (relative to the center cooling zone). Upstream, the thermal spread was relatively uniform across L_p and T_p, ranging 4.2 – 4.9 mm from the edge of the cooling zone. Downstream, the thermal spread ranged between 1.5 – 4.9 cm from the downstream edge of the cooling zone. For all $L_p \geq 3$ cm, downstream thermal spread stretched to the terminal end of the carotid independent of T_p. See Figure 4.14 for thermal spread in the edge cases (min/max L_p and T_p combination) for the percutaneous condition.

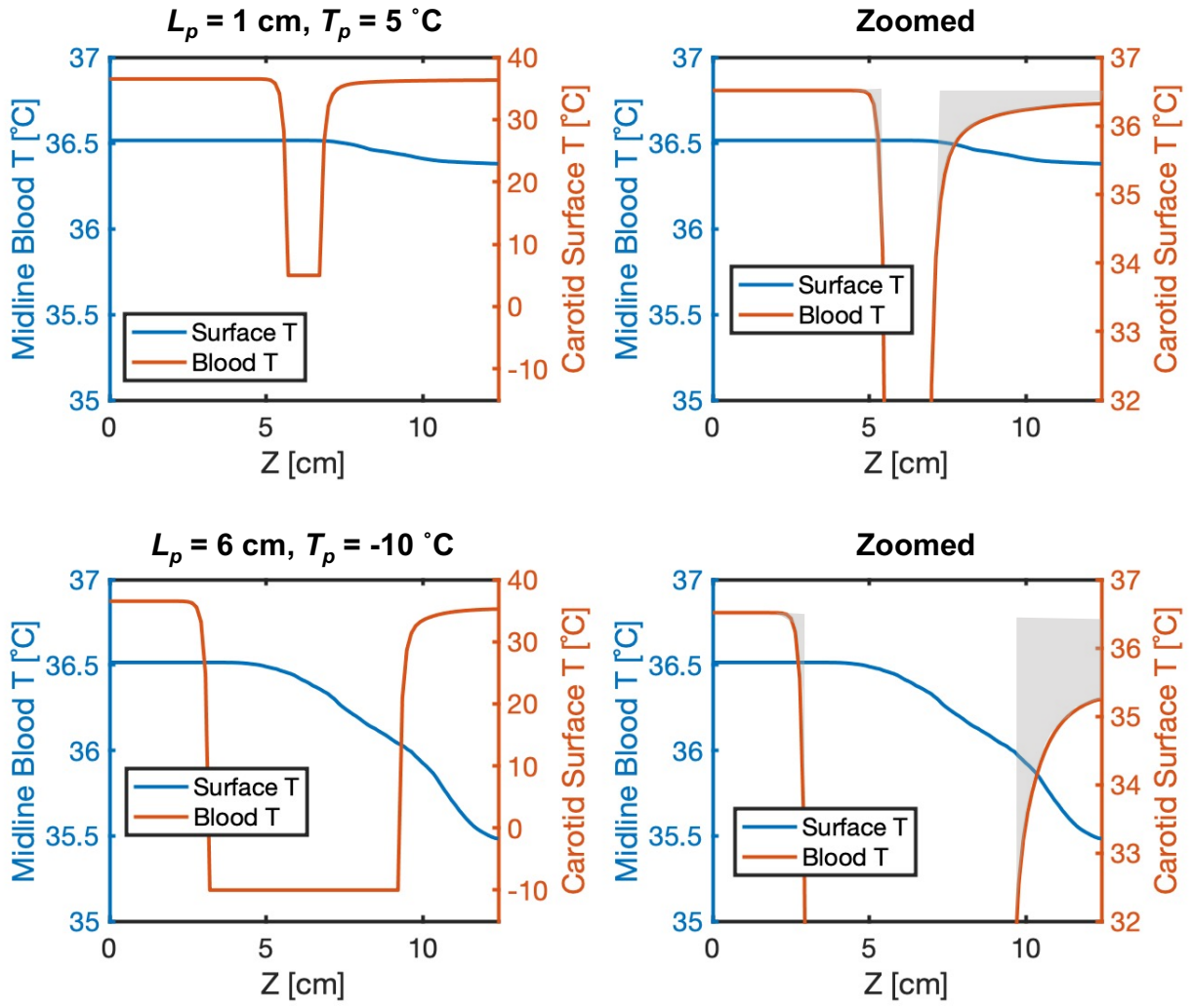

Figure 4.14. Thermal spread as measured for the edge cases in percutaneous cooling model. Right column depicts zoomed in plots of the left column, respectively. Gray areas highlight the regions of thermal spread.

To assess the impact of thermal spread on outlet blood temperature, a steady state simulation comparing k_{cca} vs $2k_{cca}$ was performed at the two edge cases. At {L_p = 1 cm, T_p = 5 ˚C}, simulations with conductivity of $2k_{cca}$ did not change upstream thermal spread length or area (area of cooled zone, or lower vessel surface temperature) relative to the k_{cca} runs, but increased downstream thermal spread area by ~20 %. This decrease in downstream vessel temperature led to an additional drop in outlet blood temperature by ~0.1 ˚C. At {L_p = 6 cm, T_p =

-10 ˚C}, doubling the vessel conductivity also did not affect upstream thermal spread length or area, but increased downstream thermal spread area by ~30 %, which resulted in an additional drop in blood temperature of ~0.6 ˚C compared to simulations at k_{cca}. For both edge cases, the additional blood cooling achieved was an approximate 50% increase in the |ΔT| at the corresponding L_p and T_p combination (See Figure 4.12 for |ΔT| at runs with k_{cca}).

4.6 Discussion

4.6.1 Rat model validation

Although rat scale model simulations with the open neck conditions correlated well with the experimental carotid measurements, key differences remain between real life conditions and the model. First, the natural convection imposed on the bottom surface of the carotid was referenced to a mean measured temperature (32 ˚C) from prior rat experiments. Our assumption of a thin, warm layer of air (at 32 ˚C) that separates the carotid underside from the rest of the neck tissue may not properly reflect real life conditions. For example, surface moisture levels affect h^{31} and k^{32}, but this was not accounted for in the rat experiments. Additionally, there could have been partial contact of the rat CCA with neck tissue, greatly increasing the effective thermal mass and potentially causing errors in transient analysis. Also, for the purpose of model validation, animal temperature measurements were averaged (as plotted in Figure 4.6). Yet, such data processing is not typical in animal work due to high variability across animals. In this case, using animals of a similar weight (thermal mass) helped to justify this averaging. Lastly, physiological measurements in animals tend to oscillate as part of a natural bodily rhythm; the averaging of the empirical data erased this phenomenon, and the oscillations are also not replicated in our simulations.

4.6.2 Extravascular blood cooling in context of clinical therapy

Clinically guided hypothermia levels (32-36 ˚C)[2] from normothermia (36.5 ˚C) require at least 1˚C drop in temperature. As such, we analyzed the feasibility of reducing CCA blood temperature by ~1-2 ˚C at the two different human extravascular cooling conditions discussed in this paper: open neck surgery and percutaneous delivery. In open neck surgery, the CCA was rapidly cooled by a large magnitude ($|\Delta T|$ of ≥ -9 ˚C at saturation), greater than the tentative goal of 1-2 ˚C drop. However, an independence of outlet temperature with L_p at steady state was noted, which implied that convection cooling from surrounding air was very impactful compared to the extravascular cooling. The change in temperature along the L_p was also trivial compared to the temperature difference at the CCA inlet from normothermia ($|\Delta T|$ at $Z = 0$ was > 8 ˚C, but $|\Delta T|$ along conduction cooling area was < 0.5 ˚C). The dominance of convective cooling over conduction cooling may be explained by several factors, including that the vessel's assumed thermal conductivity was merely 0.46 W/m/K, convection occurred over a much larger area than conduction, and the heat transfer coefficient prescribed was a relatively high number for natural convection (25 W/m^2/K)[21]. From an overview of literature modeling convection for air on tissue, we identified use of h values ranging from 8.3 to 29.3 W/m^2/K for dry and wet skin respectively[16]. As our blood vessel was moist, we considered h = 25 W/m^2/K from similar computational studies to be an appropriate value.

For percutaneous delivery, we reached a $|\Delta T|$ of ~ 1 ˚C, but only at the maximal cooling combination of L_p and T_p (6 cm, -10 ˚C). Here, only conduction cooling and insulation were considered, and the results showed outlet blood temperatures as monotonic with both L_p than T_p. The magnitude of change in outlet blood also followed with increasing cooling area, as expected. These results support our argument above on how convection dominates in open neck conditions,

overpowering the extravascular cooling with L_p. Sensitivity analysis also showed that percutaneous cooling depends more on L_p than T_p. This suggests a fundamental limitation on the feasibility of the percutaneous method in real life, considering the expected maximum length of carotid artery that can be safely accessed in clinics is around 6 cm. Saturation for percutaneous modeling was also achieved within the first minute of study. Therefore reaching lower outlet temperatures with greater application periods is highly unlikely. As a side note, this work modeled an aspect of thermoregulatory responses with metabolic rate, which decreases with levels of anesthesia in patients[33]. Model outputs showed there was minimal sensitivity of blood temperature to metabolic heat generation. Other factors of thermoregulation such as levels of vasoconstriction[34] were not studied in this work, but external heating provided by electric blankets or hot lamps were effective in maintaining core normothermia in rats[20] and similar efficacy in humans are predicted. This is because humans have greater thermal mass and body-to-brain mass ratios than rats. Thus we hypothesize that levels of CCA blood cooling will not change significantly with extended anesthesia in patients, which is beneficial as clinical guidance for hypothermia recommends 24+ hours of treatment[1].

Compared to ice helmets and neck cuffs which take at least 2 hrs for 1-3 ˚C of brain cooling[35], the percutaneous model demonstrated rapid loss of blood temperature in the first minute of application. Whether this rapid loss also results in rapid brain cooling to clinically beneficial levels (32-36 ˚C) requires further analysis. To estimate the impact of the percutaneous 1 ˚C drop in inflow blood on the adult brain, a simplified heat transfer analysis was performed. Equation 12 is a one-dimensional estimate of the temperature change in brain tissue assuming perfect heat transfer to the cooled blood. Thermal spread, brain metabolic heat generation, and blood perfusion were neglected for simplicity.

Equation 12

$$\dot{Q}_{brain} = \dot{Q}_{blood}$$

$$\dot{Q}_{brain} = m_{brain} C_{p,brain} \frac{\Delta T_{brain}}{\Delta t}, \quad \dot{Q}_{blood} = \dot{m}_{blood} C_{p,blood} \Delta T_{blood}$$

$$\Delta T_{brain} = \frac{\rho_{blood} \dot{V}_{blood} C_{p,blood} \Delta T_{blood} \Delta t}{m_{brain} C_{p,brain}}$$

Here, ρ_{blood} is blood density (1050 kg/m^3), $\dot{V}_{blood}$ is the average volumetric blood flow rate in the internal carotid (265 mL/min)[36], $C_{p,blood}$ is the specific heat of blood (3617 J/kg/˚C), ΔT_{blood} is the temperature change in the blood (assumed as -1 ˚C to match our percutaneous results), Δt is the run time, m_{brain} is the average mass of the adult male brain (1336 g)[37], and $C_{p,brain}$ is the specific heat of brain tissue (3630 J/kg/˚C). All tissue properties were sourced from IT'IS Foundation[23]. At a runtime of 300 s (equal to the percutaneous simulation time above), Equation 12 resulted in an approximate brain temperature change of -1.04 ˚C (-1.87 ˚C with CCA flow rate). Cooling both CCAs doubles the volumetric flow rate, and brain temperature drops approximately -2 ˚C. Note that Equation 12 is a linear approximation with time, but in real life there will conceivably be a saturation point for brain temperature. Future work will simulate heat transfer in the brain affected by the 1 ˚C drop in the CCA blood, as well as investigate the possible synergies of internal and external carotids (which head to the brain and scalp respectively) on overall efficacy of brain cooling.

Percutaneous models showed a thermal spread ranging 4-5 mm in length upstream of the cooling zone, which was driven by conduction in the vessel walls as blood flows in the opposite direction. The thermal spread is comparable with the experimentally measured thermal spread in electrocautery (4.4 mm)[38]. To account for the uncertainty with the k_{cca} value used in our simulations, as tissue conductivity is affected by moisture and temperature, we evaluated the

impact of k on our model in terms of thermal spread. A simple comparison of the model results with k_{cca} vs $2k_{cca}$ showed that outlet blood temperature is quite sensitive to k due to the increased cooling downstream of the vessel. Therefore, thermal spread increases the effective L_p and clearly aids in removing heat from the blood. As our model was set to 12.4 cm which is the length of the CCA before bifurcation[26], we cannot estimate thermal spread past the model's geometry.

4.6.3 Limitations of human scale models and possible sources of error

The human open neck model led to nonintuitive results for $|\Delta T|$, which were independent with increasing L_p. The primary cause of this independence was likely the convection boundary conditions that were used in the model, which dominated over any cooling effects from conduction. As a result, transient studies at this cooling condition often did not reach a saturation point during runtime (30 mins maximum due to system memory constraints) and continued fluctuations in the results were observed several minutes into the simulation (Figure 4.7). There are also inherent uncertainties in the material properties that were used in the model. Though the open boundary conditions were validated with rodent experiments, rodents are significantly different from humans in their cardiovascular system. Therefore, the physics transferred from the rat scale model may not be suitably accurate to describe the conditions in a real open neck surgery in a patient (such as initial underside CCA temperature). In addition, transient analysis of the human open neck model is susceptible to the same potential errors as the rat model it is derived from (i.e. possible contact with neck tissue increases heat capacity).

Yet another possible source of error in our model was the lack of an elastic, pulsatile CCA. Although we showed that averaged steady flow is a suitable simplification for pulsatile flow, pulsation could affect wall thickness and therefore conduction. Furthermore, autonomic

vasodilation from applied cold would affect flow conditions within the vessel. Additionally, error estimation of our human models cannot be performed without data from a clinical trial.

4.7 Conclusion

This work assessed the impact of an extravascular approach on outlet blood temperature of a human CCA at normothermia (36.5 ˚C). Analysis was performed on a simplified FEM model of a human CCA with steady uniform flow.

Extravascular cooling via open neck surgery resulted in $|\Delta T| > 9$ ˚C in 5 mins, while percutaneous cooling resulted in $|\Delta T| \sim 1$ ˚C at the maximum possible cooling. Though open surgery is highly effective in cooling, it is likely too invasive for clinical use. By contrast, percutaneous delivery is expected to be minimally invasive. However, the percutaneous approach is limited by the practical length of the average adult CCA that can be accessed. Cooling length was determined to be the most sensitive factor in lowering blood temperature in percutaneous models, both due to direct extravascular cooling and/or in combination with beneficial thermal spread along the vessel. In the context of brain hypothermia, we estimate that prolonged percutaneous cooling of both CCA will induce a 1-2 ˚C drop in brain temperature in the first several minutes. We also estimate that the brain will eventually reach a steady state point that may be warmer than chilled CCA blood temperature but within the recommendation of 32-36 ˚C[1].

In future work, we plan to conduct thermofluidic studies of the brain itself to more accurately estimate the sensitivities to input parameters and whether a 1 ˚C reduction in both common carotids is sufficient for clinical purposes. Furthermore, we plan to investigate possible technical improvements in real-life experimental extravascular systems to achieve greater heat removal (i.e. a steady power draw) from the blood while insulating from neck tissue. For

instance, our cooling probe design used with rats consists of several thermoelectric cooling elements. The number of thermoelectrics may be increased for higher cooling power. Once simulational and experimental brain cooling is satisfactorily established with percutaneous blood cooling, we will implement it for study of neuroprotection in common diseases. Disease models, such as ischemic stroke (reduced blood flow to the brain) or fevers (higher body temperature resulting in greater brain ΔT required for treatment) are of particular interest due to their medical merits.

This work informs in vivo extravascular blood cooling in the medical and technical arenas. Future improvements in the device and technique will inform clinical workflows for brain hypothermia. Finally, development of a percutaneous, minimally invasive cooling probe will add to existing thermal medical devices.

4.8 References

1. Callaway CW, Donnino MW, Fink EL, et al. Part 8: Post–Cardiac Arrest Care. *Circulation*. 2015;132(18):S465-S482. doi:10.1161/CIR.0000000000000262

2. Arrich J, Holzer M, Havel C, Müllner M, Herkner H. Hypothermia for neuroprotection in adults after cardiopulmonary resuscitation. *Cochrane Database Syst Rev*. 2016;2016(2). doi:10.1002/14651858.CD004128.pub4

3. Larsson IM, Wallin E, Rubertsson S. Cold saline infusion and ice packs alone are effective in inducing and maintaining therapeutic hypothermia after cardiac arrest. *Resuscitation*. 2010;81(1):15-19. doi:10.1016/J.RESUSCITATION.2009.09.012

4. Bernard SA, Gray TW, Buist MD, et al. Treatment of Comatose Survivors of Out-of-Hospital Cardiac Arrest with Induced Hypothermia. *N Engl J Med*. 2002;346(8):557-563. doi:10.1056/nejmoa003289

5. Deng H, Han HS, Cheng D, Sun GH, Yenari MA. Mild hypothermia inhibits inflammation after experimental stroke and brain inflammation. *Stroke*. 2003;34(10):2495-2501. doi:10.1161/01.STR.0000091269.67384.E7

6. Chihara H, Blood AB, Hunter CJ, Power GG. Effect of Mild Hypothermia and Hypoxia on Blood Flow and Oxygen Consumption of the Fetal Sheep Brain. *Pediatr Res 2003 545*. 2003;54(5):665-671. doi:10.1203/01.pdr.0000084115.31416.17

7. Polderman KH. Hypothermia, immune suppression and SDD: Can we have our cake and eat it? *Crit Care*. 2011;15(2). doi:10.1186/cc10080

8. Dietrich WD, Bramlett HM. The Evidence for Hypothermia as a Neuroprotectant in Traumatic Brain Injury. *Neurotherapeutics*. 2010;7(1):43-50. doi:10.1016/j.nurt.2009.10.015

9. Busto R, Dietrich WD, Globus MY, et al. The Importance of Brain Temperature in Cerebral Ischemic Injury. *Stroke*. 1989;20(8):1113-1114. doi:10.1161/01.STR.20.8.1113

10. Poli S, Purrucker J, Priglinger M, et al. Induction of cooling with a passive head and neck cooling device: Effects on brain temperature after stroke. *Stroke*. 2013;44(3):708-713. doi:10.1161/STROKEAHA.112.672923

11. Abou-Chebl A, Sung G, Barbut D, Torbey M. Local brain temperature reduction through intranasal cooling with the rhinochill device: Preliminary safety data in brain-injured patients. *Stroke*. 2011;42(8):2164-2169. doi:10.1161/STROKEAHA.110.613000

12. Duan Y, Wu D, Huber M, et al. New Endovascular Approach for Hypothermia with Intrajugular Cooling and Neuroprotective Effect in Ischemic Stroke. *Stroke*. 2020:628-636. doi:10.1161/STROKEAHA.119.026523

13. Woo JH, Lim YS, Yang HJ, et al. Factors associated with pneumonia in post-cardiac arrest patients receiving therapeutic hypothermia. *Am J Emerg Med*. 2014;32(2):150-155. doi:10.1016/j.ajem.2013.10.035

14. Polderman KH. Hypothermia and coagulation. *Crit Care*. 2012;16(S2):1-42. doi:10.1186/cc11278

15. Maze R, Le May MR, Froeschl M, et al. Endovascular cooling catheter related thrombosis in patients undergoing therapeutic hypothermia for out of hospital cardiac arrest. *Resuscitation*. 2014;85(10):1354-1358. doi:10.1016/j.resuscitation.2014.05.029

16. Keller E, Mudra R, Gugl C, Seule M, Mink S, Fröhlich J. Theoretical evaluations of therapeutic systemic and local cerebral hypothermia. *J Neurosci Methods*. 2009;178(2):345-349. doi:10.1016/j.jneumeth.2008.12.030

17. Li H, Chen RK, Tang Y, Meurer W, Shih AJ. An experimental study and finite element modeling of head and neck cooling for brain hypothermia. *J Therm Biol*. 2018;71(May 2017):99-111. doi:10.1016/j.jtherbio.2017.10.022

18. Wang Y, Zhu L. Targeted brain hypothermia induced by an interstitial cooling device in human neck: theoretical analyses. *Eur J Appl Physiol*. 2007;101(1):31-40. doi:10.1007/s00421-007-0451-6

19. Pennes HH. *Analysis of Tissue and Arterial Blood Temperatures in the Resting Human Forearm*. *J Appl Physiol*. 1948;1(2):93-122. doi:10.1152/jappl.1948.1.2.93

20. Lee CY, Crouch AC, Jha AK, et al. Extravascular Cooling of Blood Using a Concentrated Thermoelectric Cooling Probe. *J Med Device*. 2022;16(3):31004-31005. doi:10.1115/1.4054003

21. Dodde RE, Miller SF, Geiger JD, Shih AJ. Thermal-electric finite element analysis and experimental validation of bipolar electrosurgical cautery. *J Manuf Sci Eng Trans ASME*. 2008;130(2):0210151-0210158. doi:10.1115/1.2902858/462167

22. Azar T, Sharp J, Lawson D. Heart Rates of Male and Female Sprague–Dawley and Spontaneously Hypertensive Rats Housed Singly or in Groups. *J Am Assoc Lab Anim Sci*. 2011;50(2):175. /pmc/articles/PMC3061417/. Accessed April 18, 2022.

23. DATABASE » IT'IS Foundation. https://itis.swiss/virtual-population/tissue-properties/database/. Accessed June 29, 2022.

24. OLMSTED F, CORCORAN AC, PAGE IH. Blood Pressure in the Unanesthetized Rat. *Circulation*. 1951;3(5):727-729. doi:10.1161/01.CIR.3.5.727

25. Ku DN, Giddens DP, Zarins CK, Glagov S. *Pulsatile Flow and Atherosclerosis in the Human Carotid Bifurcation. Positive Correlation between Plaque Location and Low and Oscillating Shear Stress*. Vol 5.; 1985. doi:10.1161/01.atv.5.3.293

26. Choudhry FA, Grantham JT, Rai AT, Hogg JP. Vascular geometry of the extracranial carotid arteries: an analysis of length, diameter, and tortuosity. *J Neurointerv Surg*. 2016;8(5):536-540. doi:10.1136/NEURINTSURG-2015-011671

27. Perktold K, Resch M, Peter RO. Three-dimensional numerical analysis of pulsatile flow and wall shear stress in the carotid artery bifurcation. *J Biomech*. 1991;24(6):409-420. doi:10.1016/0021-9290(91)90029-M

28. Uematsu S, Yang A, Preziosi TJ, Kouba R, Toung TJ. Measurement of carotid blood flow in man and its clinical application. *Stroke*. 1983;14(2):256-266. doi:10.1161/01.STR.14.2.256

29. Hodges TC, Detmer PR, Dawson DL, et al. Ultrasound determination of total arterial wall thickness. 1994.

30. Xiao N, Humphrey JD, Figueroa CA. Multi-scale computational model of three-dimensional hemodynamics within a deformable full-body arterial network. *J Comput Phys*. 2013;244:22-40. doi:10.1016/J.JCP.2012.09.016

31. De Dear RJ, Arens E, Hui Z, Oguro M. Convective and radiative heat transfer coefficients for individual human body segments. *Int J Biometeorol 1997 403*. 1997;40(3):141-156. doi:10.1007/S004840050035

32. Elansari AM, Hobani AI. Effect of Temperature and Moisture Content on Thermal Conductivity of Four Types of Meat. *https://doi.org/101080/10942910701687519*. 2009;12(2):308-315. doi:10.1080/10942910701687519

33. Stevens WC, Cromwell TH, Halsey MJ, Eger EI, Shakespeare TF, Bahlman SH. The Cardiovascular Effects of a New Inhalation Anesthetic, Forane, in Human Volunteers at Constant Arterial Carbon Dioxide Tension. *Anesthesiology*. 1971;35(1):8-15. doi:10.1097/00000542-197107000-00005

34. Bindu B, Bindra A, Rath G. Temperature management under general anesthesia: Compulsion or option. *J Anaesthesiol Clin Pharmacol*. 2017;33(3):306. doi:10.4103/JOACP.JOACP_334_16

35. Qiu W, Shen H, Zhang Y, et al. Noninvasive selective brain cooling by head and neck cooling is protective in severe traumatic brain injury. *J Clin Neurosci*. 2006;13(10):995-1000. doi:10.1016/j.jocn.2006.02.027

36. Bogren HG, Buonocore MH, Gu W -Z. Carotid and vertebral artery blood flow in left- and right-handed healthy subjects measured with MR velocity mapping. *J Magn Reson Imaging*. 1994;4(1):37-42. doi:10.1002/JMRI.1880040110

37. Hartmann P, Ramseier A, Gudat F, Mihatsch MJ, Polasek W, Geisenhoff C. [Normal weight of the brain in adults in relation to age, sex, body height and weight]. *Pathologe*. 1994;15(3):165-170. doi:10.1007/S002920050040

38. Campbell PA, Cresswell AB, Frank TG, Cuschieri A. Real-time thermography during energized vessel sealing and dissection. *Surg Endosc Other Interv Tech*. 2003;17(10):1640-1645. doi:10.1007/S00464-002-8781-2/FIGURES/2

Chapter 5 Encoding of Thermosensation in the Layer V Sensory Cortex of Non-human Primates

5.1 Abstract

Background: Neural mechanisms for cold sensation and cold-induced anesthesia are important for developing non-opioid local analgesics and understanding of neuropathic diseases. Yet, coding of these mechanisms in the sensory cortex is not widely investigated. Prior studies have reported human subject scoring to imprecise cooling methods (e.g. ice, cold air) and lacked quantitative data on central nervous system (CNS) behavior to broad ranges of cold temperatures. The present work aims to identify the dynamic neural response to cutaneous thermal and tactile stimuli using non-human primate models (rhesus, male, n=2).

Methods: The present work aims to identify the dynamic neural response to cutaneous thermal and tactile stimuli using non-human primate models (rhesus, male, n=2). Animals were implanted with Utah arrays in the hand area of the primary sensory cortex, containing cortical multiunits receptive to both thermal and tactile stimuli. The device used is a custom feedback-controlled thermoelectric cooling probe (±0.001 ˚C, ≤5 ˚C/sec, dia. 0.25 in) that allows simultaneous or independent blunt poking and cooling of a target area. Experiments performed are: (1) baseline neural response to the environment (20˚C) while the animal is in a seated and restrained position (baseline data acquired prior to all trials, with position and climate maintained), (2) response to constant applied probe temperature (*T)* (-5, 0, 5, 35 ˚C), (3) response to innocuous pokes on skin cooled to a constant *T*, with stimuli spaced irregularly over a trial period of 60-90 secs to gauge the effects of cooling on poking sensation while reducing chances

of adaptation or allodynia, (4) immediately following the conclusion of (3), raising *T* to 35 ˚C (monkey normal skin temperature) with continued pokes, to test for adaptation vs. numbing from cold, and (5) response to rapid changes (stepwise or periodic) in *T* while maintaining contact.

Results: Preliminary findings show a steady decline in firing rate for a series of pokes with cooling, with a slight increase in the firing rates to pokes once the *T* was raised to 35 ˚C (skin *T*). Naïve Bayes classification of firing rates could discriminate neither tactile inputs (accuracy ~50%) nor the temperature points at constant *T* trials. However, firing rates from combined pokes with cold could be discriminated from skin *T* responses at a moderate accuracy (>70%). For periodic inputs, a low frequency response correlating to the cooling phase of the sinusoid was detected, suggesting that the brain is more sensitive to cold transients than warm.

Conclusion: Overall, firing rate of cortical multiunits and low frequency broadband signal are potential indicators of cryoanesthesia as functions of *T,* tactile pokes, and time. However, the magnitude of direct responses is minimal; there is a need to amplify responses (greater signal and wider distribution of means) to *T* and pokes, and reduce other activity. Future work will include performing additional experiments to increase datasets, improving accuracies of classification algorithms, establishing a model that predicts neural response to cold and tactile stimuli, and engaging human subject testing to pair human sensation scores to monkey neural data.

5.2 Nomenclature

Acronym/Symbol	Definition
T	Temperature; thermal stimulus train
P	Pressure
MP	Mechanical pokes; precise pokes delivered by built-in clicker (< 1 sec)

Skin T	Monkey normothermic skin temperature; 35 ˚C
Onset/Offset Event	Event of probe placed on skin; event of probe taken off of skin
$\dot{n}$	Cortical neural signal

5.3 Introduction

Thermal sensation is essential for regular functioning of bodily systems and comfort in daily activities. Through sensation, our bodies constantly monitor the temperature of the environment and respond as necessary to maintain health. At a high level, we define two pathways in which an individual's skin surface thermal stimuli is translated into personal responses: biochemical (autonomic) and psychophysical (cognitive, behavioral). In the biochemical pathway, disbalance in skin temperature can trigger fat storage (lipolysis) and affect metabolism[1], hair loss[2], and shivering[3] or sweating[4]. These biological responses to skin temperature (indirectly the temperature of the environment) are a result of heat transfer through the skin affecting core bodily processes[5,6]. The temperature change also signals the autonomic nervous system[3] to enact homeostatic measures, such as shivering to generate heat in cold weather. In the psychophysical pathway, temperature information also derives from heat conducted through skin layers and transmitted as signals to the brain; from there the signals are further translated into perception, leading to some awareness by the individual about the state of the environment (i.e. a warm day) (Figure 5.1). Unlike involuntary biological responses (i.e. sweating), the perception of hot or cold profoundly affects a person's behavior and lifestyle. For example, the perception of warmer weather could induce a decision for wearing thinner clothing, drink iced beverages or manipulate office air conditioning systems to achieve a more comfortable climate. Of course, there exist intersectionalities between these two pathways, such

as lurching away from a sizzling pan, which is a combination of the body's protective response to painful thermal damage while also being partially motivated by a person's prior perception of heat or fear of burns[7].

Along with temperature signals, pain information is transmitted via nervous pathways. The extent to which temperature and pain information can be signaled simultaneously to the brain is unknown. Anecdotally, instances of using hot or cold for pain relief and relaxation hints at the possibility of reducing the intensity of pain signals with appropriate levels of thermal stimuli[8,9]. Adding to this conjecture, people with the disease Hereditary Sensory and Autonomic Neuropathy Type IV (CIPA) do not register temperature sensation or pain, and also cannot regulate their body temperatures[10]. Either neuropathic patients are unable to take in any external stimuli information, or pain and temperature sensation are inherently correlated in both their signaling pathways as well as their intensity. Overall, *temperature sensation and perception* (hereby jointly termed "thermosensation") is a relatively under-investigated subject that could inform the fields of medicine, heat transfer, psychology, biophysics and neural engineering.

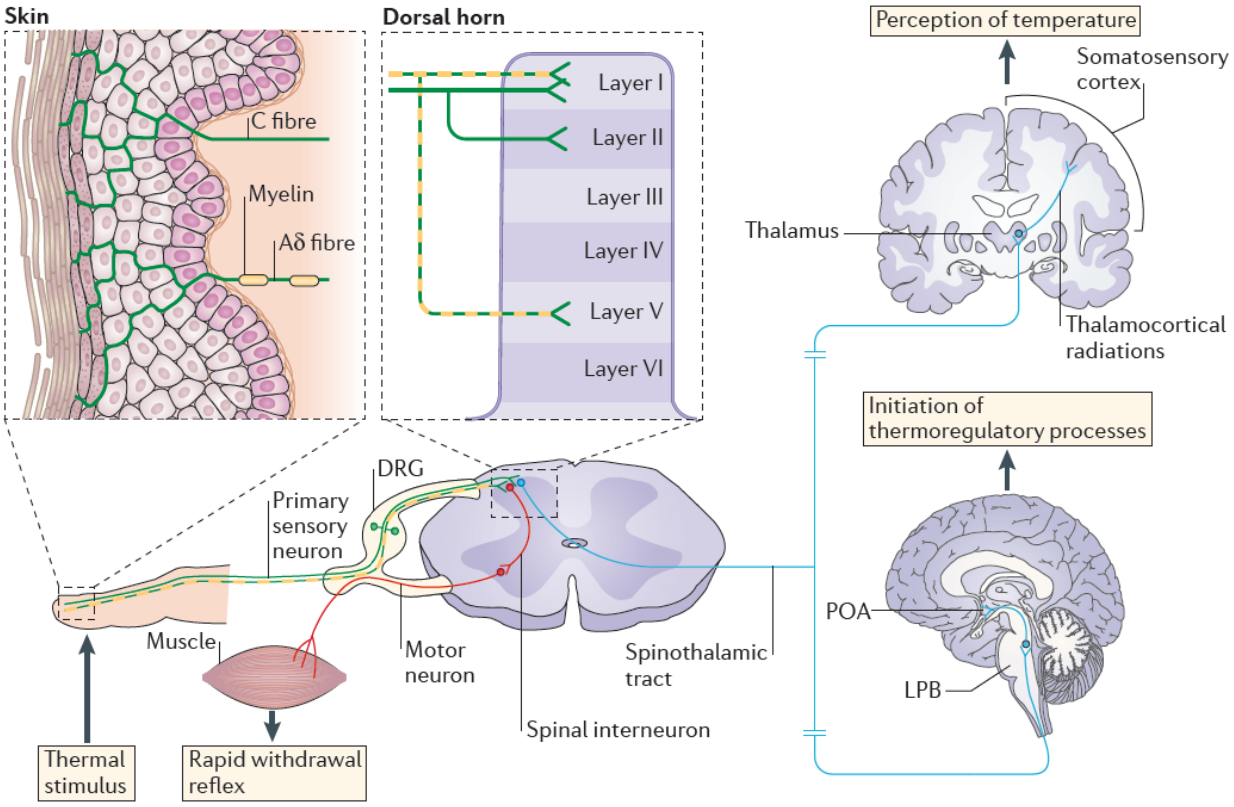

Figure 5.1 Taken from Vriens et al[7]. Neural pathway of thermosensory signals from peripheral neurons into the sensory cortex, where it is processed as perception

Reverse engineering of thermosensation would enable thermosensory interventions in the technical and medical arenas. Technical examples include improving of haptic interfaces and HVAC systems. Medical interventions could involve treatments for neuropathy[10], cryoanesthesia for acute and chronic pain[11], or sports medicine[12]. Specifically, cold sensation has significant potential in these arenas, but the understanding of cold sensation is far less studied than warm due to high engineering and power requirements. Throughout the rest of this work, we focus on cold sensation and its applications (i.e., cryoanesthesia).

State of the art cryoanesthesia methods range in levels of sophistication and engineering. Ice packs remain the standard for reducing pain and swelling in local injuries, and are one of the oldest forms of thermal medicine[13]. More recent innovations in cryoanesthesia are less adopted in society and medicine, but serve unique purposes. For reducing pain of needles and reduce

anxiety in children at doctor's offices, devices that combine vibration with cold are effective at drowning out pain sensation[14] (Figure 5.2). Also for needle injection applications, a high power, specialty precision cooling device for intravitreal injections[15] was introduced (Figure 5.3). While the efficacy of these methods are validated with subject scoring in clinical trials, they were not utilized for researching the neural mechanisms for cryoanesthesia.

Figure 5.2 A commercial cryoanesthesia package consisting of vibrating cold packs. The combination of vibration and cold are thought to minimize pain. Image sourced from Pain Care Labs[14]

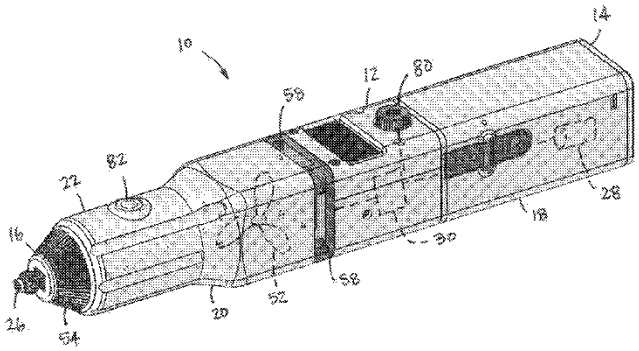

Figure 5.3 Applicator for cryoanesthesia for use before intravitreal injections[15]

Current scientific knowledge on thermosensation is divided into three spatial scales, ion channels, peripheral, and cerebral (perception). While unknowns remain, extensive research performed in the first two spatial scales determined molecular[16] and peripheral[7,17] pathways for

thermosensation. Modeling work on terminal nerve endings and in the periphery recreated action potential generation in response to a temperature input on the skin (-0.6 to -1.2 ˚C/s pulses)[18]. However, investigations in the brain itself and with regards to perception is currently limited to wide-area mapping at higher spatial scales (i.e. MRI[19]), or subject scoring tests for cryoanesthesia[11,20]. To the best of our knowledge, there currently is no information on the encoding of cold sensation in the cortical units at varied thermal stimuli. In addition, the convolution of thermosensation and pain signals at the cortical level is yet uninvestigated.

Despite the numerous possible uses for thermosensation, the field lacks for sophisticated cryoanesthesia devices and research projects in the cortex. There are three major drivers for this need. First, there is an unbalanced focus on hot sensation and heat stimulus more so than cold. This is primarily because cold delivery is far more difficult to perform and control than heat, particularly in the temperature ranges and time scales that matter in scientific and medical research (i.e. for hypothermia therapy at least a 2 ˚C decrease in brain temperature must be maintained for >24 hrs[21]). This lack of a sophisticated experimental apparatus for cold sensation is an outstanding issue that has spanned thousands of years of cryoanesthesia use in human history. Second, cold is more energy intensive than hot, and until recently was unsustainable to use for long periods of time (e.g. melting ice packs). Third, sensation -- particularly cold sensation -- tends to be quite subjective and there is significant variability among subjects.

In order to dive into the cortical neural response of cold sensation and devise improved cryoanesthesia methods, this work aims to investigate the following questions: 1) can we resolve thermal and tactile sensation from a receptive zone on the skin using direct spike recordings from the sensory cortical units? 2) Using this data, can we discriminate when a tactile (nonpainful pressure) stimulus is given, 3) can we discriminate responses to cold vs warm temperatures? and

4) can we identify the neural activity of cryoanesthesia? Experiments are performed using non-human primate models with the intention of pairing with human subject scores for sensation in the future[17].

5.4 Assumptions

The following assumptions hold in this study:

- As the Utah array's 96 electrode pitch is 400 μm pitch, each electrode (channel) records from multiunits
- Firing rate is a reliable feature to examine as the standard feature of interest for cortical spikes
- Sensory information as we are attempting to resolve can be captured from a small patch of the sensory cortex via Utah arrays.
- Synchronous application of thermal and tactile stimuli as outlined in experimental protocol.
- Data collected over 3 years with the same animals are not significantly different.

5.5 Experimental setup and protocol

5.5.1 Thermoelectric skin cooler and mechanical poker (clicker)

The cooling device used is a custom feedback-controlled thermoelectric probe that allows simultaneous or independent blunt poking and cooling of a target area. It was built with the following features: 1) a changeable tip for wider/smaller cooled contact area. For this study, a 0.5" dia. tip was used. 2) A mechanical poker (clicker) built into the center of the probe. The clicker can deliver uniform and painless pokes (or "mechanical pokes" aka *MP*) to the skin. 3) A precise (±0.001 ˚C) and rapid (≤5 ˚C/sec) feedback-controlled tip temperature (*T*), with a range of -10 to 50 ˚C (TEC controller: Meerstetter Engineering, Germany). The probe concentrates the cooling power of 12 thermoelectric cooling units (TECs, 6.6 x 6.6 mm^2 contact area, Custom Thermoelectrics LLC, Bishopville, MD) integrated onto an aluminum center bar (Figure 5.4). Waste heat from the TECs are funneled away by the copper heat spreaders and water cooling

blocks surrounding the probe center (Figure 5.5). The cooling probe is a modified version of the cryoanesthesia eye cooling probe designed by Besirli et al[15]. Key differences between the original design by Besirli et al and the current device are in the material, the changeable tip, the mechanical clicker and the water cooling system that is depicted in Figure 5.5.

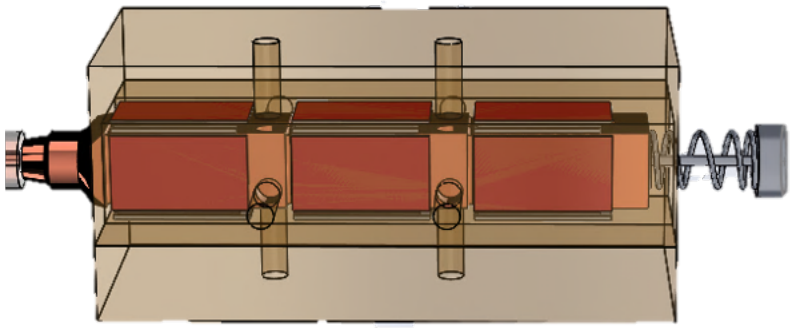

Figure 5.4 Rendering of probe inner design, with TECs, mechanical clicker, and heat spreaders (copper plates) on the center bar

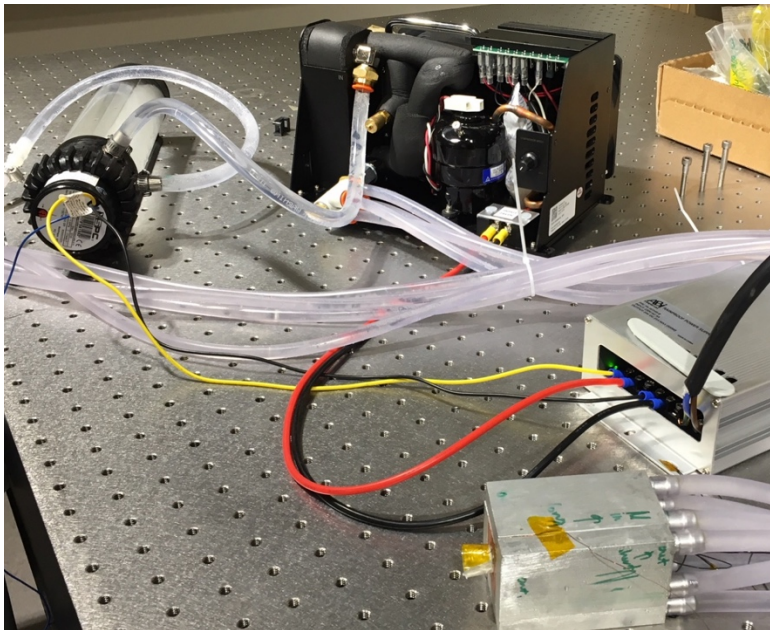

Figure 5.5 Skin cooling system. From left to right: water pump and reservoir, water chiller, power supply, cooling probe.

The mechanical clicker was built using a thin, steel rod (< 1 mm dia.) with a blunted tip that was attached to a plastic stopper and metal spring (Figure 5.4). The probe center rod was built with a through hole that the clicker could be placed in a loose fit, coming to rest where the stopper was placed at the other end of the clicker. During experiments, the user could press the clicker down towards the experimental site, and the clicker would deliver a precise poke (*MP*) at a depth equal to the spring displacement allowed by the plastic stopper. Once the poke is delivered, the spring on the clicker returns the clicker back to its original position. This clicker was used in experiments that required simultaneous thermal (*T*) and mechanical/tactile (*P*) sensory inputs, but was not used in experiments requiring only thermal inputs.

5.5.2 Animal preparation and selection

All animal protocols were approved by IACUC at the University of Michigan. Prior to all experiments, animals were implanted with Utah arrays (Blackrock Microsystems, Salt Lake City, UT) recording from the layer V multiunits of the somatosensory cortex. Units in the sensory cortex are receptive to both thermal and tactile stimuli[22]. All surgeries were performed by a neurosurgeon in the animal laboratory and were not part of this experimental design. The author did not choose the sensor, sensor location, or the implantation procedure. Animals were selected from a pre-instrumented group of monkeys. Criteria for selecting animals included animal availability, temperament, and location of the Utah array (i.e., sensory cortex). Age, weight, and sex were not factors in this study beyond considerations for general good health.

Adult male Rhesus Macaque monkeys (n = 2) were used for protocol development and data collection respectively over the course of 4 years, with 2-3 hour long trials performed 3-4 months apart. The animals were kept in a temperature (~22 ˚C) controlled vivarium. No tranquilizers, sedatives or other chemical interventions were used before and during the trials.

Most data presented in later sections were from a single animal, with the exception of baseline and ice trials. The criteria for exclusion of data/animals from further participation in the study were changes to the animal's initial availability (logistical constraints), temperament (ability to adjust to experimental demands, cooperate and maintain stillness), and signal quality of the implanted sensory array. One monkey from the cohort was removed partway through the experiments due to scheduling constraints. That monkey was therefore used primarily for protocol development and preliminary data collection, but most of its data was not included in the results below.

5.5.3 Experimental procedure

The animal was placed in a wheeled, box-chair keeping its torso and arms gently in seated position (Figure 5.6). The seat had the monkey's arms fixed in frontal plane movement (side-to-side, lateral), with room for comfort and minor movement in its fingers. The animal was unrestricted in movement of arms in the sagittal plane (forwards and backwards). This required that the handler gently grasp the monkey's hand during experiments to prevent retraction of the arm. The monkey's head is also kept in a comfortable, upright position. The animal was previously trained for seating in such implements. All restraints were familiar and nonpainful to the animal. Minimizing the monkey's movement is critical to reducing movement artifacts in the data. Then the animal was wheeled into the testing room (Figure 5.7) where its Utah array was plugged into the data acquisition system (Cerebus) and display panel (Figure 5.8).

From the display panel, the handlers verified the monkey's receptive zone by gently applying nonpainful pressure on portions of the monkey's skin until the display panel became active. This is to ensure the multiunits we record from are receptive to stimuli to our testing site. During protocol development, the receptive zone was identified to be the monkey's inner wrist

and pinky. The receptive zone's fur was shaved as much as possible and marked for direct access to the skin (Figure 5.6). During this time, the cooling probe was also powered and primed for use. Prior to the start of a trial, the door to the test room was closed, the lights turned off, and all power supplies connected to a common ground (or floated using battery packs) to minimize electrical noise.

Experimental trials were conducted as outlined in Table 5.1, Table 5.2, Table 5.3 and Figure 5.9. Experiments were designed and performed with the aim of answering the following questions: 1) can thermal and tactile sensation from a receptive zone on the skin be resolved from the spike recordings? 2) Using this data, can we discriminate when a tactile (nonpainful pressure) stimulus occurs, 3) can we discriminate responses to cold vs warm temperatures? and 4) can we identify the neural activity of cryoanesthesia? The baseline, constant T and cold-induced numbing experiments directly inform the above research questions. The dynamic T experiments supplement findings for question 4.

All experiments were completely nonpainful and vocal encouragement and treats were provided to the monkey periodically.

Figure 5.6 (Left): Monkey in restraint chair. (Right): Probing and shaving receptive zone (marked in black square)

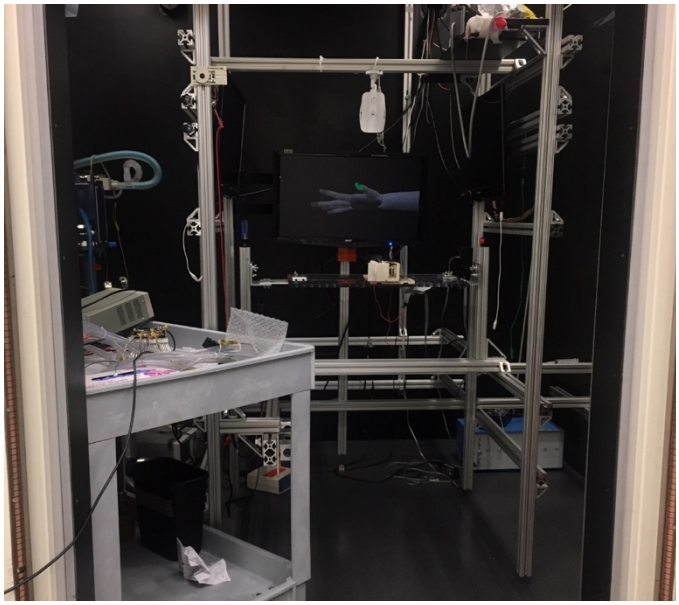

Figure 5.7 Experimental rig and cerebral data acquisition system (Cerebus) inside a faraday cage, which is used as the primary experimental theater

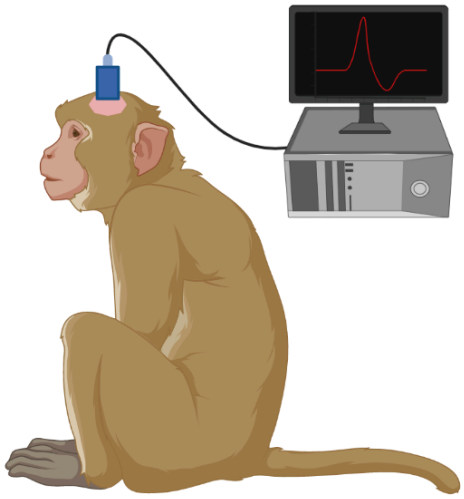

Figure 5.8 Conceptual drawing of a monkey plugged into neural data acquisition system. Monkey's seat, restraints, or other apparatus not shown. Graphic created using Biorender.com (2022)

Table 5.1 Types of experiments performed. T: thermal stimuli, P: pressure/tactile stimuli

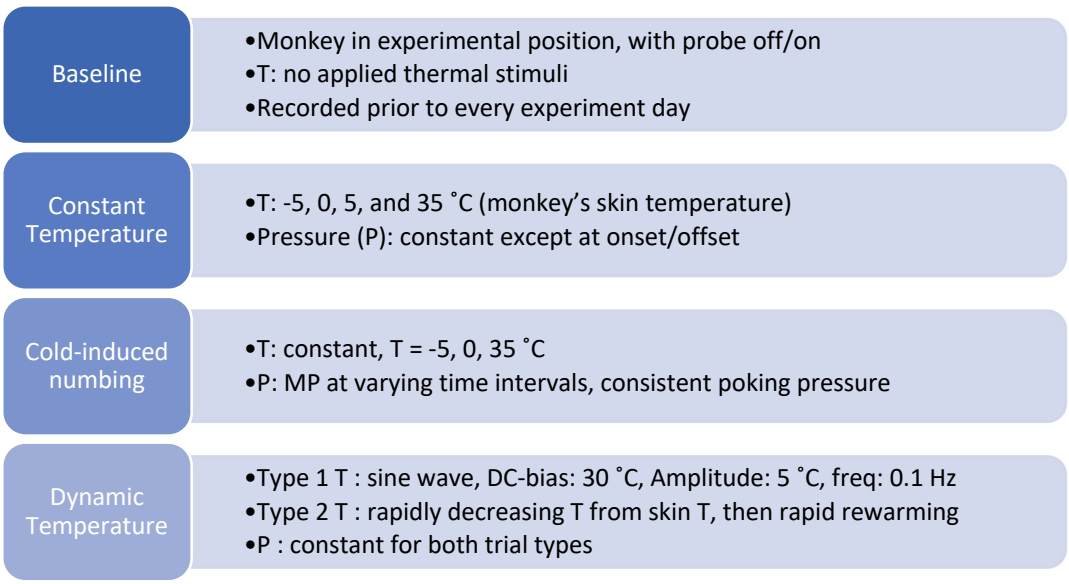

Baseline: baseline trials were performed prior to every experiment immediately following animal preparation and setup. Recordings were taken of animal baseline neural activity at the present ambient temperature, and seated position. General observations of the animal's mood were also noted.

Constant *T*: constant *T* trials applied the probe tip, primed to a steady temperature onto the receptive zone of the monkey for a specified duration. These trials were repeated for multiple temperature points for at least 5 runs each for 10 secs minimum (Table 5.2). Constant *T* trials assume a constant pressure of the probe tip as a consequence of placing the probe on the monkey's skin. This is separate from deliberate clicker stimuli (*MP*) which are short, uniform pressure, painless blunt pokes delivered within a fraction of a second, much like the clicking of a dull pen.

Table 5.2 Constant temperature trial sequence. Onset: placement of probe on the skin. Offset: removal of the probe from the skin/end of a trial. Each trial was repeated 5x minimum.

T	t = 0	t = 10 s	Rest for 30 s

35	Onset	Offset	No probe
5	Onset	Offset	No probe
0	Onset	Offset	No probe
-5	Onset	Offset	No probe

Constant *T* with *MP (cold-induced numbing)*: these trials combined the constant *T* trials with irregularly placed, innocuous *MP* using the built-in clicker. The *MPs* were applied irregularly in time to reduce the monkey's anticipation of the event. The trials could be performed for at least a minute in length, or extended to include a reheating period after which more *MP* were applied. This was intended to test the effect temperature has on level of tactile sensation, and if we could resolve the change in sensation with the recorded multiunits (Table 5.3).

Table 5.3 Constant T with MP trial sequence. MP: poking with the clicker. From 0-90 s, the probe T is held constant until at 91 s the probe is brought to 35 ˚C. The length of time to reach stable constant T varies with initial probe T, which results in longer wait times for restarting MP

T/Time	**0 s**	**5 s**	**10 s**	**20 s**	**35 s**	**55 s**	**75 s**	**90 s**	**91 s**	**100 s**	**115 s**	**120 s**
35 ˚C	Onset	*MP*	*MP*	*MP*	*MP*	*MP*	*MP*	*MP*	35 ˚C	*MP*	*MP*	Offset
T/Time	**0 s**	**5 s**	**10 s**	**20 s**	**35 s**	**55 s**	**75 s**	**90 s**	**91 s**	**120 s**	**140 s**	**150 s**
5 ˚C	Onset	*MP*	*MP*	*MP*	*MP*	*MP*	*MP*	*MP*	35 ˚C	*MP*	*MP*	Offset
0 ˚C	Onset	*MP*	*MP*	*MP*	*MP*	*MP*	*MP*	*MP*	35 ˚C	*MP*	*MP*	Offset
T/Time	**0 s**	**5 s**	**10 s**	**20 s**	**35 s**	**55 s**	**75 s**	**90 s**	**91 s**	**140 s**	**150 s**	**160 s**
-5 ˚C	Onset	*MP*	*MP*	*MP*	*MP*	*MP*	*MP*	*MP*	35 ˚C	*MP*	*MP*	Offset

Dynamic *T* trials: Two types of dynamic trials were performed, 1) a stepwise ramp and 2) a sinusoidal input *T*. Dynamic trials in which a nominal stepwise *T* ramp was applied (Figure

5.9) proved difficult to perform in practice due to the high thermal inertia of the probe. Actual probe temperature traces appeared more as a gradual decrease in temperature rather than structured steps. This was an expected result given the probe's maximum ramping rate and thermal inertia. Data analysis was performed with actual measured temperature. Unlike the stepwise dynamic trials, the probe could apply a sinusoidal thermal input with high fidelity to the planned waveform, the details of which are described in Table 5.1.

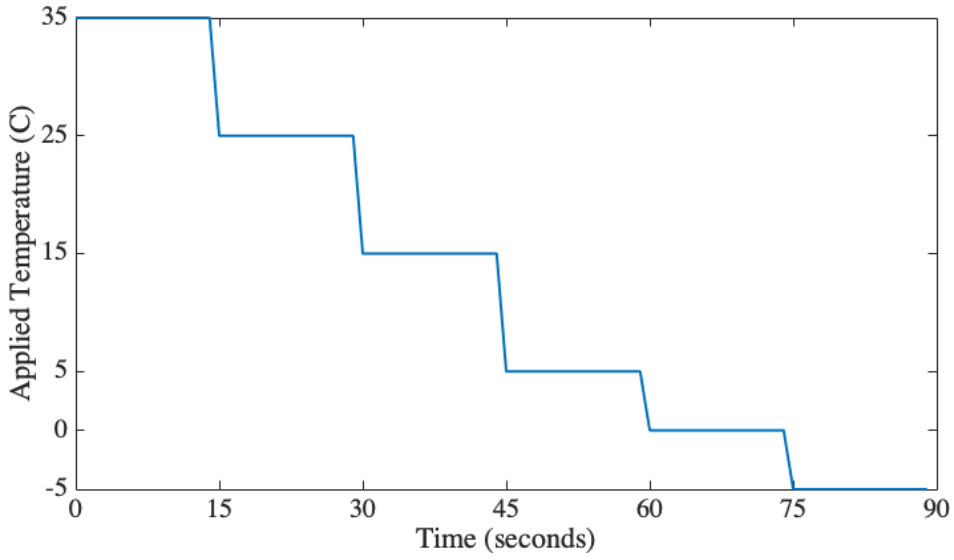

Figure 5.9 Nominal T input for a rapidly changing T (dT/dt) trial, with no MP. This temperature trace was followed by a stepwise ramp up to 35 ˚C.

5.6 Data processing, machine learning, and statistics

Data methods were performed with in-house MATLAB (MathWorks, Natick, MA) and Python scripts. Overall, we sought to identify trends (linear, quadratic) in the spiking data that indicate a correlation in *T* and *MP* (i.e. transient spiking data vs *T*), which could answer the research questions above. We also examined the data for possible minima/maxima, which could indicate for min/max neural response at a specific input stimulus combination. High dimensional

trends that cannot be visualized or extracted in a low dimension were used in machine learning algorithms for classification (described below).

5.6.1 Data preprocessing

Raw data from sensory array (in μV with time; broadband signal) require significant pre-processing prior to feature extraction. The process was performed as follows: 1) on experiment day, visually identify the viable channels (channels with normal spike waveforms), 2) take the subset of viable channels from whole array, and synchronize timestamps of all applied stimuli and probe data with sensory neural data, 3) subdivide dataset into relevant snippets of data (i.e. a data snippet per trial), 4) common average reference all datasets[23], and 5) filter re-referenced data to 300-5000 Hz range using a 6^{th} order Butterworth filter[24,25]. This bandwidth is chosen as it is the frequency range in which spiking activity occurs. This work used direct recordings from multiunits, and did not perform spike sorting. However this is an option in future studies.

5.6.2 Feature extraction

In this study several features were considered, including features from spiking multiunits as well as broadband signal.

Firing rates (spikes per second): firing rates are the primary feature of interest in this study due to its relevance in resolving motor inputs[26]. From the pre-processed data snippet in the previous section, a 1 s moving threshold of *-4.5 x RMS* value is imposed; spikes are defined as the synaptic biphasic event that crosses this threshold (Figure 5.10). Spikes are counted and binned at desired time windows to calculate firing rate. This work looked at time bins of 100 ms to 1 s.

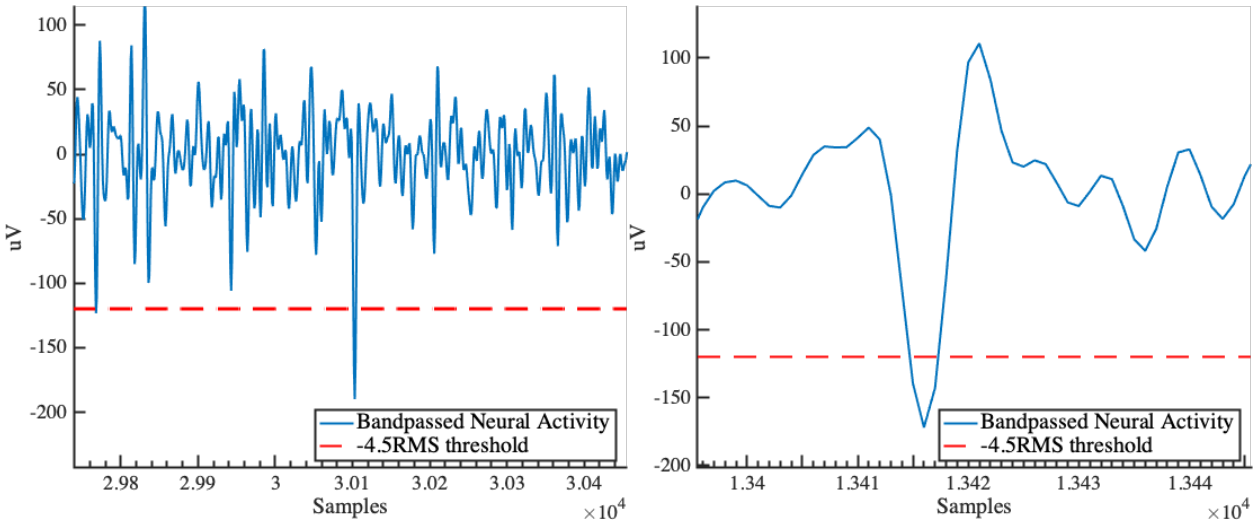

*Figure 5.10 (Left): Referenced, broadband signal bandpass filtered to 300-5000 Hz range, with a moving -4.5*RMS threshold (red-dashed). (Right): Zooming in on the spikes that cross the thresholds*

Peak time: peak time is defined as the timestamp at which the "maximum" firing rate occurs for a particular channel and event. For example, for an onset event captured at 100 ms time bins may result in a surge in firing rate followed by a decay, or adaptation period. The peak time is the most optimal peak time value for that time window. Peak times identify when the maximal "sensation" occurred in relation to the time the stimulus was applied. Peaks are detected via a moving window for which threshold crossings are calculated. The threshold is arbitrarily set to:

Equation 13

$$1.5\left[\frac{1}{n}\sum firing\ rates\right]$$

where n is the total number of time bins in the data snippet. All firing rates that cross the threshold are considered potential peaks. Actual peak times are determined via a conditional decision tree as described in Figure 5.11. Custom scripts are included in Appendix C.

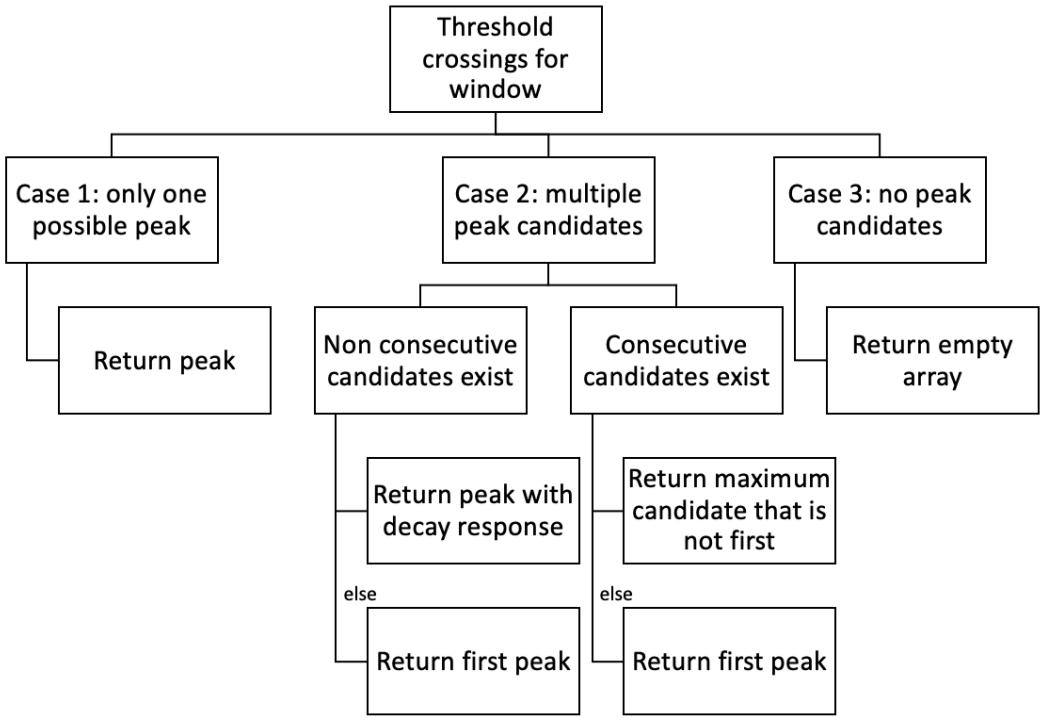

Figure 5.11 Conditional decision tree for returning optimal peak time value

Latency: latency is calculated for *MP* inputs to assess the speed of neural response to the stimuli.

Equation 14

$$Latency = actual\ response\ time - expected\ response\ time$$

Phase: the phase is calculated for sinusoidal trials, and is defined as the time difference between the local maximum of a power spectra relative to a point on the sinusoid. Here, the cooling inflection point is used.

Equation 15

$$Phase = peaking\ time - inflection\ point\ time$$

5.6.3 Visual encoding analysis:

We preliminarily identified a subset of channels that are producing viable results using visual and qualitative analysis. Plotting firing rates versus time with timestamps for events (i.e. *MP*) isolates channels that are response to that particular event (Figure 5.12).

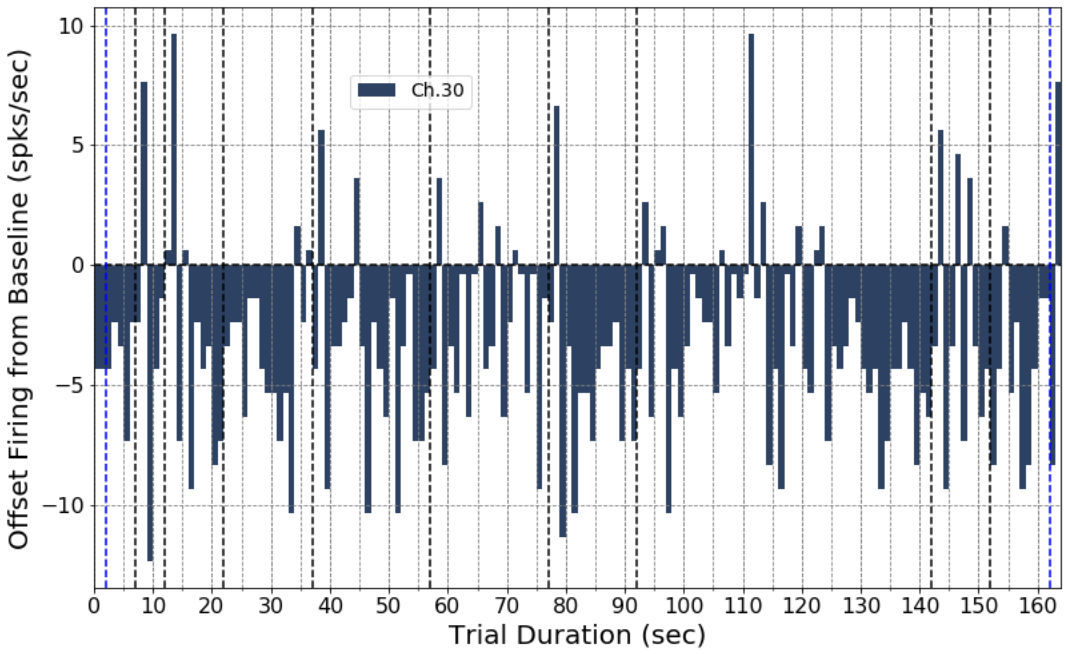

Figure 5.12 Sample plot of firing rates vs time for a given channel and trial; this channel is clearly sensitive to MPs (dashed-black vertical lines) but less so to onset of cold T (1st blue-dashed line, 2nd line indicates probe offset).

5.6.4 Population analysis and classification

Population analysis, consisting of all viable channels in a trial, aimed to identify population wide patterns in response to a stimulus. Given the variability in firing behavior, multiunits are analyzed independently or as a collective—averaging of signals from multiple electrodes are not recommended. Two modes of population analysis were used: 1) qualitatively with rasterplots of channels (Figure 5.13), and 2) using machine learning techniques to classify and decode spike samples from multiple units. Supervised classifiers were used, such as Naïve Bayes and logistic regression. Linear regression was used to train and test models based on batches of spiking multiunits.

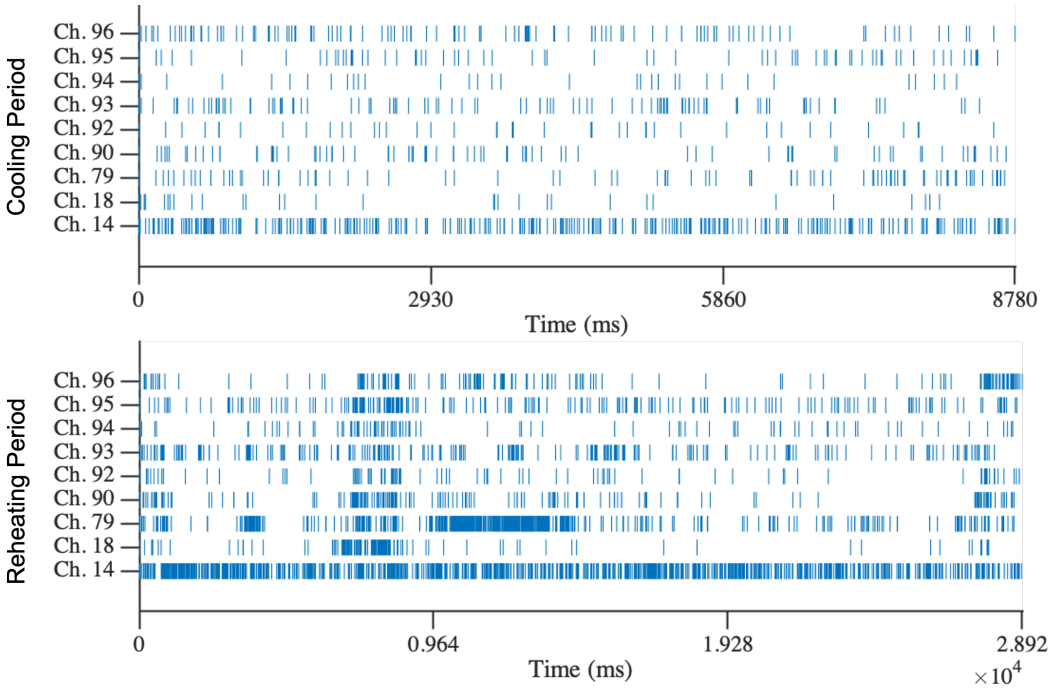

Figure 5.13 Rasterplot of viable channels in a sample trial to visually assess for response to specific stimuli. (Top): no visible response to constant cold temperature; (Bottom): when probe is offset and skin rewarms to normal temperature, there is a surge of firing in all channels

Datasets containing firing rates per channel per trial were reorganized to be fed into machine learning algorithms. For supervised classifiers, a random subset of total firing rates were taken to maintain equal amounts of data per class. A minimum of 100 iterations of randomized 75% holdout training and testing was used to determine mean accuracy of the classifier. Algorithms were run in-batch and for offline predictions.

5.6.5 Other machine learning techniques

This work also utilized various machine learning techniques such as independent component analysis, support vector machines, principal components analysis, and k-means clustering. However, these techniques are not discussed further due to lack of interesting results and samples.

5.6.6 Broadband signal processing: FFT, Wavelet transformation

Parallel to feature extraction and analysis of firing rates, broadband signal was assessed using the following tools and algorithms: fast Fourier transform, wavelet transformation, power spectral analysis, and spectrograms.

5.6.7 Statistical analysis

To determine the fit and predictive capabilities of the generated model vs actual data, mean squared error, correlation, and accuracy were calculated. To determine the statistical significance of datasets being compared, a one-way analysis of variance (ANOVA) was used. To determine the statistical significance of calculated values against the mean, the Student's t-test was used. Statistical significance was defined as a p-value < 0.05.

5.7 Results

To investigate and prove the hypotheses for this study, the following measurements were performed: (1) baseline neural response to the environment (20˚C) while the animal is in a seated and restrained position (baseline data acquired prior to all trials, with position and climate maintained), (2) response to constant *T* (-5, 0, 5, 35 ˚C), (3) response to innocuous pokes on skin cooled to a constant *T*, with stimuli spaced irregularly over a trial period of 60-90 secs to gauge the effects of cooling on poking sensation while reducing chances of adaptation or allodynia, (4) immediately following the conclusion of (3), raising *T* to 35 ˚C (monkey normal skin *T*) with continued pokes, to test for adaptation vs. numbing from cold, and (5) response to a sinusoidal *T* profile while maintaining contact. All results presented below are from one monkey, except for the results from ice tests.

5.7.1 Baseline neural response to the environment (20˚C) versus the probe

The baseline neural response (defined as the spiking activity of recorded multiunits with no input stimulus) was examined as firing rates and compared against the probe being turned on and off, as well as gentle presses onto the monkey's skin. This was to distinguish whether our probe added significant electrical noise to the system. The firing rates did not increase significantly ($p > 0.05$) with the probe being on/off. Visually, the probe also did not add significant noise during experiments as identified via the display panel on the Cerebus (Figure 5.14).

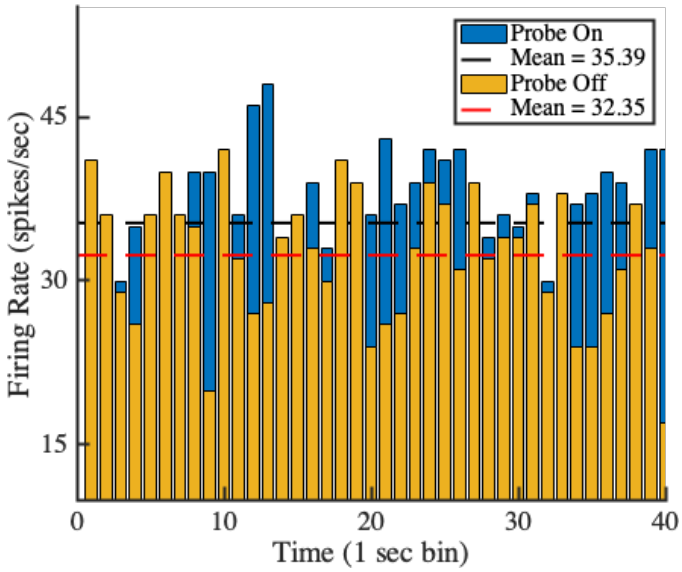

Figure 5.14 From a representative channel from a trial, baseline recording during probe on vs off.

5.7.2 Response to constant T (-5, 0, 5, 35 ˚C)

Firing rates were the primary feature of interest in this study. At four constant *T*: 35 ˚C (skin), 5 ˚C, 0 ˚C, and -5 ˚C, firing rates showed little to no change in firing pattern. Aside from an initial burst in firing at the onset and adaptation, throughout the rest of the trial period firing occurred uniformly and with no distinction with applied *T* ($p > 0.5$) (Figure 5.15). In addition to the probe stimuli, a flat cube of ice (approximately 4 x 4 x 4 cm^2) was used as a control for

electrical noise added by the probe to the system. Probing with ice (approximately 0 ˚C) resulted in a more prominent firing curve with obvious signals for the initial cooling period, adaptation, and rewarming (Figure 5.16). Transient periods in ice trials (onset/offset events) were captured in both firing rate as well as broadband wavelets (Figure 5.17). Constant *T* trials with the probe were performed with one monkey, while the ice trial was performed in the other monkey.

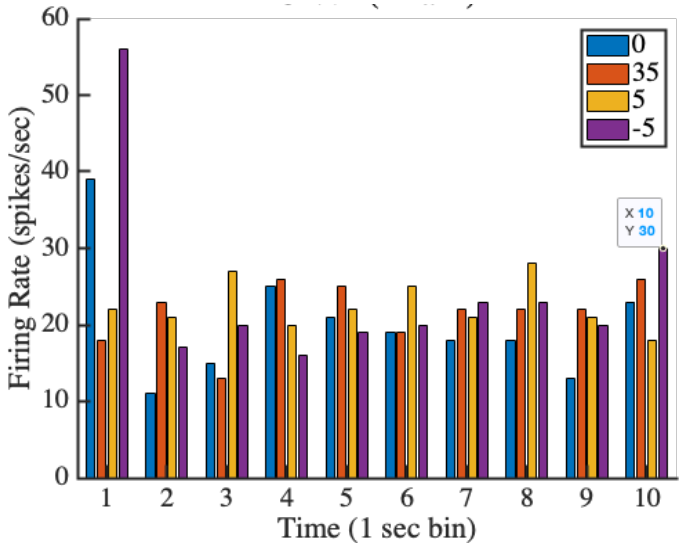

Figure 5.15 Firing rates from a sample channel with constant T inputs only at four T points

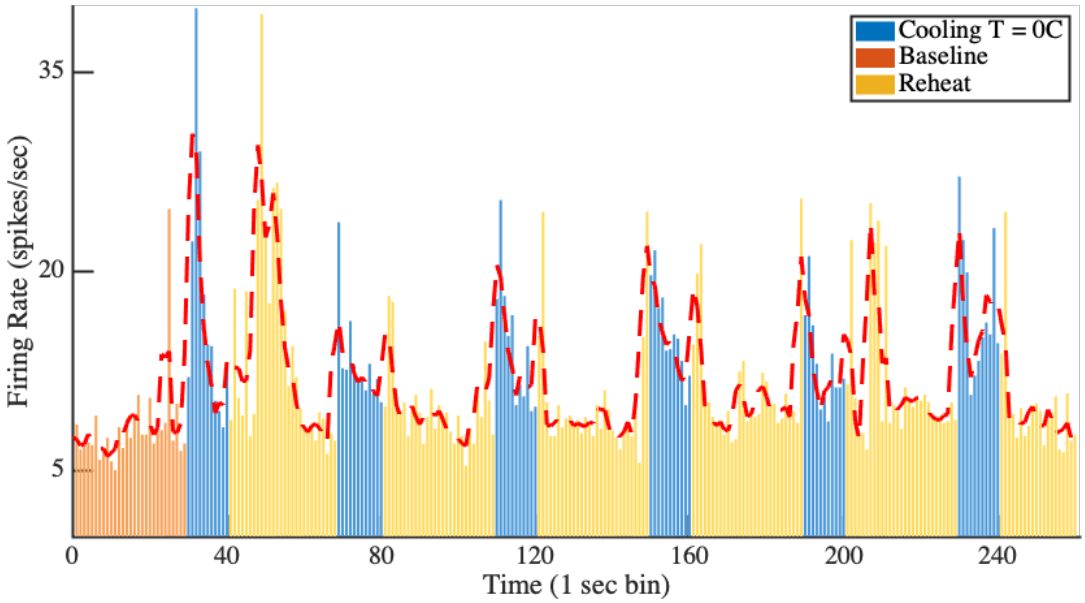

Figure 5.16 Firing rates for a sample channel with onset/offset of ice, or 0 ˚C (blue), and the subsequent rewarming period (yellow). Red-dashed lines indicate a moving average of the firing rates.

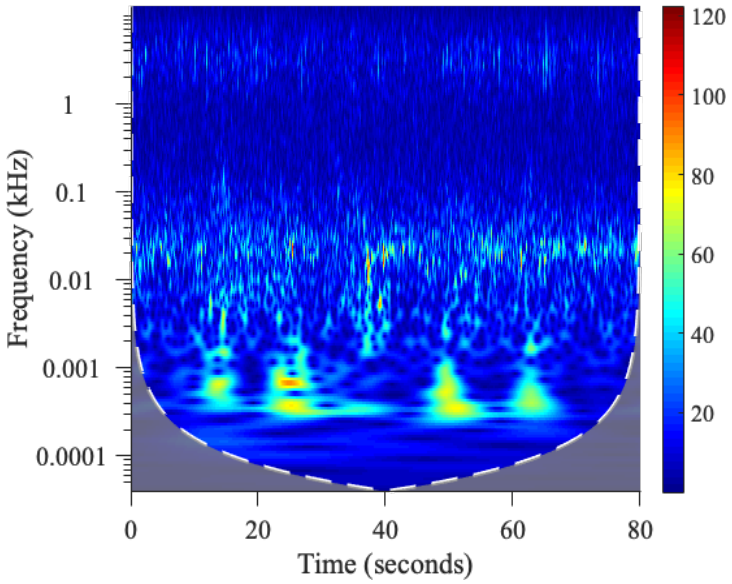

Figure 5.17 Wavelet plot of ice trial, capturing the first two onset/offset pairs. Onset/offset are visible as hot spots in the wavelet plot.

5.7.3 Response to constant T (-5, 5, 35 ˚C) and innocuous MP (cold-induced numbing)

Classification of sensory inputs: to assess whether the multiunit response could be used to discriminate for sensory signals, three sets of classification were performed in succession. First,

we assessed whether we could highly discriminate *MP* vs no *MP*. Given the success of this first classification, we assessed if we could discriminate between cold and normal skin *T* (35 ˚C). Finally, given success in the previous classification, determine whether all *T* could be discriminated.

In classifying for *MP* vs no *MP* signals, this resulted in chance accuracy (mean accuracy of ~50%) for all collected data and its randomly generated subsets. For classifying a cold vs. skin *T*, data subsets containing equal and random sets of -5 ˚C vs 35 ˚C firing rates resulted in higher than chance overall accuracy (76%) for a particular dataset, with 5 ˚C vs 35 ˚C also resulting in ~73% mean overall accuracy for the same dataset (Table 5.4). Using this dataset, a preliminary linear model was generated to predict input *T* (-5 and 35 ˚C) and *MP* (1 for no *MP*, 2 for *MP*) with supplied output firing rates (Figure 5.18). The mean squared error and correlation values for both *T* and *MP* were poor, with higher correlations with *MP* than *T*. Discriminating between all temperature points was not highly accurate but were greater than chance (Figure 5.19). High classification accuracy is defined as over 80% correct prediction.

Table 5.4 Mean accuracies for classification of population response in firing rates

Dataset	**% accuracy *(param1, param2, overall)***			**Param1 vs Param2**
Aug	52	51.2	51.6	*MP* vs no *MP*
May	50.5	58.6	54.5	
Aug	51.3	75.7	63.5	35 ˚C vs -5 ˚C
May	77.4	75.1	76.2	
Aug	55.3	76.1	65.7	35 ˚C vs 5 ˚C
May	75.2	70.3	72.8	

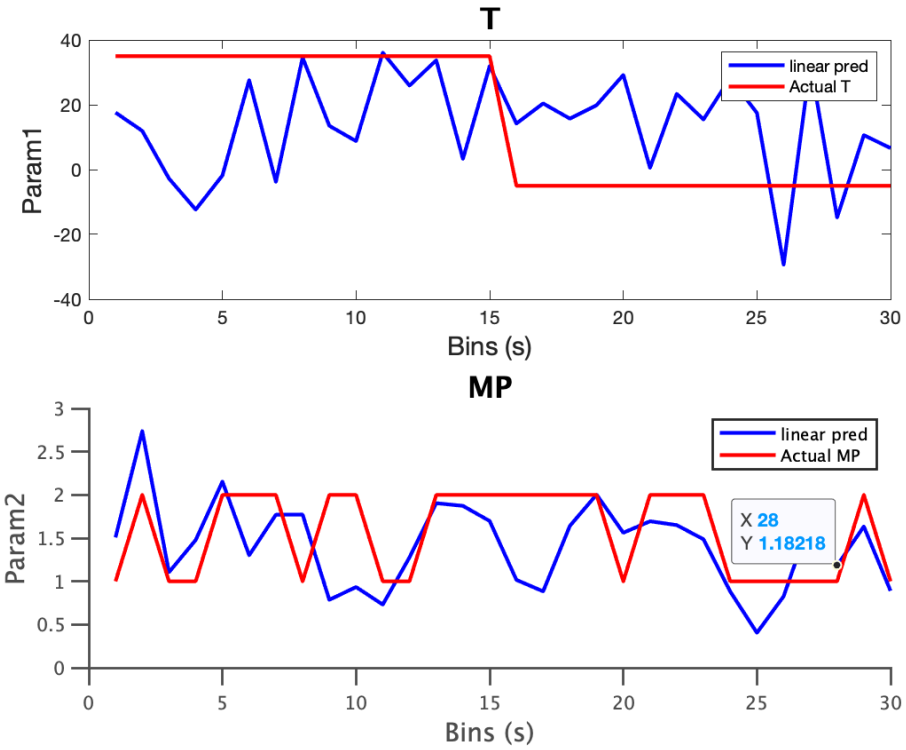

Figure 5.18 Preliminary attempt at decoding of T and MP stimuli with 16 viable channels. The actual T applied were 35 ˚C and -5 ˚C. MP = 1 indicates no stimuli and MP = 2 indicates with MP. Mean squared error for T: 608.6, MP: 0.31; Correlation for T: 0.07, MP: 0.42.

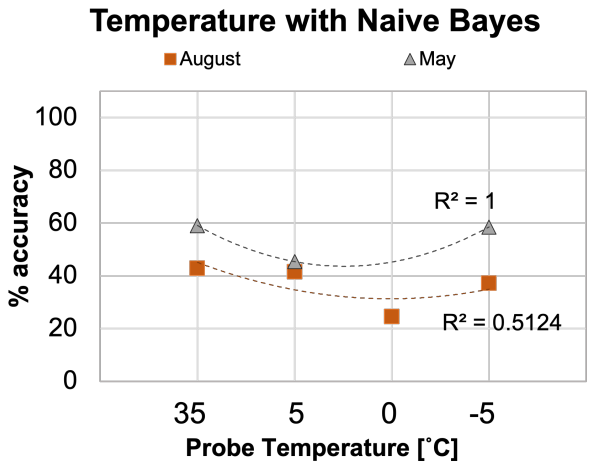

Figure 5.19 Mean accuracies for classification of applied T using population response in firing rates.

Position dependence of firing rates: to determine whether there was position dependence on channels, k-means clustering determined that there was no explicit relationship with position of the channels on the electrode array (Figure 5.20).

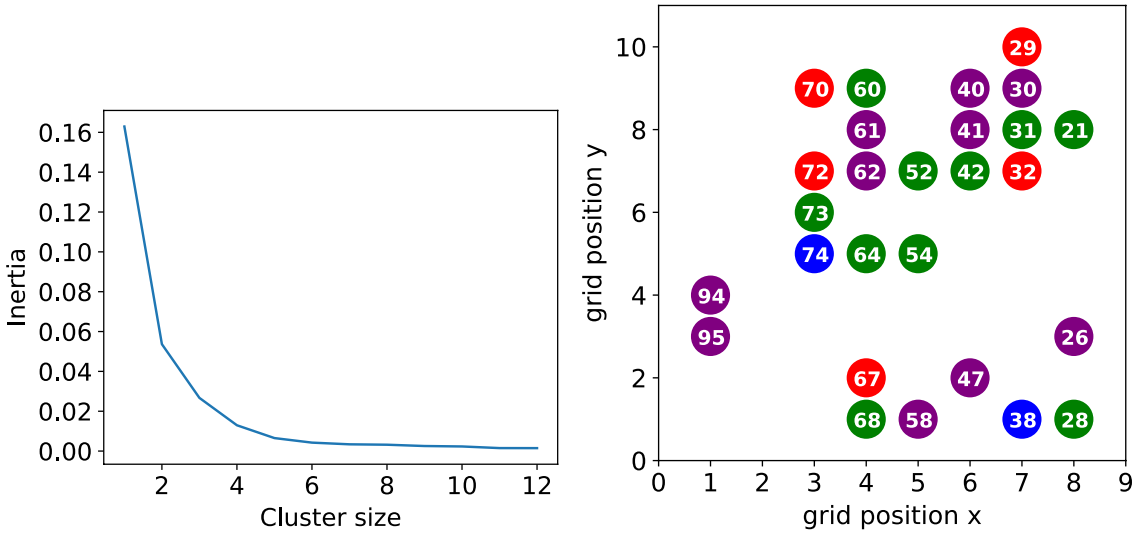

Figure 5.20 Position dependence and clustering based on k-means clustering. Figures created by Agnes M. Resto

Latencies (actual response time – expected response time) calculated for each *T* were compared in unique pairs (i.e. 0 vs 35 ˚C) for all channels. Preliminary analysis detected little notable change in latency with time at cold *T* versus at 35 ˚C. The comparisons were also not found to be statistically significant in most channels. For the few channels that were significantly different across cold and skin temperatures, only one channel consistently reported $p < 0.05$ at each cold/skin combination (Table 5.5).

Table 5.5 Statistical comparisons of latency values per trial and channels. Data from Aug 2019 dataset.

T1	T2	Channels at p < 0.05 for T1 vs T2
-5	5	21, 32, 64
-5	0	52, 61, 64, 73, 95
5	0	26, 40, 61
35	-5	30, 32, 61, 64, 95

35	5	21, 40, 60, 61, 95
35	0	52, 64, 95

5.7.4 Response to reheating after constant cooling

Heating the skin back to skin *T* (35 ˚C) from it's cooled state visibly increased firing rate at the warmer *T* (Figure 5.21), but this difference was notable only for -5 vs 35 ˚C comparisons. *T* closer together did not show any obvious change. Statistical analysis for this section was not rigorously performed, as most of the data collected is within the same constant *T* range (and therefore not statistically significant), with only the last two datapoints possibly showing a difference. This observation was also only noted in 2-3 out of all channels recorded (20+), which indicated it to be a poor response and therefore did not pursue this avenue of study further.

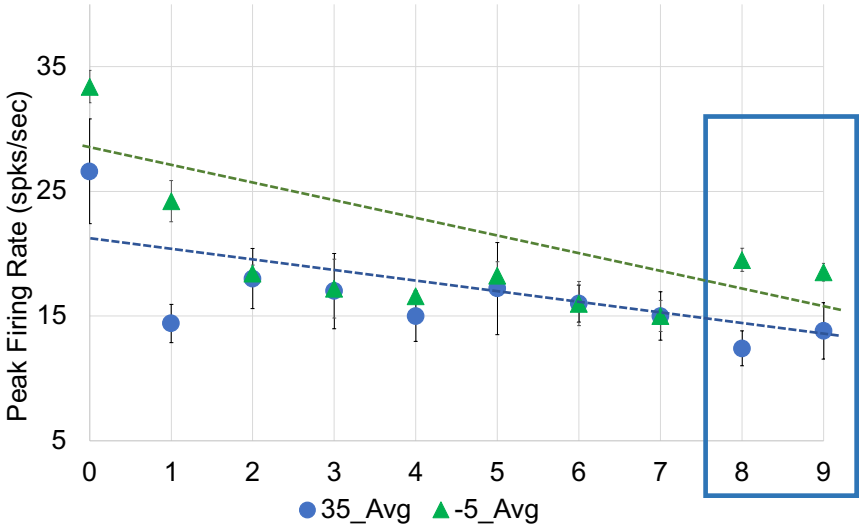

Figure 5.21 For a sample responsive multiunit, firing rate for constant T and irregularly spaced MP, with return to skin T at MP 8-9. Horizontal labels indicate the i-th MP that was applied, not time. Trendlines are placed as a visual guide and are not regression lines.

5.7.5 Response to a rapidly fluctuating temperature (|dT/dt| > 0)

To determine the relationship between neural activity and changing *T* inputs, preliminary firing rates from cortical multiunits and moving RMS values of filtered (300-5000 Hz) broadband signal were compared against input *T* and dT/dt values. Initial analysis indicates for a surge in firing rate with instances of greatest dT/dt, and with onset/offset (Figure 5.22). Onset/offset are also moments of high dT/dt. A moving RMS animation charting RMS values throughout time showed a similar, RMS trace for both Trials 1 and 2, if slightly out of phase (Figure 5.23). The phase shift may be due to a timing error in experiments.

Note that these are preliminary results considering the lack of quality data and iterations. Thus no conclusive results, beyond observations, can be drawn at this point in time.

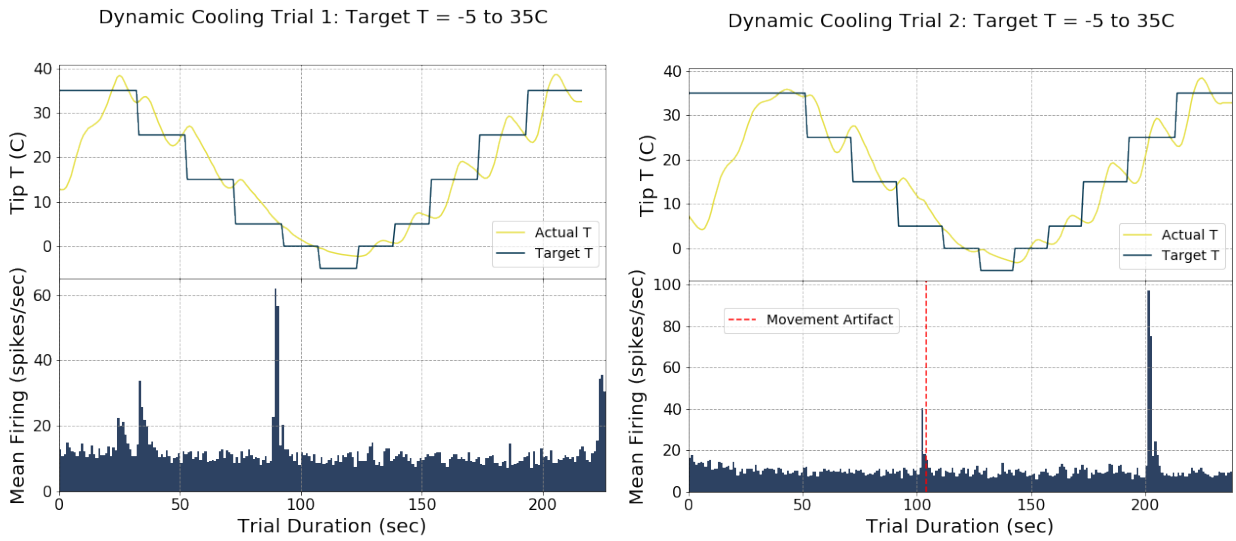

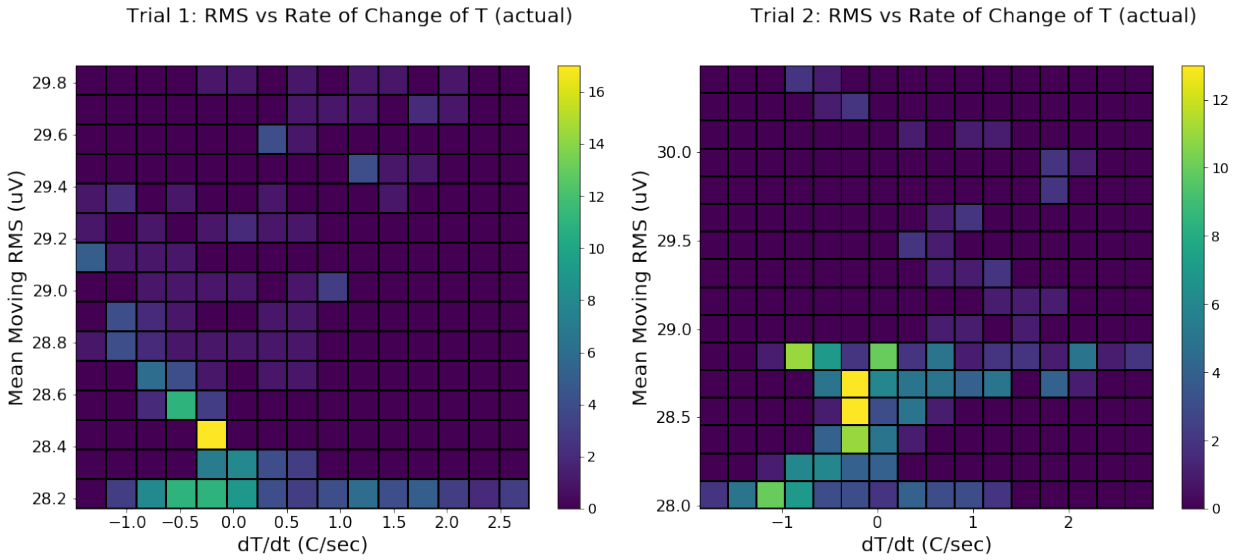

Figure 5.22 Response from a sample channel to dynamic T inputs. (Top row): firing rates from a sample channel compared to changing input T. (Bottom row): Mean moving RMS calculated from a sample channel for values of dT/dt. Only two trials are reported due to unforeseen experimental challenges with monkey cooperation.

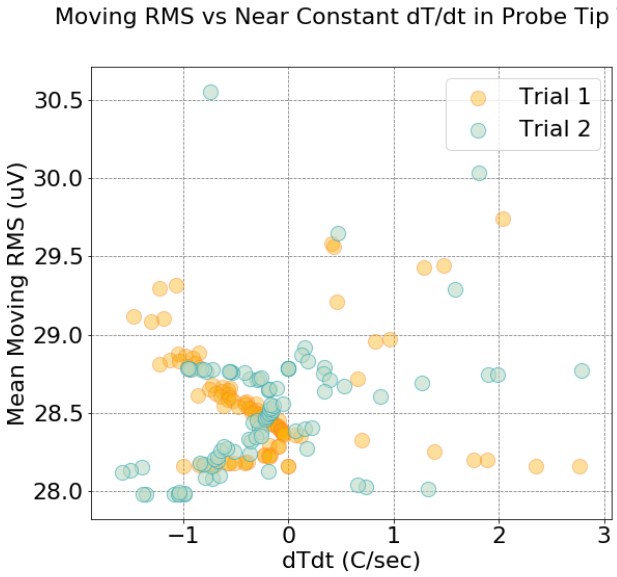

Figure 5.23 Average MRS for a moving window (1 s) at points of constant dT/dt. An animation for the full rms trace is available in Appendix D

5.7.6 Response to a periodic temperature

Periodic *T* stimuli resulted in power surges at low frequency bands (0.01 – 10 Hz) (Figure 5.24Figure 5.25). At 0.1 Hz, the preliminary phase calculation for each timepoint of the power

spectra local maxima averaged -0.95 s from the cooling inflection point (Figure 5.26), or shifted by an entire cycle (std: 3.95 s).

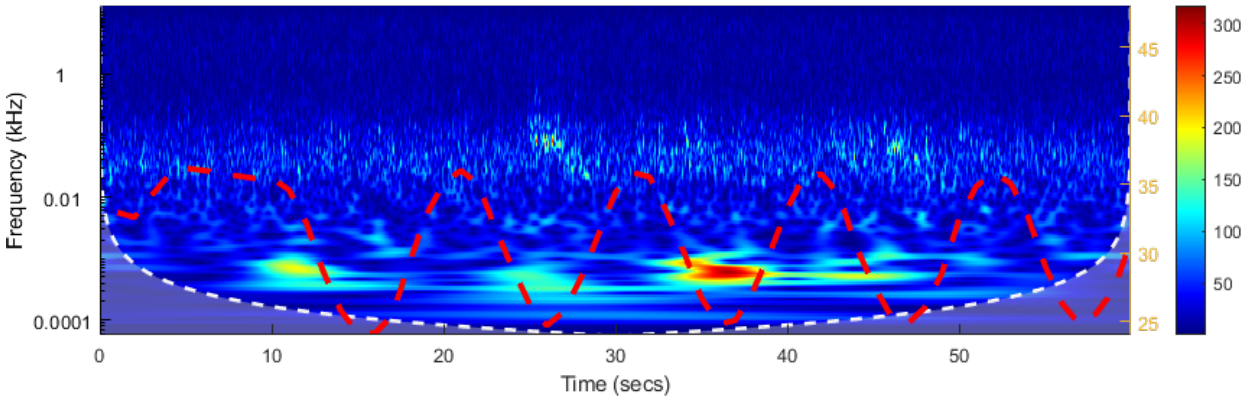

Figure 5.24 Wavelet analysis for a sample trial and channel for the first 60 seconds. Red-dashed indicates input T, colors indicate power of signal

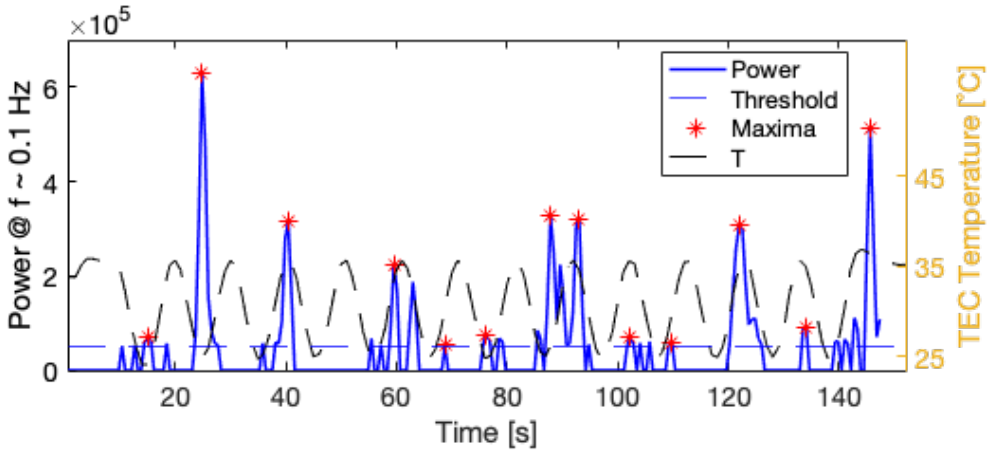

Figure 5.25 Power spectra at ~ 0.1 Hz, red indicates peaks and black-dashed indicates T input, blue-dashed-horizontal line indicates threshold to define a peak.

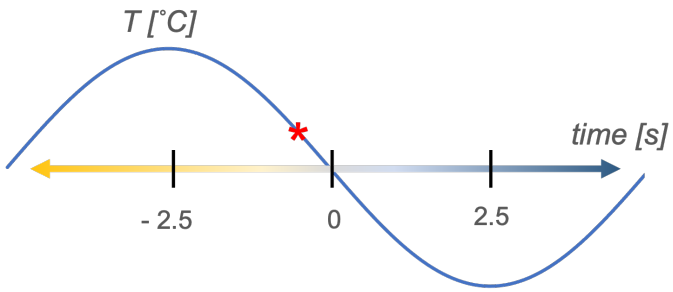

Figure 5.26 Mean peak time vs sinusoidal input shows mean value falls during cooling period. Phase: -0.95 s ± 3.95 s at 0.1 Hz signal.

5.8 Discussion

5.8.1 Ice vs probe cooling

Although we determined the probe does not add significant noise to the system, the ice trials showed a marked response to the cold stimulus than with 0 ˚C probe trials. At the same time bins of 1 s, the firing rates corresponding to 0 ˚C input from the probe displayed far weaker and less distinguishable signals, with no clear adaptation period for cooling onset (even accounting for the lack of a rewarming period in the trial design). On the other hand, ice shows a clear onset/offset response with adaptation. It's possible that this is a biological difference between monkeys. However, considering that noise interference was not notable with the probe, it may be that the greater contact area with ice caused a more prominent signal. In addition, the moisture from the melting ice could aid in heat transfer from the ice to the skin. A simple future test with wider probe tips could check for stronger and more robust neural signals to constant *T*.

5.8.2 On the accuracy of classification and linear model generation

In both individual and population response of multiunits, there were ambiguity in the results. With firing rates, no clear response to *T* or changing *T* could be identified across dates, animals, and even same day trials. The low accuracy of our classifier is partly due to similar

statistical means of firing rates across input constant *T*. This implies that either firing rate is not the most optimal feature for thermosensation, or there is a flaw in experimental design (i.e. low intensity of input stimulus). The classifier is also unable to highly discriminate *MP*, despite the visible surges in firing rate of multiunits at select trials. Clearly, there is a need to amplify the magnitude of responses to only cold and poking, and reduce other activity caused by movement or electrical noise.

Attempts to generate linear models with latency, phase, or firing rate were also unsuccessful in predicting *T* or *MP*. With latency, changes in latency over time at different *T* were statistically significant in ~10-15 channels at most. This is from a population size of 20-25 viable channels. There are too few channels and data to develop a highly accurate linear decoder. Phase and firing rates also faced this same dilemma.

In order to establish a model that predicts neural response to cold and mechanical stimuli, we must improve experimental and signal processing methods to collect data from more units and trials. Developing a highly accurate model with neural data is a priority to prove the encoding of cold sensation in cortical units, and must be accomplished before engaging human subject testing to pair human sensation scores to monkey neural data.

5.8.3 Limitations

The data thus far is limited in its ability to decode input stimuli with high accuracy. The cause of this may be due to experimental or signal processing pitfalls. Experimentally, the probe delivered cold to a small contact area for a short length of time (ranging 10 sec to 2 mins per trial). Therefore intensity of stimulus was low and temporal effects could not be resolved at a high frequency. Increasing the intensity of the stimulus could involve using lower temperatures, increasing trial durations, applying cold to a wider contact area, or choosing another receptive

zone on the animals' skin. We also did not investigate pressure sensation (caused by the probe tip pressing onto the arm while delivering cold) in conjunction with cold. Testing varying levels of pressure with constant T would allow decoupling of temperature with pressure sensation. Also, the animals were few in number (due to lack of resources), trained minimally and would occasionally twitch, chew and vocalize, causing artifacts in the data. Sufficient training and preparation is necessary for animals' cooperation and plentiful data collection. Lastly, the experiments were performed over years, likely leading to considerable changes in the electrode array and its sensitivities.

In terms of data analysis and signal processing, the lack of sample data, trial durations, and number of viable channels hindered the drawing of accurate conclusions. Ultimately, of the 96 total electrodes only 20-25 channels were deemed healthy, which is a tiny fraction of the total units in the sensory cortex. Even if an accurate model could be developed with this data, it would only represent a section of the cortex. The brain is a highly complex and noisy organ, and any argument for a portion of multiunits affecting thermosensation would require additional justification.

Other limitations center on the fact that this is a highly exploratory project with many unknowns. For instance, efforts to unmix pressure and temperature responses failed; not only does independent component analysis change results with every run, but also because there is no baseline knowledge for cross checking. The lack of signposts to identify what signals belong to what stimulus has excessively complicated this study. Visual encoding and statistical analysis of neural activity was unable to identify a large population of multiunits for each type of stimulus. A clinical study with MRI, EEG, and subject scoring would be more suited to identifying responses to stimulus types while resolving a wide area population response and developing a

predictive model accordingly. This would effectively achieve the goal of engineering enhanced cryoanesthesia.

5.9 Conclusion

We have investigated the cortical neural response to thermal and tactile stimuli on monkeys' skin. While prior works in thermosensation have focused on heating responses[20] or peripheral neural response to steady cold inputs[11,18], our work examined the response of cortical multiunits (single channel as well as set of all channels) to thermomechanical stimuli (constant and transient) using visual, statistical, and machine learning techniques. Results confirmed that the cortex is more sensitive to transient inputs (i.e. changing *T* or *MP* trains) than constant inputs. Using data from both constant *T* and *MP*, cold vs normal skin *T* could be discriminated to 70-75% accuracy. This was not possible for constant *T* data without the occasional *MP* stimulation. Sinusoidal thermal stimuli resulted in peak neural response at the cooling transient regime, with no visible response for heating regimes. Linking such neural behavior to psychophysiological responses must be performed to understand the impact of the data.

This work aims to inform how the sensory cortical multiunits encode for thermosensation. With this knowledge, we envision both clinical and technical advancements. Clinically, we may engineer sensation, or induce enhanced cryoanesthesia. This will inform pain relief methods as well as research on CIPA (sensory neuropathy). Technically, the knowledge may inform the engineering of haptic interfaces, HVAC systems, and more.

Future work will include the gathering of further data using monkey modes with an improved protocol, and create a higher accuracy model to predict neural responses to stimuli. We will also explore use of other features, neural spatial scales (i.e. MRI), or human trials. The

ultimate goal is to create a dynamic model of temperature and pressure, correlated with subject scores to pair sensation to neural activity.

5.10 Acknowledgements

This work is made possible through collaboration with the Chestek lab. Special thanks to: Cindy Chestek, Eric Kennedy, Samuel Nason, and Autumn Bullard for enabling this study and assisting in experiments.

5.11 References

1. Fredholm BB, Johansson S, Wang Y-Q. Adenosine and the Regulation of Metabolism and Body Temperature. In: *Advances in Pharmacology*. Vol 61. Academic Press; 2011:77-94. doi:10.1016/B978-0-12-385526-8.00003-5

2. Can COVID-19 cause hair loss? https://www.aad.org/public/diseases/hair-loss/causes/covid-19. Accessed June 26, 2022.

3. Sessler DI. Perioperative thermoregulation and heat balance. *Lancet*. 2016;387(10038):2655-2664. doi:10.1016/S0140-6736(15)00981-2

4. Ogawa T, Asayama M. Quantitative Analysis of the Local Effect of Skin Temperature on Sweating. *Jpn J Physiol*. 1986;36(2):417-422. doi:10.2170/JJPHYSIOL.36.417

5. Pennes HH. *Analysis of Tissue and Arterial Blood Temperatures in the Resting Human Forearm*. *J Appl Physiol*. 1948;1(2):93-122. doi:10.1152/jappl.1948.1.2.93

6. Havenith G. Temperature regulation, Heat balance and climatic stress. *Extrem Weather Events Public Heal Responses*. 2005:69-80. doi:10.1007/3-540-28862-7_7/COVER/

7. Vriens J, Nilius B, Voets T. Peripheral thermosensation in mammals. *Nat Rev Neurosci*. 2014;15(9):573-589. doi:10.1038/nrn3784

8. YARNITSKY D, OCHOA JL. RELEASE OF COLD-INDUCED BURNING PAIN BY BLOCK OF COLD-SPECIFIC AFFERENT INPUT. *Brain*. 1990;113(4):893-902. doi:10.1093/brain/113.4.893

9. Melzack R. Gate control theory: On the evolution of pain concepts. *Pain Forum*. 1996;5(2):128-138. doi:10.1016/S1082-3174(96)80050-X

10. Rosemberg S, Nagahashi Marie SK, Kliemann S. Congenital insensitivity to pain with anhidrosis (hereditary sensory and autonomic neuropathy type IV). *Pediatr Neurol*.

1994;11(1):50-56. doi:10.1016/0887-8994(94)90091-4

11. Ingraham FD, Matson DD. Inhibition of Cutaneous Pain Responses By the Local Application of Cold. *N Engl J Med*. 1947. http://www.nejm.org/doi/pdf/10.1056/NEJM194711202372104. Accessed November 9, 2017.

12. Lloyd EL. ABC of Sports Medicine: Temperature and Performance I: Cold. *BMJ*. 1994;309(6953):531-534. doi:10.1136/BMJ.309.6953.531

13. Karnatovskaia L V., Wartenberg KE, Freeman WD. Therapeutic Hypothermia for Neuroprotection: History, Mechanisms, Risks, and Clinical Applications. *The Neurohospitalist*. 2014;4(3):153. doi:10.1177/1941874413519802

14. Vibracool - Muscle & Join Pain Relief – Pain Care Labs. https://paincarelabs.com/pages/vibracool. Accessed July 6, 2022.

15. Besirli CG, Smith S, Kim G-H, Pipe K. Applicator for cryoanesthesia and analgesia. March 2016. https://patents.google.com/patent/US9956355B2/en. Accessed October 16, 2018.

16. Bautista DM, Siemens J, Glazer JM, et al. The menthol receptor TRPM8 is the principal detector of environmental cold. *Nature*. 2007;448(7150):204-208. doi:10.1038/nature05910

17. Harrington T, Merzenich M. Neural coding in the sense of touch: Human sensations of skin indentation compared with the responses of slowly adapting mechanoreceptive afferents innervating the hairy skin of monkeys. *Exp Brain Res*. 1970;10(3):251-264. doi:10.1007/BF00235049

18. Olivares E, Salgado S, Maidana JP, et al. TRPM8-Dependent Dynamic Response in a Mathematical Model of Cold Thermoreceptor. McKemy DD, ed. *PLoS One*. 2015;10(10):e0139314. doi:10.1371/journal.pone.0139314

19. Craig AD, Chen K, Bandy D, Reiman EM. Thermosensory activation of insular cortex. *Nat Neurosci*. 2000;3(2):184-190. doi:10.1038/72131

20. Yarnitsky D, Ochoa JL. Studies of heat pain sensation in man: perception thresholds, rate of stimulus rise and reaction time. *Pain*. 1990;40(1):85-91. doi:10.1016/0304-3959(90)91055-N

21. Arrich J, Holzer M, Havel C, Müllner M, Herkner H. Hypothermia for neuroprotection in adults after cardiopulmonary resuscitation. *Cochrane Database Syst Rev*. 2016;2016(2). doi:10.1002/14651858.CD004128.pub4

22. Filingeri D. Neurophysiology of Skin Thermal Sensations. In: *Comprehensive Physiology*. Vol 6. Hoboken, NJ, USA: John Wiley & Sons, Inc.; 2016:1429-1491. doi:10.1002/cphy.c150040

23. Ludwig KA, Miriani RM, Langhals NB, Joseph MD, Anderson DJ, Kipke DR. Using a common average reference to improve cortical neuron recordings from microelectrode arrays. *J Neurophysiol*. 2009;101(3):1679-1689. doi:10.1152/jn.90989.2008

24. Irwin ZT, Thompson DE, Schroeder KE, et al. Enabling Low-Power, Multi-Modal Neural Interfaces Through a Common, Low-Bandwidth Feature Space. *IEEE Trans Neural Syst Rehabil Eng*. 2016;24(5):521-531. doi:10.1109/TNSRE.2015.2501752

25. Stark E, Abeles M. Predicting movement from multiunit activity. *J Neurosci*. 2007;27(31):8387-8394. doi:10.1523/JNEUROSCI.1321-07.2007

26. Nason SR, Vaskov AK, Willsey MS, et al. A low-power band of neuronal spiking activity dominated by local single units improves the performance of brain–machine interfaces. *Nat Biomed Eng 2020 410*. 2020;4(10):973-983. doi:10.1038/s41551-020-0591-0

Chapter 6 Summary and Future Work

6.1 Summary

Thermoelectric cooling was demonstrated to cool local tissue in living systems, for studies on selective hypothermia and thermosensation. Compared to pre-existing cooling techniques such as ice packs, ice baths, and single Peltier coolers, the approach described in this work delivered more concentrated, rapid, and controlled cooling. In the projects relating to blood and selective brain cooling, concentrated cooling effectively reduced blood and brain temperature, opening the possibility for targeted hypothermia therapies at the treatment site and inform clinical workflows. This is a breakthrough technology as existing hypothermia methods are systemic and cannot selectively cool a part of the body. The prototype blood/brain cooling device proposed could also serve as a tool for optimizing studies or other cooling studies in the future. While a computational analysis of the prototype has revealed possible power deficiencies in cooling human vasculatures to a desired level, the technical improvements required are not impossible to achieve (i.e., can add more thermoelectric elements).

In our study of the encoding of cold sensation in the brain, the thermoelectric cool was also highly utilized for precise cold delivery and quantification of input stimuli. Neural firing rates from the sensory cortex of non-human primate models showed a correlation to the applied probe temperature. Though the statistical relevance of these parameters could be strengthened, thus far we can reliably decode (~73% accuracy) firing rates for input probe temperature. To the best of our knowledge, such a quantitative study for cold sensation was not performed and we envision eventually reverse-engineering thermosensation in patients for therapy.

6.2 Future work

In future work, the prototype blood cooling probe will be improved in its cooling power and delivery mechanism to allow minimally invasive percutaneous cooling. Then the efficacy of the percutaneous cooling will be tested in swine/human trials. Ultimately, we hope to submit our device for FDA approval and partake in clinical studies to expand the uses for hypothermia therapy for various diseases.

Regarding the cold sensation study, more neural data will be collected from monkeys. The collective data will be used for training and testing the decoder and other machine learning algorithms. Aside from increasing the training data pool, we aim to improve the preliminary decoder in its accuracy by modifying its architecture (i.e. adjusting weights, adding more factors, etc). Concurrently to animal work and algorithm development, human trials will be performed to pair monkey neural data with sensation scores.

Appendices

-

Appendix A: Description of Rat Experimental Setup

Appendix Figure 1. Rat surgical space setup. 1) Kopf stereotaxic frame, 2) anesthesia induction box and shaving area, 3) Vetamac isoflurane vaporizer, 4) oxygen tank with regulator, 5) 10x microscope, 6) surgical benchtop with anesthesia nose cone and cooling probe tip, 7) Koolance cooling probe chiller and power supply, 8) biohazardous waste disposal, 9) charcoal canister for waste isoflurane recovery, with another under the surgical benchtop.

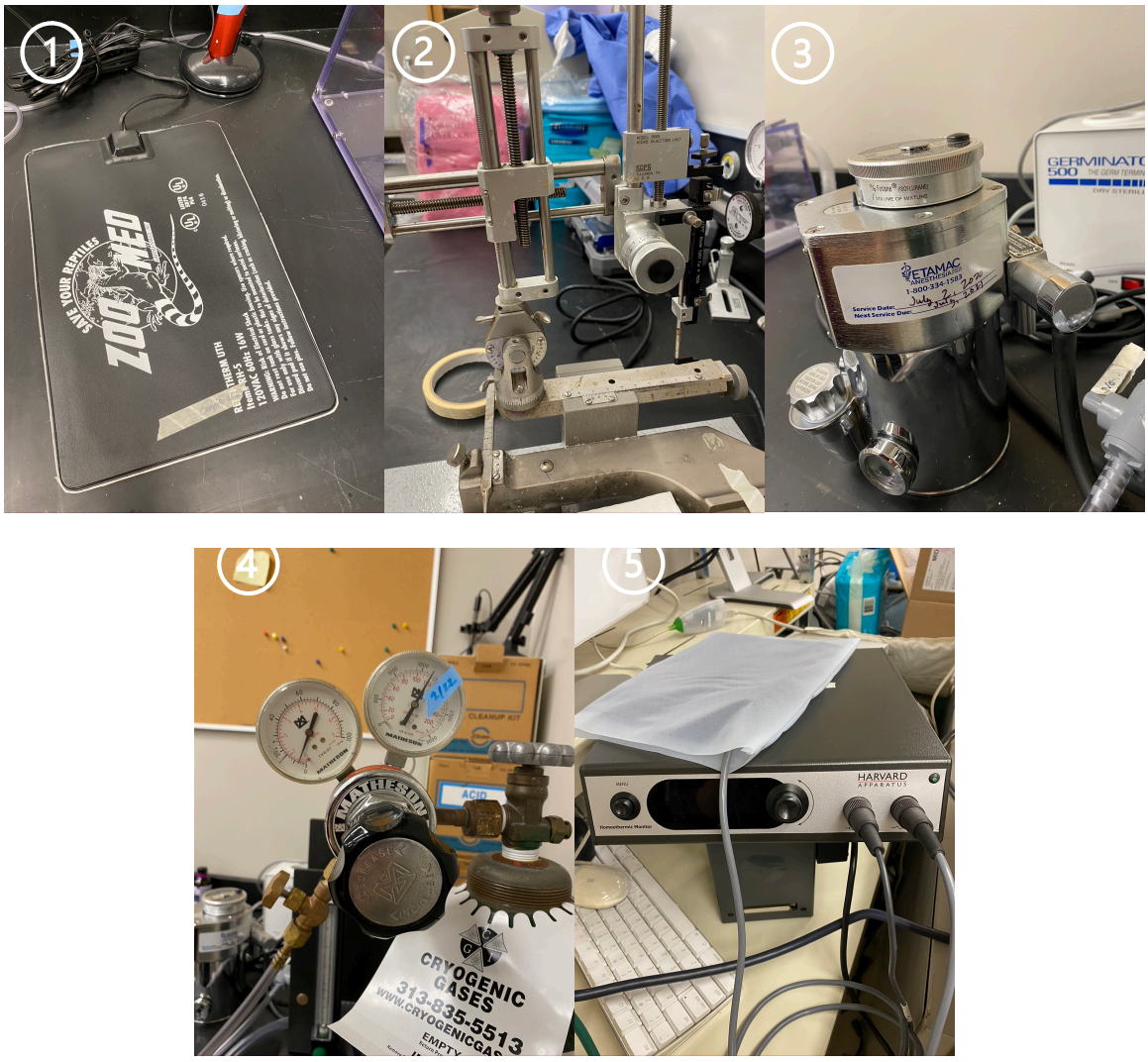

Appendix Figure 2. Close up images of equipment used in surgical lab. 1) Zoomed heating pad for induction of anesthesia, 2) Kopf stereotaxic frame, 3) Vetamac vaporizer for isoflurane, 4) oxygen regulators, 5) Harvard Apparatus feedback controlled heating pad with rectal probe.

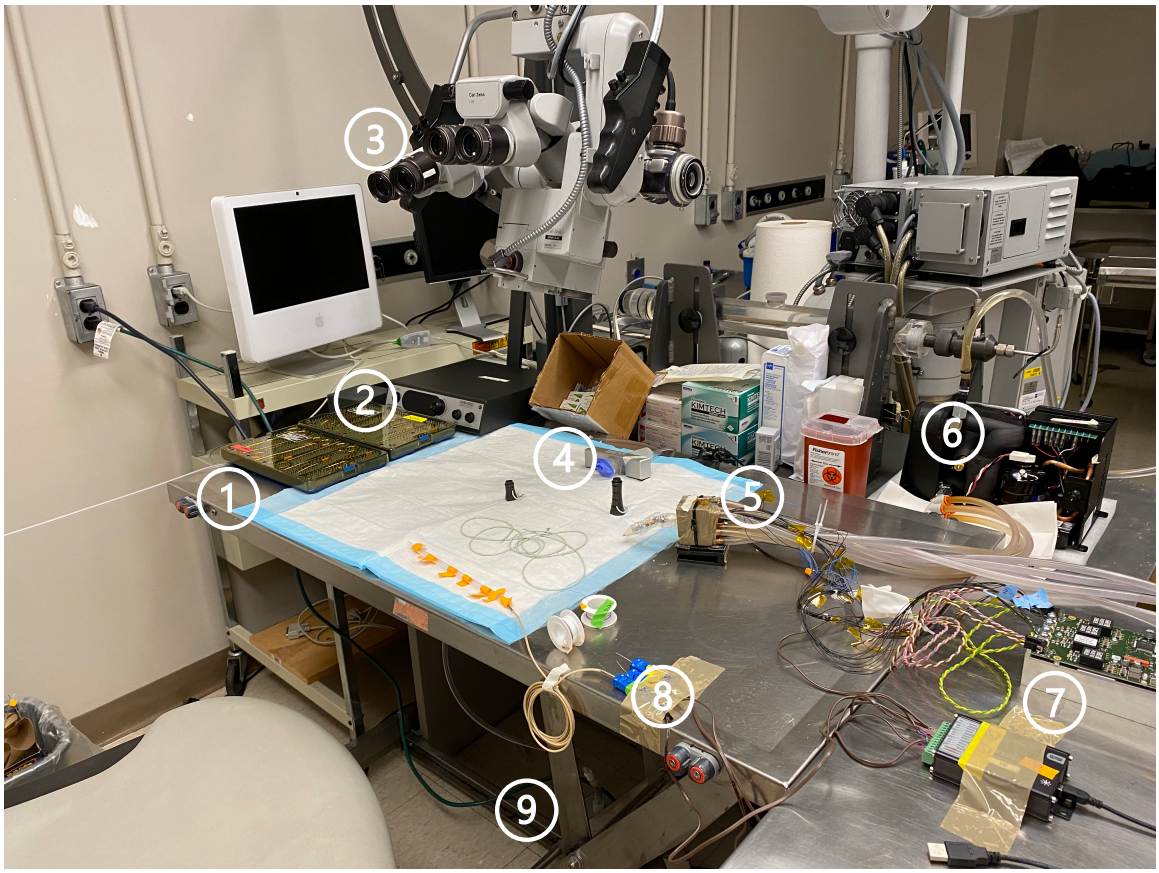

Appendix Figure 3. Close up of the surgical bench. 1) Surgical tools and anesthesia line from vaporizer (thin white tube to the left), 2) Harvard Apparatus feedback controlled heating pad, with the pad under the white surgical benchtop area, 3) 10x microscope, 4) 1"-1.25" diameter nose cone made with a syringe and latex gloves, 5) cooling probe tip, 6) Koolance water chiller, 7) Meerstetter TEC high voltage controller and Siteview data logger, 8) thermocopules, 9) hidden charcoal canister for waste isoflurane collection.

Appendix B: Description of Parts in Cooling Probes (Rat and Monkey)

Components list:

- TECs (Custom Thermoelectrics, Bishopville, MD; Part# 03101-9B30-30RU7)
- TEC controller (Meerstetter Engineering, Germany; Part# 1123HV-NTC56K, and CAB6155 cables)
- Water pump and reservoir (measured 3.6 – 9.6 L/min flow rate)
- Water chiller (Koolance, South Korea; Part #VLX 450)
- Power supply (24V, 500W)
- Aluminum water blocks
- NTC Thermistor (Mouser Electronics, Mansfield, TX; GA10K3MCD1)

TEC elements:

TEC Specification Sheet

CUSTOM THERMOELECTRIC
Your Thermoelectric Partner

Part #	I_{max} (Amps)	Q_{max} (Watts)	V_{max} (Volts)	DT_{max} (°C)	T_{max} (°C)
03101-9B30-30RU7	3.0	6.75	3.75	69°C	200°C

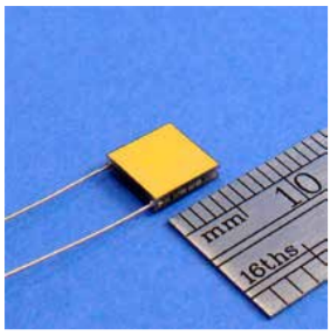

Custom Options:

Call for custom wire types and other custom options.

Notes:

Typical power input is 40% to 80% of I_{max}

Maximum Waste Heat (exiting the hot side) at 100% input power, $I=I_{max}$, $V=V_{max}$ is;

$(I_{max} * V_{max}) + Q_{max}$ = **18.0 watts**

Use of a properly sized heat sink or water block is required to remove waste heat.

Bottom Plate				Top Plate				Metallized Height		Lapped Height	
A		B		C		D		H		H	
mm	in	mm	in	mm	in	mm	in	mm	in	mm	in
6.6	0.260	6.6	0.260	6.6	0.260	6.6	0.260	1.5	0.059	NA	NA

Appendix Figure 4. TEC specifications for rat (and monkey) probes. Manufactured by Custom Thermoelectrics.

Appendix C: Custom Scripts and Functions for Study of Cold Sensation.

Detectdecay:

% function for detecting adaptation response in firing rate of units (written in MATLAB)

```
function rec = detectDecay(data, ind_peak, N, exp)
%Inputs:
% data: firing rates for one unit
% ind_peak: indices of the peaks
% N: window size
% exp: true/false for making an exponential amplification on the data or not

rec = [];

%make sure that the datapoint we are looking at doesn't exceed the boundaries
of the dataset
if (ind_peak+N) <= length(data)
    fin = ind_peak+N;
else
    fin = length(data);
end

%recall we had taken the exponential of the data
if exp == 1
    sample = log(log(data(ind_peak:fin)));
else
    sample = log(data(ind_peak:fin));
end

%test that there are any zero values in this sample
zero_vals = find(sample==0, 1);
if isempty(zero_vals) == 0
    return
else
    [p, S] = polyfit(1:length(sample), sample, 1);
    %arbitrary thresholds of S.normr (norm of the residuals) being < 1. Can
    %make it smaller if necessary.
    if (p(1) < 0) && (S.normr < 1)
        rec = ind_peak;
        disp('1')
    else
        return
    end
end
end
```

Findbestresponse:

% function to find the best response peak out of a number of candidate peaks to a single stimulus

```
function peak_index = findBestResponse(data, stimulations, window, time,
thres, exp)
%Inputs:
%data: input data, often it is in the form of one channel firing rates that
are taken from a myZ struct. Ex: data = myZ(3).FiringRates100bin./time;
%stimulations: expected time of stimulations (MPs), according to the data.
This already includes any padding accounted for when data was extracted.
%window: how much time after the stimulation time to search for the "best
response"
%time: a correction factor to count the indices of the data, ex: 100 ms
binned firing rates would have a time = 10 factor. time = 1000/binsize;
%thres: a threshold to detect the peaks by. ex: 1.5*mean(data), or
1.5*mean(baseline)
%exp: a logical True/False to indicate if data is exp(FiringRates) or just
firing rates.

%Outputs:
%peak_times: a cell array containing the indices of the extracted "best
%peak times", in terms of indices (ex: index = 10 would be equivalent to 1s
%in a 100 ms binned data. To convert to elapsed seconds, multiply index
%with time/binsize, ex: index_i*(time/binsize) [=] seconds.

peak_index = {};
for i = 1:length(stimulations)
    %Calculate a conversion factor to convert the indices for snippet to
    %whole dataset, as well as a starting offset for the snippet.
    B = stimulations(i)-(window(1)*time);
    if B == 0
        B = 1;
    end

    snippet = data(B: stimulations(i) + window(2)*time);

    %Set a threshold for a peak at some reasonable value unless defined in
    %the function statement inputs
    if isempty(thres) == 1
        thres = 1.5*mean(snippet); %(1.5)*mean(data);
    end

    %find the index of the datapoints in the snippet that are >= threshold
    %snippet = testcase1_1;
    ind_peaks = find(snippet >= thres);

    if numel(ind_peaks) == 1  %only one possible peak
        %return the best index, in terms of indices for the WHOLE dataset,
        %not the snippet.
        response_index = ind_peaks+(B-1);
        disp('Case 2')

    elseif numel(ind_peaks) == 0 %no peak candidates, return empty array
```

```
        response_index = [];
        %disp('No qualifying peak detected')
        disp('Case 3')
    else  %numel(ind_peaks) > 1, more than one possible peak, determine
        % best peak time to return by assessing decay response or
consecutivity.

        %first check if indices of peaks are next to each other. If they
        %are consecutive, return the very first index
        N = 1; % Required number of consecutive numbers following a first one
        x = diff(ind_peaks')==1;
        f = find([false,x]~=[x,false]);
        g = find(f(2:2:end)-f(1:2:end-1)>=N,1,'first');
        ind_cons_peak = ind_peaks(f(2*g-1));  %If they are next to each
other, just report the first value

        %If there is a consecutive peak value that's not preceded by a
        % greater than or equivalent peak, return that first time bin.
        if (~isempty(ind_cons_peak) == true) %&& (isempty(any_earlier_peaks)
== 1)
            ind_first_peaks = ind_peaks(ind_peaks < ind_cons_peak);

            %return the value of the first peak that is greater/equivalent to
            %the consecutive peak, if any.
            good_first_peaks = ind_first_peaks(snippet(ind_first_peaks) >=
snippet(ind_cons_peak));

            if (~isempty(good_first_peaks) == true)
                response_index= good_first_peaks(1)+(B-1);
                disp('Case 1.11')
            else
                response_index = ind_cons_peak+(B-1);
                disp('Case 1.1')
            end
            clear ind_first_peaks good_first_peaks

        %If there does not exist peak values that are consecutive, then check
for decay
        %response in at least one of the values.
        else
            rec = [];
            k = 1;
            %while loop terminates when it finds the "first" decay response
            %peak value or gives up when it runs out of peaks.
            while (isempty(rec) == 1) && (k <= numel(ind_peaks))
                %N = 3;  %arbitrary; # of expected trailing decay response
bins.
                % When choosing N, consider the time bin of your data.
                rec = detectDecay(snippet, ind_peaks(k), 3, exp);
                disp(k)
                k = k+1;
            end
            if isempty(rec) %Of all the candidate peaks, no peaks return a
decay response. Then return the first peak timepoint
                response_index = ind_peaks(1)+(B-1);
```

```
                disp('Case 1.3')
            else  %if there is a good candidate with a decay response, return
rec
                response_index = rec+(B-1);
                disp('Case 1.2')
            end

        end

    end
    peak_index{i} = response_index;
end
end
```

Appendix D: Cold Sensation Study-- Stepwise Dynamic Trials

Moving RMS of neural data from stepwise dynamic trials. Animation showing RMS values (calculated at moving window of 1 second lengths) at instantaneous probe cooling rate as it varies with experiment time (RMS vs dT/dt and t).

Link:

https://drive.google.com/file/d/1tneGsOZffpAcBp3Z7YAn35L64lOXj7l6/view?usp=sharing